The Astrophysical Journal Supplement Series, 173:185–255, 2007 December

THE *GALEX* ULTRAVIOLET ATLAS OF NEARBY GALAXIES

Armando Gil de Paz,[1] Samuel Boissier,[1] Barry F. Madore,[1,2] Mark Seibert,[3] Young H. Joe,[1,4] Alessandro Boselli,[5] Ted K. Wyder,[3] David Thilker,[6] Luciana Bianchi,[6] Soo-Chang Rey,[3] R. Michael Rich,[7] Tom A. Barlow,[3] Tim Conrow,[3] Karl Forster,[3] Peter G. Friedman,[3] D. Christopher Martin,[3] Patrick Morrissey,[3] Susan G. Neff,[8] David Schiminovich,[3] Todd Small,[3] José Donas,[5] Timothy M. Heckman,[9] Young-Wook Lee,[4] Bruno Milliard,[5] Alex S. Szalay,[9] and Sukyoung Yi[4]

Received 2006 January 6; accepted 2006 March 15

ABSTRACT

We present images, integrated photometry, and surface-brightness and color profiles for a total of 1034 nearby galaxies recently observed by the *Galaxy Evolution Explorer* (*GALEX*) satellite in its far-ultraviolet (FUV; $\lambda_{\rm eff} = 1516$ Å) and near-ultraviolet (NUV; $\lambda_{\rm eff} = 2267$ Å) bands. Our catalog of objects is derived primarily from the *GALEX* Nearby Galaxies Survey (NGS) supplemented by galaxies larger than $1'$ in diameter serendipitously found in these fields and in other *GALEX* exposures of similar of greater depth. The sample analyzed here adequately describes the distribution and full range of properties (luminosity, color, star formation rate [SFR]) of galaxies in the local universe. From the surface brightness profiles obtained we have computed asymptotic magnitudes, colors, and luminosities, along with the concentration indices C31 and C42. We have also morphologically classified the UV surface brightness profiles according to their shape. This data set has been complemented with archival optical, near-infrared, and far-infrared fluxes and colors. We find that the integrated (FUV $-$ K) color provides robust discrimination between elliptical and spiral/irregular galaxies and also among spiral galaxies of different subtypes. Elliptical galaxies with brighter K-band luminosities (i.e., more massive) are redder in (NUV $-$ K) color but bluer in (FUV $-$ NUV) (a color sensitive to the presence of a strong UV upturn) than less massive ellipticals. In the case of the spiral/irregular galaxies our analysis shows the presence of a relatively tight correlation between the (FUV – NUV) color (or, equivalently, the slope of the UV spectrum, β) and the total infrared-to-UV ratio. The correlation found between (FUV $-$ NUV) color and K-band luminosity (with lower luminosity objects being bluer than more luminous ones) can be explained as due to an increase in the dust content with galaxy luminosity. The images in this Atlas along with the profiles and integrated properties are publicly available through a dedicated Web page.

Subject headings: atlases — galaxies: evolution — galaxies: fundamental parameters — galaxies: photometry — ultraviolet: galaxies

Online material: extended figure set, machine-readable tables

1. INTRODUCTION

There are several compelling reasons for observing nearby galaxies in the ultraviolet (UV). First of all, massive, young stars emit most of their energy in this part spectrum and at least in star-forming galaxies they outshine the emission from any other stage of the evolution of a composite stellar population (e.g., Bruzual & Charlot 2003). Therefore, the flux emitted in the UV in spiral and irregular is an excellent measure of the current star formation rate (SFR; Kennicutt 1998; Donas et al. 1987). In the case of quiescent elliptical galaxies the analysis of the UV upturn (the rising part of the FUV spectrum of these galaxies) promises to provide fundamental clues in our understanding of the evolution of low-mass stars on the horizontal branch. Due to its remarkable sensitivity to the physical properties of these stars, the UV upturn could be used, once fully understood, as a powerful diagnostic of old stellar populations (Burstein et al. 1988; O'Connell 1999; Yi et al. 1999; Brown 2004; Rich et al. 2005; R. M. Rich et al. 2008, in preparation; Boselli et al. 2005). The UV has also revealed the presence of residual star formation in a non-negligible fraction of low-redshift elliptical galaxies (Yi et al. 2005).

Second, the light emitted in the UV can be very efficiently absorbed by dust and then re-emitted at far-infrared (FIR) wavelengths. Therefore, an analysis of the energy budget using a comparison of the infrared and UV emission is a powerful tool to determine the dust attenuation of light at all wavelengths (see Buat et al. 2005 and references therein). In this sense, it is worth

[1] The Observatories, Carnegie Institution of Washington, 813 Santa Barbara Street, Pasadena, CA 91101; agpaz@ociw.edu, boissier@ociw.edu, young@ociw.edu; A. G. d. P.'s current address: Departamento de Astrofísica, Universidad Complutense de Madrid, Madrid 28040, Spain; S. B.'s current address: Laboratoire d'Astrophysique de Marseille, BP 8, Traverse du Siphon, 13376 Marseille Cedex 12, France.

[2] NASA/IPAC Extragalactic Database, California Institute of Technology, MS 100-22, Pasadena, CA 91125; barry@ipac.caltech.edu.

[3] California Institute of Technology, MC 405-47, 1200 East California Boulevard, Pasadena, CA 91125; mseibert@srl.caltech.edu, wyder@srl.caltech.edu, screy@srl.caltech.edu, tab@srl.caltech.edu, tim@srl.caltech.edu, krl@srl.caltech.edu, friedman@srl.caltech.edu, cmartin@srl.caltech.edu, patrick@srl.caltech.edu, ds@srl.caltech.edu, tas@srl.caltech.edu; S.C.R.'s current address: Department of Astronomy and Space Sciences, Chungnam National University, 220 Gung-dong, Yuseong-gu, Daejeon 305-764, Korea.

[4] Center for Space Astrophysics, Yonsei University, Seoul 120-749, Korea; ywlee@csa.yonsei.ac.kr, yi@astro.ox.ac.uk.

[5] Laboratoire d'Astrophysique de Marseille, BP 8, Traverse du Siphon, 13376 Marseille Cedex 12, France; alessandro.boselli@oamp.fr, jose.donas@oamp.fr, bruno.milliard@oamp.fr.

[6] Center for Astrophysical Sciences, The Johns Hopkins University, 3400 North Charles Street, Baltimore, MD 21218; dthilker@pha.jhu.edu, bianchi@pha.jhu.edu.

[7] Department of Physics and Astronomy, University of California, Los Angeles, CA 90095; rmr@astro.ucla.edu.

[8] Laboratory for Astronomy and Solar Physics, NASA Goddard Space Flight Center, Greenbelt, MD 20771; neff@stars.gsfc.nasa.gov.

[9] Department of Physics and Astronomy, The Johns Hopkins University, Homewood Campus, Baltimore, MD 21218; heckman@pha.jhu.edu, szalay@pha.jhu.edu.

emphasizing that dust attenuation is the most vexing problem that one has to face when analyzing the observational properties of composite stellar populations and galaxies.

Finally, the observation of nearby galaxies in the UV is fundamental if we are to understand the evolution of galaxies from the high-redshift universe (where their properties are commonly derived from rest-frame UV observations) to the present.

There have been many attempts in the past to address some of these issues. Sullivan et al. (2000, 2001, 2004) studied the star formation histories in a relatively large and complete sample of UV-selected local galaxies, from which Treyer et al. (1998) derived the SFR density of the local universe. The nature of the UV upturn in elliptical galaxies has been widely studied by several groups, including O'Connell (1999), Brown et al. (2000), and Deharveng et al. (2002). Studies on the dust attenuation in galaxies based on either photometric or spectroscopic UV studies are numerous, including Calzetti et al. (1994), Heckman et al. (1995), Meurer et al. (1995, 1999), Buat & Xu (1996), Gordon et al. (2000, 2003), Buat et al. (2002), and Roussel et al. (2005). The analysis of the UV morphology of nearby galaxies as a local benchmark for studies in the optical at high redshift have been also carried out by several authors, including Kuchinski et al. (2000, 2001), Marcum et al. (2001), Windhorst et al. (2002), and Lauger et al. (2005).

However, the results of some of these studies were not conclusive mainly due to the small size of the samples used, which were not representative of the overall population of galaxies in the local universe. This is particularly true for studies on the dust attenuation in star-forming galaxies and on the rest-frame UV morphology in nearby galaxies. In the case of the UV-upturn studies in early-type galaxies this limitation adds to the lack of spatial resolution and depth of previous UV data and, in some cases, to the availability of UV data in only one band, which leads to a loss of sensitivity to the strength of the UV upturn, best traced by the FUV $-$ NUV color (see Gil de Paz et al. 2005a and references therein).

The availability of deep UV observations with moderately good spatial resolution for large numbers of well-known nearby galaxies is now possible thanks to the launch of the *Galaxy Evolution Explorer* (*GALEX*) on 2003 April 28. The compilation of *GALEX* UV data carried out as part of this paper will allow us (and other researchers making future use of this data set) to provide fundamental clues for solving some of the many open questions regarding the UV properties of galaxies in the local universe. In particular, we will show how the strength of the UV upturn is function of the stellar mass of the galaxy, with more massive elliptical galaxies showing stronger UV upturns. We will also demonstrate that in a sample like ours, which adequately represents the bulk of the galaxy population in the local universe, the slope of the UV continuum is well-correlated (although with a significant dispersion) with the infrared-to-UV ratio and, therefore, with the UV extinction, and that the (FUV $-$ K) color provides and excellent segregation between early-type (ellipticals and lenticulars) and late-type (spirals and irregulars) galaxies.

In this *GALEX* Ultraviolet Atlas of Nearby Galaxies we present surface photometry in the two *GALEX* ultraviolet (FUV and NUV) bands, providing integrated photometry and structural parameters for a total of 1034 nearby galaxies, including extensively studied objects like M31, M32, M33, M51, M81, M82, M83, M87, M101, etc. We compare the UV properties of this sample with corollary data in the optical, NIR, and FIR, available for the majority of the galaxies in the Atlas. This comparison allows us to obtain insight into fundamental correlations such as the "red sequence" found in the color-magnitude diagram of ellipticals and lenticulars, and a better definition of the IRX-β relation in normal star-forming galaxies.

In § 2 we extensively describe the sample of galaxies. Section 3 provides a summary of the *GALEX* observations. The analysis and results are given in §§ 4 and 5, respectively. The conclusions are summarized in § 6.

2. SAMPLE

2.1. *Selection*

The sample of objects in this Atlas includes galaxies in the *GALEX* Nearby Galaxies Survey (NGS; Gil de Paz et al. 2004; Bianchi et al. 2003a, 2003b) plus galaxies serendipitously found in NGS fields or in fields with similar or greater depth obtained as part of other *GALEX* imaging surveys that have optical diameters at the $\mu_B = 25$ mag arcsec^{-2} isophote larger than $1'$ according to the Third Reference Catalog of Bright Galaxies (de Vaucouleurs et al. 1991, hereafter RC3). Note also that $1'$ is the apparent diameter for which RC3 is reasonably complete (H. G. Corwin 2005, private communication).

As mentioned above the answers to some of the most fundamental open questions on galaxy evolution in general and on the UV properties of galaxies in particular are largely dependent on the (sometimes very large) corrections for dust extinction that must be applied. With this in mind, the NGS survey was constructed to optimally sample the UV as provided by *GALEX* and the FIR (where most of the UV light absorbed by dust is reemitted) as seen by the *Spitzer Space Telescope* that would give us a bolometric view of galaxies in the local universe. Thus, we began building the NGS sample using *Spitzer*'s Reserved Observations Catalog (ROC ver. 2.0), which guarantees that both UV and infrared data will be eventually made publicly available to the community for all these galaxies. This includes not only the *Spitzer* Infrared Nearby Galaxies Survey legacy project (SINGS; Kennicutt et al. 2003), but also data from Guaranteed Time Observer (GTO) programs like The Mid-IR Hubble Atlas of Galaxies (PI: G. Fazio), Starburst Activity in Nearby Galaxies (PI: G. Rieke), Probing a sample of Interacting and Ultraluminous Galaxies (PI: G. Fazio), etc. The total number of (targeted) NGS galaxies represents approximately one-fourth of the total sample of 1034 galaxies in the present Atlas. The vast majority of the UV images of the galaxies observed as part of NGS have exposure times of 1 *GALEX* orbit or more ($\sim$1700 s). See § 3 for a detailed description of the *GALEX* spacecraft and instrument.

In order to cover a wider range of physical properties (see § 3.1) and taking advantage of the large field of view of the *GALEX* instrument (1.2° in diameter) we added to the Atlas sample all galaxies in RC3 with D25 diameter larger than $1'$ that were serendipitously observed within NGS fields and/or within other *GALEX* surveys of similar or greater depth that were available to the *GALEX* team, namely the Medium Deep, Deep, and Ultradeep Imaging Surveys (MIS, DIS, and UIS, respectively). We also added galaxies that were targeted by *GALEX* because they had been observed by previous UV missions like UIT or FOCA (as an additional calibration test for *GALEX*) and galaxies from dedicated observations of the central 12 deg^2 of the Virgo cluster (Boselli et al. 2005).

Of the original 1136 galaxies compiled 26 were found in images that have failed the quality assurance (QA) test of the image aspect solution that is included as part of the standard *GALEX* pipeline. A total of 55 additional galaxies were excluded either because were observed in regions of high background, high Galactic extinction, during very short orbits and/or they showed extremely low surface brightness in the UV. After excluding these

TABLE 1
GALEX Atlas Sample

Object Name (1)	R.A. (J2000.0) (2)	Decl. (J2000.0) (3)	$2\times A$ (arcmin) (4)	$2\times B$ (arcmin) (5)	P.A. (deg) (6)	Distance d (Mpc) (7)	Distance DM (8)	Distance Ref. (9)	$E(B-V)$ (mag) (10)	Morphological Type (11)	T (12)	Spectral Type (13)
WLM	00 01 58.2	−15 27 39.3	11.5	4.0	4	0.98	24.96	2	0.04	IB(s)m	10.0 ± 0.3	
NGC 7808	00 03 32.1	−10 44 40.8	1.3	1.3	...	124	35.48	1	0.04	(R′)SA0*0*:	−2.0 ± 1.2	Sy1?
UGC 00017	00 03 43.3	+15 13 06.0	2.5	1.7	160	13	30.62	1	0.05	Sm:	9.3 ± 0.6	
PGC 00282	00 04 01.5	−11 10 27.3	1.1	0.9	0	161	36.04	1	0.04	SB(rs)c:	5.0 ± 1.0	
NGC 0024	00 09 56.5	−24 57 47.3	5.8	1.3	46	8.2	29.57	3	0.02	SA(s)c	5.0 ± 0.3	
UGC 00128	00 13 50.9	+35 59 39.0	2.1	1.7	65	67	34.13	1	0.06	Sdm	8.0 ± 0.7	
NGC 0055	00 14 53.6	−39 11 47.9	32.4	5.6	108	2.0	26.51	4	0.01	SB(s)m: sp	9.0 ± 0.7	
Arp 256 NED 02	00 18 50.1	−10 21 41.8	1.1	0.8	0	116	35.32	1	0.04	SB(s)c pec	4.5 ± 0.6	H II
Arp 256 NED 01	00 18 50.9	−10 22 36.6	1.1	0.6	0	115	35.30	1	0.04	SB(s)b pec?	3.0 ± 1.3	H II
UGC 00226	00 23 48.2	+14 41 02.8	1.1	0.6	4	77	34.43	1	0.06	Sb	...	

Notes.—Col. (1): Galaxy name. Cols. (2)–(3): R.A. and decl. (J2000.0) of the galaxy center. Units of right ascension are hours, minutes, and seconds, and units of declination are degrees, arcminutes, and arcseconds. Col. (4): Major-axis diameter of the D25 ellipse. Col. (5): Minor-axis diameter of the D25 ellipse. Col. (6): Position angle (P.A.) of the D25 ellipse. In those cases where the D25 ellipse is approximately circular the P.A. is undefined. Col. (7): Distance to the galaxy in Mpc. Col. (8): Distance modulus. Col. (9): Reference from which the distance to the galaxy was taken (see below). Col. (10): Galactic color excess from Schlegel et al. (1998). Col. (11): Morphological type from NED. Col. (12): Morphological type T from RC3 when available. Col. (13): Spectral type from NED. Table 1 is available in its entirety in the electronic edition of the *Astrophysical Journal Supplement*. A portion is shown here for guidance regarding its form and content.

References.—References for determining the distances: (1) from the Virgo-infall–corrected radial velocity adopting $H_0 = 70$ km s^{-1} Mpc^{-1}; (2) Rejkuba et al. 2000; (3) Kennicutt et al. 2003; (4) Van de Steene et al. 2004; (5) van den Bergh 2000; (6) Freedman & Madore 1990; (7) LEDA's Tully-Fisher relationship value; (8) Karachentsev et al. 2003a; (9) Freedman et al. 2001; (10) Tikhonov & Galazutdinova 2002; (11) Freedman, Wilson, & Madore 1991; (12) Tully 1988; (13) assumed to be at the same distance as IC 0159; (14) Gallart et al. 2004; (15) Tonry et al. 2001; (16) Silbermann et al. 1996; (17) assumed to be at the same distance as NGC 1023; (18) Bland-Hawthorn et al. 1997; (19) Bottinelli et al. 1984; (20) Karachentsev et al. 1996; (21) Madore et al. 1998 (Fornax cluster); (22) Perrett et al. 1997; (23) assumed to be at the same distance as NGC 1512; (24) assumed to be at the same distance as NGC 1553 (Dorado group); (25) Jensen et al. 2003; (26) Makarova & Karachentsev 2003; (27) Tosi et al. 2001; (28) Tolstoy et al. 1995; (29) assumed to be in the NGC 2442 group; (30) Sersic & Donzelli 1993; (31) Davidge 2003; (32) Sharina, Karachentsev, & Tikhonov 1999; (33) Gil de Paz et al. 2000b; (34) Karachentsev et al. 2002; (35) Gil de Paz et al. 2003; (36) Macri et al. 2001; (37) Karachentsev et al. 2003b; (38) Drozdovsky & Karachentsev 2000; (39) Östlin 2000; (40) Freedman et al. 1994; (41) Sakai & Madore 1999; (42) assumed to be at the same distance as M81; (43) Paturel et al. 2002; (44) assumed to be at the same distance as NGC 3109; (45) assumed to be at the same distance as NGC 3190; (46) Verdes-Montenegro et al. 2000; (47) Schulte-Ladbeck et al. 1999; (48) GOLDMINE database (Gavazzi et al. 2003); (49) assumed to be at the same distance of NGC 3923; (50) assumed to be at the same distance as NGC 3923; (51) using the average of NGC 4038/NGC 4039; (52) Gavazzi et al. 1999 (Virgo M); (53) GOLDMINE database (Gavazzi et al. 2003) (Virgo Bckg); (54) Gavazzi et al. 1999 (Virgo N); (55) Karachentsev et al. 2004; (56) assumed to be at the same distance as M106; (57) Herrnstein et al. 1999; (58) assumed to be at the same distance as NGC 4278; (59) Gavazzi et al. 1999 (Virgo S+E); (60) Gavazzi et al. 1999 (Virgo A); (61) Karachentsev & Drozdovsky 1998; (62) GOLDMINE database (Gavazzi et al. 2003) (Virgo A); (63) assumed to be at the same distance as NGC 4490; (64) assumed to be at the same distance as NGC 4625; (65) assumed to be at the same distance as NGC 4631; (66) Makarova et al. 1998; (67) assumed to be at the same distance as NGC 5055; (68) Rejkuba 2004; (69) assumed to be at the same distance as NGC 5169; (70) Feldmeier et al. 1997; (71) assumed to be at the same distance as M51a; (72) Thim et al. 2003; (73) Kelson et al. 1996; (74) assumed to be at the same distance as NGC 5713/NGC 5719; (75) using the average of NGC 5713/NGC 5719; (76) assumed to be at the same distance as NGC 6340; (77) assumed to be at the same distance as NGC 7496; (78) assumed to be at the same distance as NGC 7552; (79) assumed to be at the same distance as NGC 0300.

galaxies and those objects with no published redshift (21) we ended up with a total of 1034 galaxies; 893 of them having both FUV and NUV high-quality observations.

2.2. *Positions, Sizes, Morphological Types, and Distances*

In Table 1 we give some basic parameters for the galaxies included in this Atlas, including their positions, sizes, distances, Galactic color excesses [$E(B-V)$], and morphological and spectroscopic types.

The coordinates shown (cols. [2] and [3]) correspond to those given by NED, which are known to be more accurate than those in RC3 from which a significant fraction of these galaxies were selected (H. G. Corwin 2005, private communication). A few objects (29) had NED coordinates that were clearly offset from the position of the galaxy both in the UV and the DSS images. In these cases, the new, correct positions were determined by eye after inspecting the corresponding UV images and Table 1 corrected accordingly. Finally, for two of the objects in the Atlas (UGC 08650 and UGC 11859) a missing/incomplete World Coordinate System (WCS) solution was recomputed using the positions of nearby stars in the USNO-B catalog (Monet et al. 2003). Sizes are the major (col. [4]) and minor (col. [5]) axis diameters at the B-band 25 mag arcsec^{-2} isophote (computed from the corresponding D25 and R25 values in RC3). For those few objects in our sample not included in RC3 we used the major and minor axis diameters available in NED. Position angles (PA; col. [6]) missing or incorrect in RC3 were determined by eye for a total of 90 of the galaxies in the sample after inspecting the corresponding UV images. Note that the PA is undefined in those galaxies for which the D25 isophote is approximately circular according to RC3.

The distances (cols. [7]–[9]) to objects with heliocentric recession velocities larger than 500 km s^{-1} were determined using a Virgo-infall–corrected radial velocity and a Hubble constant of 70 km s^{-1} Mpc^{-1}. The correction from heliocentric to Virgo-infall–corrected velocity was performed in the same way as in the LEDA database (see also Yahil et al. 1977; Theureau et al. 1998; Sandage & Tammann 1990). The distances to a total of 801 galaxies were computed in this way. Galaxies with radial velocities less than 500 km s^{-1} had distances computed from a variety of methods, including (in approximate order of preference) the period-luminosity (PL) relation of Cepheids, measurement of the I-band magnitude of the tip of the red giant branch (TRGB), the proper motion of masers, surface brightness fluctuations (SBFs), the globular cluster luminosity function, the Tully-Fisher relationship, or the brightest stars method (see Table 1 for

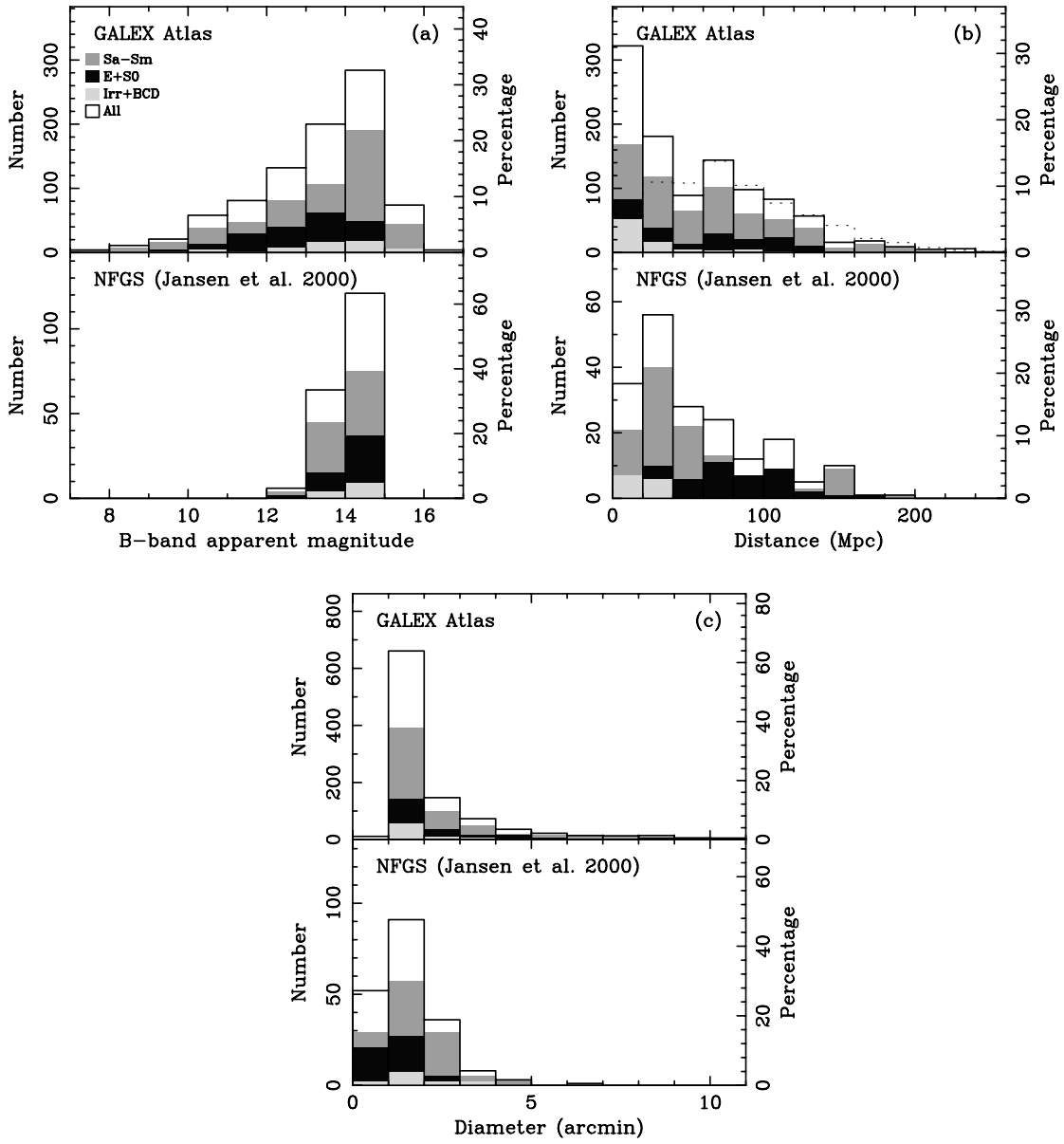

FIG. 1.—Comparison of the *GALEX* Atlas sample and the Nearby Field Galaxy Survey (NFGS) of Jansen et al. (2000). Galaxies classified as ellipticals/lenticulars are shown in dark gray, spiral galaxies in gray, and irregulars and blue compact dwarf (BCD) galaxies in light gray. The outlined solid-line histogram represents the distribution for all galaxies. (*a*) Distribution in *B*-band apparent magnitude. Note that the sharp cutoff in magnitude for the NFGS is due to the fact that this survey was extracted from the magnitude-limited CfA survey sample (Huchra et al. 1983). (*b*) Distribution of distances in Mpc (see § 2.2 for a detailed description of how the distances to galaxies in the *GALEX* Atlas were determined). The dashed-line histogram represents the distribution of 10,663 galaxies with measured redshifts in RC3. (*c*) Distribution of major-axis diameters in arcmin. Note that the size limit for the serendipitous part of the *GALEX* Atlas was set to $1'$.

individual references on each galaxy). For some galaxies believed to be members of interacting pairs, groups, or clusters we adopted the distance to the corresponding pair, group, or cluster. Examples of this are NGC 1510 and NGC 1512, and NGC 5713 and NGC 5719 as members of interacting pairs; NGC 1546, NGC 1549, and NGC 1553 as part of the Dorado group; ESO 059-G007 and ESO 059-G010 as likely members of the NGC 2442 group; NGC 1316, NGC 1317, NGC 1381, NGC 1387, NGC 1399, etc., all members of the Fornax Cluster. For a total of 104 galaxies in the Virgo Cluster area the distances were either derived by adopting a three-dimensional structure of the Virgo Cluster and subdivision into clouds, very similar to that of Gavazzi et al. (1999), or directly from the GOLDMINE database (Gavazzi et al. 2003). In the case of the SINGS galaxies we adopted the distances given by Kennicutt et al. (2003).

Galactic color excesses $E(B-V)$ (col. [10]) are those available through NED, which correspond to those given by Schlegel et al. (1998).

Regarding the morphological types (cols. [11] and [12]), we have adopted those given in RC3. Galaxies were broadly binned as elliptical/lenticular galaxies when their morphological type, T, was less than -0.5, spirals if T was between -0.5 and 9.5, and irregulars when T exceeded 9.5 (RC3). For the blue compact dwarf galaxies NGC 1705, NGC 2537, NGC 3125, NGC 4344, and NGC 4861 (see Gil de Paz et al. 2003, Gil de Paz & Madore 2005), originally classified in RC3 as ellipticals or spirals, we changed their morphological type to compact irregulars ($T = 11$). Regarding the morphological classification of mergers we should mention that depending on (1) the stage of evolution of the particular merger, (2) distance and resolution of the images from which the

TABLE 2
GALEX Observations

Object Name (1)	Date Observed (2)	Exp. (s) (3)	Tile (4)	FUV Sky Background Mean (counts s^{-1}) (5)	FUV Sky Background $\langle\sigma\rangle$ (counts s^{-1}) (6)	FUV Sky Background σ(Mean) (counts s^{-1}) (7)	NUV Sky Background Mean (counts s^{-1}) (8)	NUV Sky Background $\langle\sigma\rangle$ (counts s^{-1}) (9)	NUV Sky Background σ(Mean) (counts s^{-1}) (10)	Notes (11)
WLM	2003 Oct 23	1442	NGA_WLM	2.657E−04	4.595E−04	1.133E−05	2.968E−03	1.681E−03	8.973E−06	
NGC 7808	2003 Sep 17	592	MISDR1_29571_0650	2.403E−04	6.984E−04	3.168E−05	3.119E−03	2.688E−03	1.062E−05	
UGC 00017	2004 Aug 26	1705	MISDR2_28657_0750	4.114E−04	4.988E−04	1.217E−05	3.018E−03	1.500E−03	9.886E−06	(1)
PGC 00282	2003 Sep 17	592	MISDR1_29571_0650	2.228E−04	7.111E−04	2.995E−06	3.116E−03	2.730E−03	1.126E−04	
NGC 0024	2003 Sep 16	1602	NGA_NGC 0024	2.434E−04	4.232E−04	3.274E−05	2.789E−03	1.537E−03	8.181E−05	
UGC 00128	2003 Sep 09	1405	NGA_UGC 0128	5.992E−04	8.596E−04	1.123E−05	3.526E−03	1.794E−03	4.927E−05	
NGC 0055	2003 Sep 14	1511	NGA_NGC 0055	2.564E−04	4.457E−04	5.672E−05	2.503E−03	1.512E−03	1.213E−04	
Arp 256 NED 02	2003 Sep 19	1429	MISDR1_29523_0652	2.269E−04	4.122E−04	7.915E−06	3.016E−03	1.627E−03	2.816E−06	
Arp 256 NED 01	2003 Sep 19	1429	MISDR1_29523_0652	2.272E−04	4.123E−04	1.762E−06	3.011E−03	1.627E−03	8.552E−06	
UGC 00226	2003 Aug 29	3537	MISDR1_28652_0417	5.036E−04	4.411E−04	7.978E−06	3.283E−03	1.148E−03	6.477E−05	

Notes.—Col. (1): Galaxy name. Col. (2): Date the galaxy was observed. Col. (3): Total exposure time in seconds for each of the *GALEX* bands. Col. (4): Tile name assigned by the *GALEX* mission. It includes the name of the survey as part of which the galaxy was observed and the name of the targeted field. Col. (5): Mean sky background of the FUV image (in counts per second). Col. (6): Mean standard deviation of the sky in the FUV image measured by averaging the standard deviation within several regions around the position of the object. Col. (7): Standard deviation of the mean values of the sky measured in these regions. Cols. (8)–(10): The same for the NUV image. Col. (11): Notes for individual objects: (1) Nominal galaxy position angle changed; (2) nominal galaxy coordinates changed; (3) special pipeline processing; (4) NUV-only; (5) very shallow FUV image; (6) very bright star near or on top of the galaxy; (7) nominal galaxy size changed; (8) crowded field, uncertain photometry. Table 2 is available in its entirety in the electronic edition of the *Astrophysical Journal Supplement*. A portion is shown here for guidance regarding its form and content.

system was classified, and (3) the criterion of the person classifying the object, mergers might appear classified as (1) two galaxies each with its own morphological type (e.g., NGC 4038/4039), (2) one single peculiar (NGC 0520) or even spiral (NGC 6052) object, or (3) they might lack any morphological classification (Mrk 8). Finally, spectroscopic types (col. [13]) were taken from NED.

In Figure 1*a* (*top*) we show the distribution of galaxies in the Atlas as a function of the *B*-band apparent magnitude for different morphological types (*dark gray histogram for ellipticals, gray for spirals, light gray for irregulars*) and for the total sample (*solid-lined histogram*). Figure 1*b* (*top*) shows the distribution of distances. The shape of this latter distribution appears to be the result of combining the RC3 redshift distribution (*dashed-line histogram*) with a large number of very nearby galaxies with distances closer than 50 Mpc included in this Atlas as part of NGS. It is worth noting here that because our sample is effectively limited in magnitude and (to a lesser extent) in diameter we might be missing a fraction of faint, low-luminosity, low surface brightness galaxies compared with what we would find in a volume-limited sample of the local universe. In this sense, objects such as the Antlia Dwarf or the dwarf spheroidal satellites around the Milky Way might be common in the field, but they would certainly be underrepresented in either a magnitude-limited or a diameter-limited sample. This limitation should be kept in mind when comparing our results with those obtained from the analysis of a volume-limited sample, such as the 11 HUGS sample (Funes et al. 2007) or the Virgo-cluster sample analyzed by Boselli et al. (2005).

3. *GALEX* OBSERVATIONS

GALEX is a NASA small explorer class mission that orbits the Earth at an altitude of approximately 700 km. The single instrument on board consists of a 50 cm aperture Ritchey-Chrétien telescope equipped with a dichroic beam splitter that allows simultaneous observation in two separate bands, FUV and NUV, within a circular field of view of 1.2° in diameter. The dichroic also acts as a field-aberration corrector. The UV light is detected using microchannel plates with crossed delay-line anodes. The effective wavelength of the two *GALEX* bands are 1516 and 2267 Å, and their full widths at half-maximum are 269 and 616 Å, respectively, for the FUV and NUV channels. The observations are carried out only at night-time with a typical total usable time per orbit of ∼1700 s. For a more detailed description of the spacecraft and the instrument the reader is referred to Martin et al. (2005) and Morrissey et al. (2005).

The observations for this Atlas were carried out by the *GALEX* satellite between 2003 June 7 and 2005 April 29. The typical exposure time per field was one orbit (specific exposure times are given in Table 2). During periods of intense solar activity, including the historical solar storm occurred on 2003 October–November, or during sporadic overcurrent events the FUV detector was turned off to avoid any damage of the electronics. Although in some occasions the NUV detector had also to be turned off, in most cases the scheduled observations were still carried out through the NUV channel. Due to this, a total of 141 galaxies in this Atlas (14% of the sample) were observed only in the NUV band. These galaxies are identified as NUV-only in Table 2. Nineteen galaxies were found to be too faint in our FUV imaging data and were analyzed as NUV-only targets as well. Table 2 also provides information regarding the FUV and NUV background for each of the fields along with the mean standard deviation of the sky and the standard deviation of the mean value of the sky across different regions in the field (see § 4.2 for details).

Using the *GALEX* pipeline the photon lists generated by the detectors for each of the bands were processed to produce the corresponding intensity maps in counts per second. The final output products of the pipeline also include a high-resolution response map, which is the product of the effective exposure time by the flat field at a given position and that was used to estimate the photon noise in our images. Note that the images taken as part of the mosaics of M31 and of the center of the Virgo cluster were generated using a slightly modified version of the pipeline that, nevertheless, preserve both the image quality and absolute flux calibration generated by the standard *GALEX* pipeline.

The point spread function (PSF) of the images was found to vary as a function of the count rate with bright point sources usually leading to a wider PSF than faint sources and as a function of the position of the image. For the average count rates usually

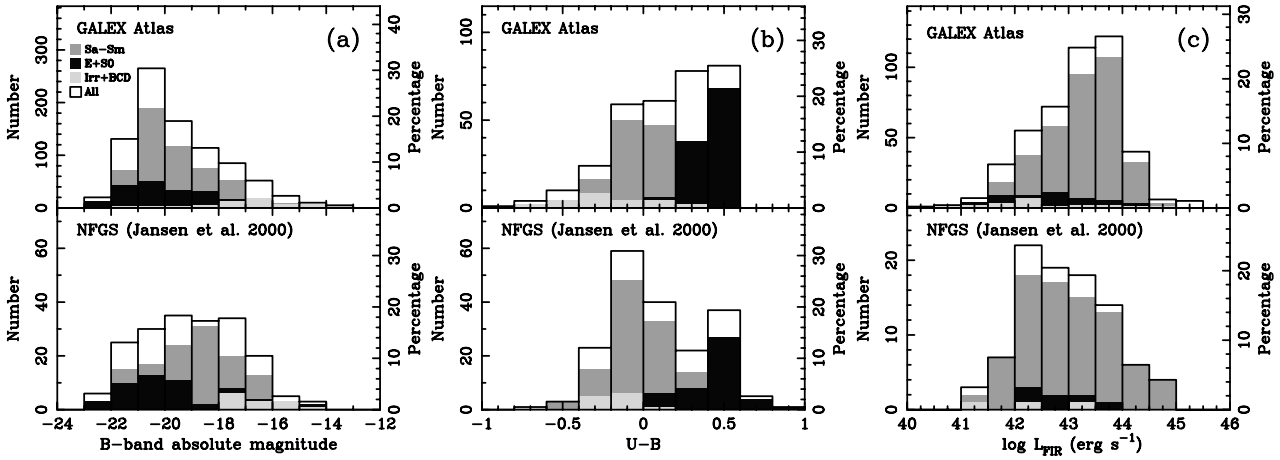

FIG. 2.—Comparison of the properties of the *GALEX* Atlas sample and the NFGS. Color coding is as in Fig. 1. (*a*) *B*-band absolute magnitude. Note that the *GALEX* Atlas sample covers the full range of properties of the galaxies in the local universe as described by the magnitude-limited NFGS sample. The distribution is quite similar in the case of elliptical/lenticular and irregular galaxies with only a moderate excess of intrinsically bright spirals in the case of the *GALEX* Atlas sample compared with field galaxies. It is worth noting that there are still almost 3 times more low-luminosity spiral galaxies in the *GALEX* Atlas than in the NFGS. The relative fractions of elliptical/spiral/irregular galaxies is also very similar between the *GALEX* Atlas sample and field galaxies (see text for details). (*b*) $U - B$ color. (*c*) FIR luminosity obtained from the *IRAS* 60 and 100 μm fluxes using the recipe of Lonsdale et al. (1985).

obtained from nearby galaxies and for objects located within the central 0.5° of the *GALEX* field, the PSF full width at half-maximum (FWHM) is in the range 4.0″–4.5″ and 5.0″–5.5″, respectively, for the FUV and NUV bands.

3.1. *Comparison with a Magnitude-limited Sample*

Because of the rather arbitrary criteria involved in selecting the objects in this Atlas, a comparison of the properties of these galaxies with the overall population of galaxies in the local universe is in order if the conclusions derived from this work are to be applied beyond the limits of this Atlas. We have therefore compared the distribution of properties of the galaxies in the Atlas with those included in the Nearby Field Galaxy Survey (NFGS) of Jansen et al. (2000). The NFGS is composed of a total of 196 galaxies that were selected as a representative subsample of the magnitude-limited CfA survey (Huchra et al. 1983).

The *B*-band magnitude distributions obtained for both the *GALEX* Atlas and the NFGS (see Fig. 1*a*) are a direct consequence of the limits of the surveys from which they are derived. That is, while the faint end of the distribution for the *GALEX* Atlas is a result of the effective completeness limit of ∼15.5 mag inherent in RC3 (note again that the completeness of RC3 is also limited to objects larger than 1′); galaxies in the NFGS show a sharp cutoff in their apparent magnitudes at the limit of the CfA survey, $B \sim 14.5$ mag.

In Figure 1*b* we compare the distribution of distances of both samples and for the whole RC3. Both distributions are similar, with most of the galaxies found at distances closer than 100 Mpc, with a relatively long tail extending to distances up to 200 Mpc and somewhat beyond. The peak in the NFGS distance distribution is intermediate between the local peak in the Atlas sample associated with NGS and the more distant peak of RC3 (which is slightly deeper in apparent magnitude).

Figure 1*c* shows the comparison between the D25 major-axis diameter of our sample and the NFGS. The major-axis diameters of galaxies in the NFGS were obtained using the UGC catalog major-axis diameters and the morphological-type–dependent transformation coefficients given by Table 6 of RC3. We find that a total of 52 galaxies in the NFGS (∼27%) are smaller than 1′ in D25 major-axis diameter and would be missed by the size limit imposed to the serendipitous part of the Atlas sample. Of these galaxies, approximately half are elliptical/lenticular and half spiral galaxies.

Figure 1 demonstrates that the *GALEX* Atlas and the NFGS, at least in terms of their apparent magnitudes and redshift distributions, are sampling the same volume of the universe and represent a similar population of galaxies. It is therefore fair to now carry out a more detailed comparison between the intrinsic properties of the galaxies in these two samples, including their luminosities, colors, and SFR. At this point it is also worth noting that the relative numbers of ellipticals/spirals/irregulars (22%, 62%, 8%)[10] in the *GALEX* Atlas are similar to those found in the field by the NFGS (28%, 65%, 7%).

In Figure 2*a* we compare the distribution in *B*-band absolute magnitude of both the *GALEX* Atlas and the NFGS samples. The distribution of both ellipticals/lenticulars and irregulars is pretty similar between both samples. However, in the case of the spirals, although the range of properties covered is also similar, we find a moderate excess of intrinsically bright spirals ($-21 < M_B < -20$) and a small paucity of low-luminosity spirals ($-19 < M_B < -18$) compared with the field for the same number of ellipticals/lenticulars and spirals outside these luminosity bins. Note that thanks to the large number of objects in our sample there are still more than twice as many low-luminosity spirals ($M_B > -19$ mag) in this Atlas as in the NFGS sample. Similar behavior is seen when the $(U - B)$ colors of both samples are compared (see Fig. 2*b*). In this case the Atlas sample shows a slight paucity of relatively blue (and probably also faint) spirals. Finally, we use the 60 μm and 100 μm *IRAS* fluxes to compute the FIR luminosity using the recipe of Lonsdale et al. (1985). The comparison of the FIR luminosities derived for each sample shows that they both cover the same range of properties with a comparable distribution except for the slight excess (paucity) of high (low) FIR luminosity spirals in the Atlas sample (see Fig. 2*c*).

The origin of this small difference in the luminosity distribution of our sample and that of the NFGS might due in part to the size limit of 1′ in D25 major-axis diameter imposed to the serendipitous part of the Atlas sample. However, since only 23% of the spirals in the NFGS are smaller than 1′, this effect only

[10] Note that about 9% of the galaxies in the Atlas do not have morphological types available in RC3.

accounts for part of the problem. The other reason for this difference in luminosity is probably intrinsic to the rather heterogeneous selection criteria in the original *GALEX* NGS, which basically includes all galaxies that were in the *Spizter* ROC at the time the *GALEX* surveys were planned. In the *GALEX* NGS we can find targets from many different *Spitzer* programs, which are in many cases biased to large, bright, nearby galaxies with expectedly bright infrared emission (i.e., bright, nearby spirals).

4. ANALYSIS

4.1. *Color Images*

The left panels of Figure Set 3 show false-color RGB maps of the galaxies in our sample. The images used are "asinh" scaling versions (Lupton et al. 2004) of the 2 pixel smoothed FUV image (*blue*), the original NUV image (*red*), and a linear combination of the two (*green*). The coefficients used to obtain the green-channel image are 0.2 and 0.8, respectively, for the smoothed FUV and original NUV images. For those galaxies with NUV-only data we give the asinh-scaled NUV image. Shown in green is the RC3 D25 ellipse, which was originally derived from *B*-band photometry.

In most of the cases (891 galaxies) the maps shown correspond to a region 1.5 times the D25 major axis diameter in size. In those cases where the UV emission is comparatively more extended than the optical light this factor was increased up to 5 times D25 for the most extreme cases. The size of the horizontal tick mark plotted at the bottom of each map corresponds to 2 kpc at the distance of the galaxy, except for the case of the Phoenix Dwarf (ESO 245-G007), where it represents a physical size of 0.2 kpc. For comparison purposes the central panels of Figure Set 3 show DSS-1 images for the same field of view.

4.2. *Surface Brightness and Color Profiles*

Using the central position, ellipticity (derived from the corresponding axial ratio), and position angle of the D25 ellipse given in Table 1, we compute the mean surface brightness within elliptical annuli of fixed center and position angle increasing from $6''$ in major-axis radius to at least 1.5 times the D25 radius. The outermost point where the surface photometry was computed corresponds to the size of the postage stamps shown in Figure Set 3, which in turn depends on the extension of the UV emission for each individual galaxy. In some cases a few of the outermost points had to be removed from the profiles shown in Figure Set 3 because either the mean flux in the isophote was below the level of the sky or the photometry errors were extremely large (see below). Point sources with colors redder than $(\mathrm{FUV} - \mathrm{NUV}) = 1$ were automatically identified as foreground stars and masked in the *GALEX* images. These masks were then visually inspected in order to (1) include blue foreground stars and, in a very few cases, to (2) exclude from this automatically generated mask the nuclei of some galaxies that had been misclassified as foreground stars.

In order to determine the errors in the surface photometry we used the expressions and methodology described in Gil de Paz & Madore (2005). Errors in the inner parts of the profiles are commonly dominated by photon noise, while in the very outer parts the background subtraction uncertainties dominate. It is important to note here that because the background in these images is very low (see Table 2), especially in the FUV channel, the statistics of the background are highly Poissonian, therefore the common estimators, the mean, median, and mode can be very different. In particular, the mode in shallow FUV images can be zero. Thus, since our surface photometry uses the mean as the measure of the flux within each isophote, we consistently use the mean of the sky as a consistent estimate of the background, after all SExtractor-detected sources are carefully masked (Bertin & Arnouts 1996). We further masked all pixels in a 5×5 pixel box around each detected-source pixel so as to avoid possible contamination from the light in the extended wings of the sources.

The background was computed as the mean of the sky value of a total of 90 different regions of 4000 pixels each located around the source and arranged in two concentric elliptical patterns at a distance never closer than 1.5 times the size of the corresponding D25 ellipse. From a comparison of the mean of the standard deviation within each sky region with the standard deviation of the mean of each region we also determine the impact of low-frequency variations in the background (due, for example, to flat-fielding errors) on the total error budget (see Gil de Paz & Madore 2005 for details).

In the right panels of Figure Set 3 we show the FUV and NUV surface-brightness (*bottom*) and $(\mathrm{FUV} - \mathrm{NUV})$ color profiles (*top*) each corrected for Galactic extinction in units of AB magnitudes per square arcsec along with the corresponding 1 σ errors. Here we have adopted the Galactic color excesses given by Schlegel et al. (1998) and the parameterization of the Galactic extinction law given by Cardelli et al. (1989) for a total-to-selective extinction ratio of $R_V = 3.1$. The conversion factors are $A_{\mathrm{FUV}} = 7.9E(B - V)$ and $A_{\mathrm{NUV}} = 8.0E(B - V)$. The FUV surface-brightness profile shown in Figure Set 3 is given in blue, the NUV profile in red, and the $(\mathrm{FUV} - \mathrm{NUV})$ color profile is in green. The profiles are plotted against the equivalent radius $(ab)^{1/2}$ of the corresponding ellipse (expressed both in arcsec and kpc). The white error bar at the top right corner of each diagram represents the ± 1 σ uncertainty on the *GALEX* zero points, which is estimated to be ± 0.15 mag for both the FUV and NUV channels. Note that all panels are scaled to the same range in surface brightness and color. Hereafter when we refer to $(\mathrm{FUV} - \mathrm{NUV})$ it will be the color corrected for Galactic extinction.

In all cases, except the Antlia Dwarf, the outermost point represented in these plots corresponds to the position beyond which either the intensity in the image falls below the level of the sky, or the error in the surface photometry for the NUV band is larger than 0.8 mag, whichever happens first. In the case of the Antlia Dwarf galaxy, we limited the radial range to that where the contamination from a diffuse Galactic cirrus, located near the position of the galaxy, was still found to be negligible.

4.3. *Asymptotic Magnitudes, Colors, and Structural Parameters*

Using the surface brightness profiles derived and the area of each elliptical annulus we obtained the asymptotic magnitudes by extrapolating the growth curve to infinity. We first computed the accumulated flux and the gradient in the accumulated flux (i.e., the slope of the growth curve) at each radius and perform an error-weighted linear fit to the accumulated flux versus slope of the growth curve plot. After an appropriate radial range was chosen we took the value of the *y*-intercept of this fit as the asymptotic magnitude of the galaxy. This technique is described in detail in Cairós et al. (2001). These authors also tested the stability of this method against the choice of radial range used for the fit and verified its reliability by comparing their results with those obtained using alternative extrapolation techniques. Note that obtaining growth curves and deriving the corresponding asymptotic magnitudes of galaxies at UV wavelengths have been already done in the past (see Rifatto et al. 1995).

In Table 3 we give the observed asymptotic and aperture (inside the D25 ellipse) AB magnitudes in both the FUV and NUV bands along with the corresponding computed from the growth

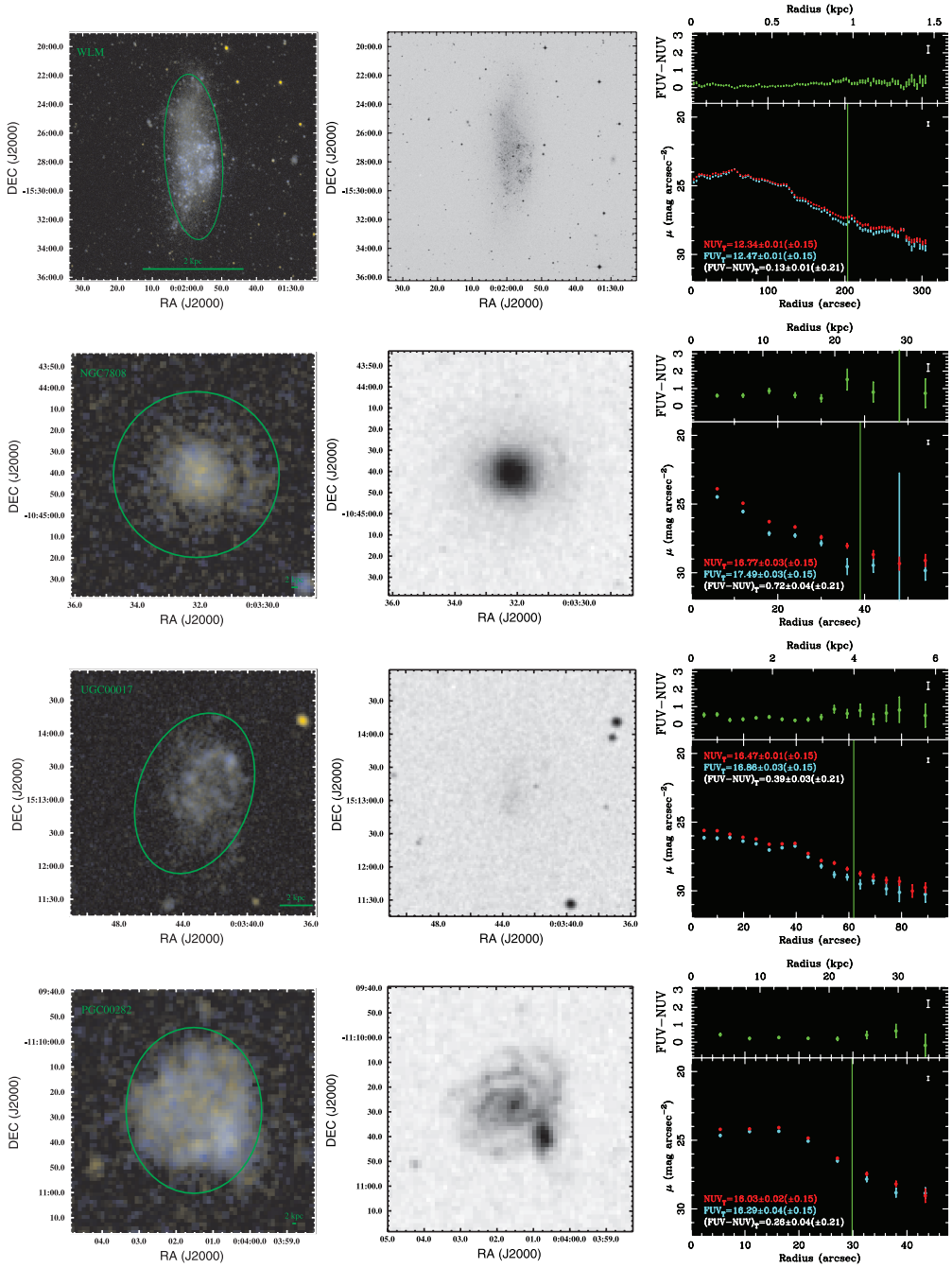

FIG. SET 3.—False-color *GALEX* images (*left*), DSS-1 images (*center*), and surface brightness and color profiles (*right*) of the galaxies in the Atlas (see text for details). All panels are available online at http://nedwww.ipac.caltech.edu/level5/GALEX_Atlas/. [*See the electronic edition of the Supplement for Figs.* 3.1–3.259.]

curve (FUV − NUV) colors. The errors quoted correspond to the error associated with the fit to the growth curve alone. The mean differences obtained between the asymptotic magnitudes and the D25 aperture magnitudes are -0.19 ± 0.20 mag and -0.23 ± 0.20, respectively, for the FUV and NUV, with the asymptotic magnitudes being brighter. The corresponding foreground-extinction–corrected values are given in Table 4. The corrected asymptotic luminosities (in watts) are also provided in this table. Foreground-extinction–corrected asymptotic magnitudes and colors along with their corresponding errors are also shown in one of the corners of the panels on the right of Figure Set 3. In this case the errors are composed of a term derived from the error-weighted fit of the growth curve plus a term (in parentheses) due exclusively to uncertainties in the *GALEX* FUV and NUV zero points (± 0.15 mag).[11]

From the growth curve obtained we also computed the effective radius as the equivalent radius at which the accumulated flux was equal to the asymptotic magnitude plus 0.7526 mag [2.5 log (2)]. In a similar way we derived the radii containing the 20%, 25%, 75%, and 80% of the light (r_{20}, r_{25}, r_{75}, and r_{80},

[11] Note that due to the poor handling of fractional pixels by the IRAF task ELLIPSE additional errors in the asymptotic magnitudes (and to a lesser extent in the colors) might be present. We estimate that this error might be larger than the error quoted in only a very small fraction (<5%) of the sample, either the most concentrated or inclined galaxies.

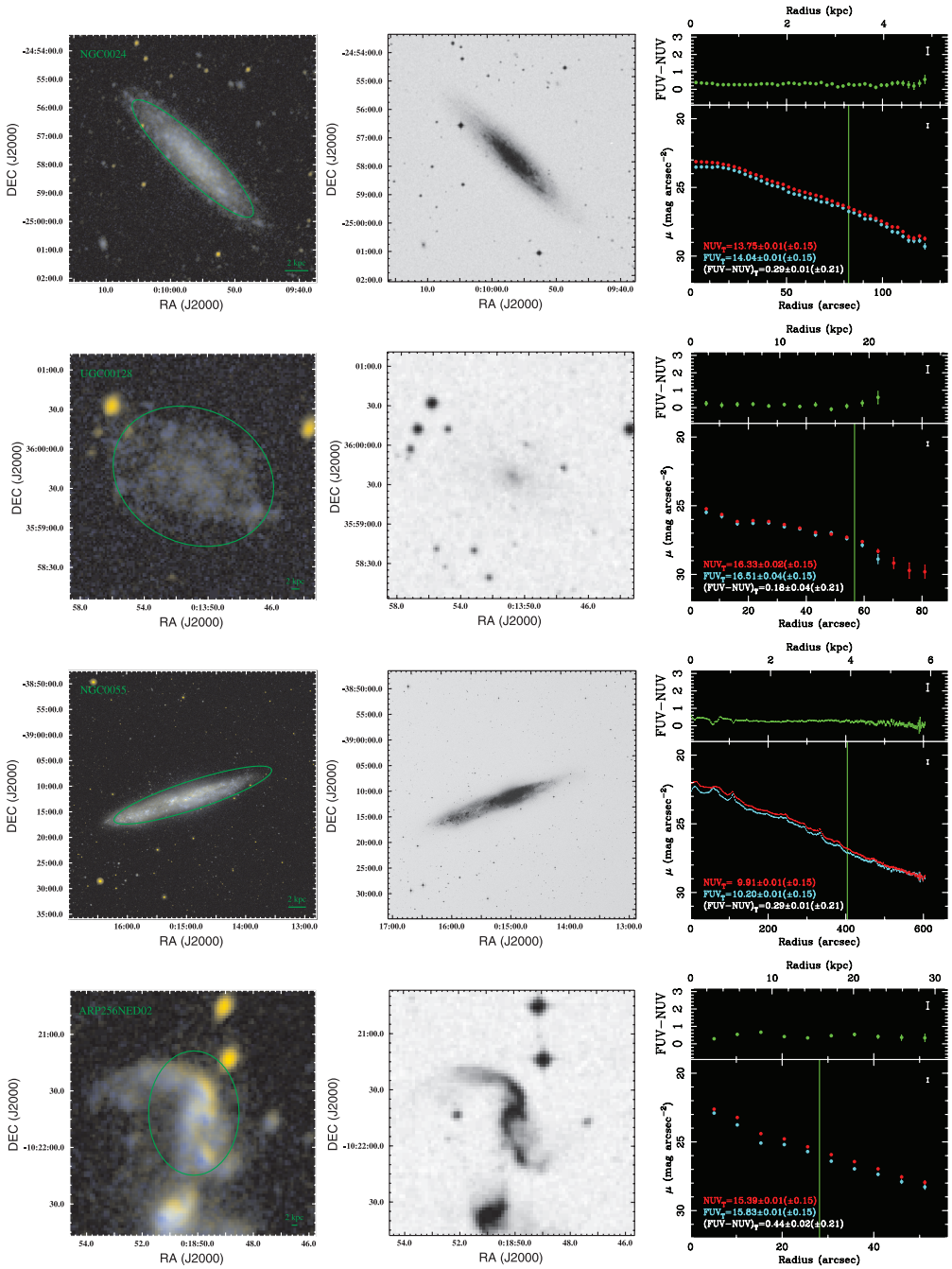

FIG. 3 — *Continued*

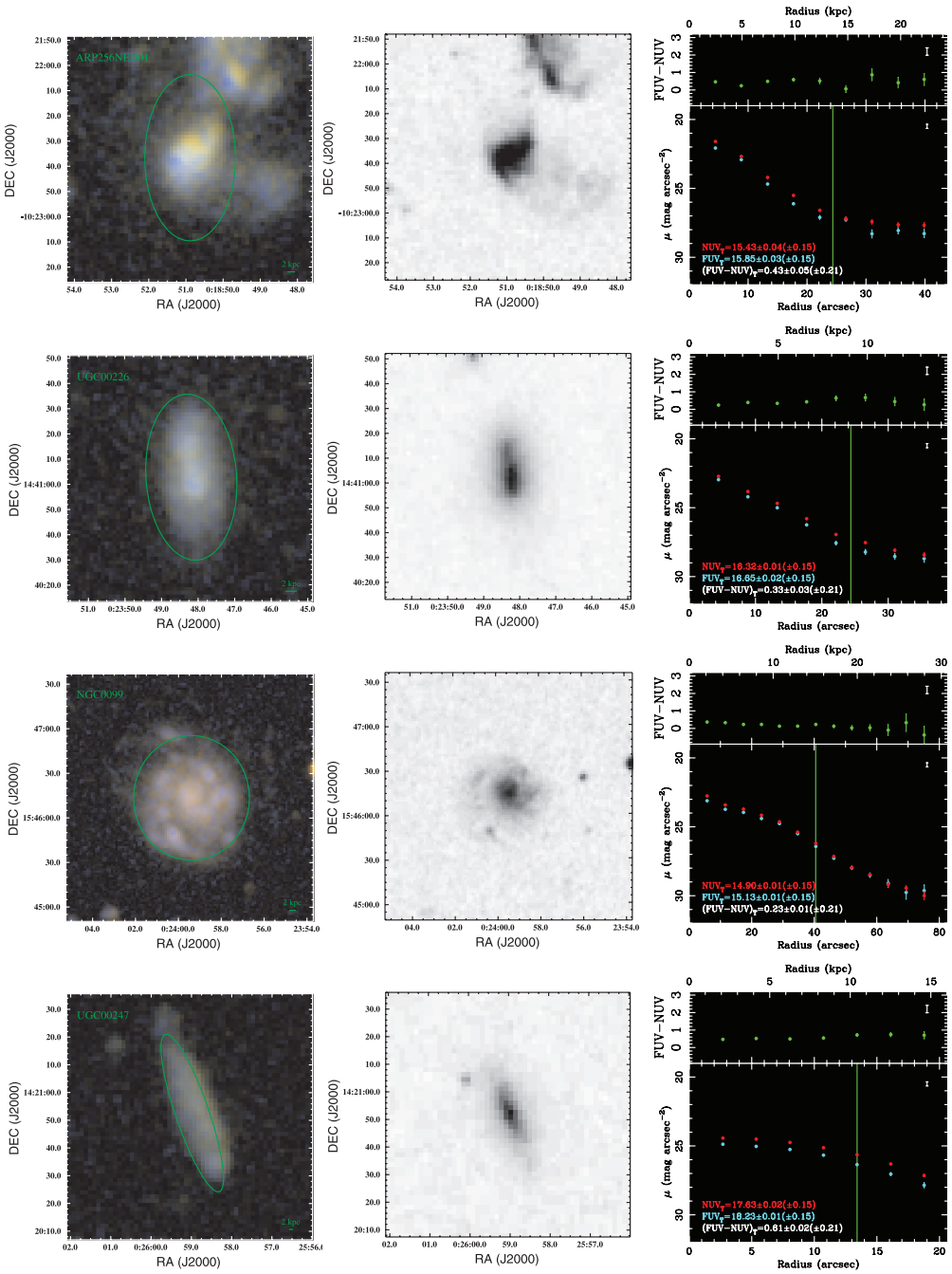

FIG. 3—*Continued*

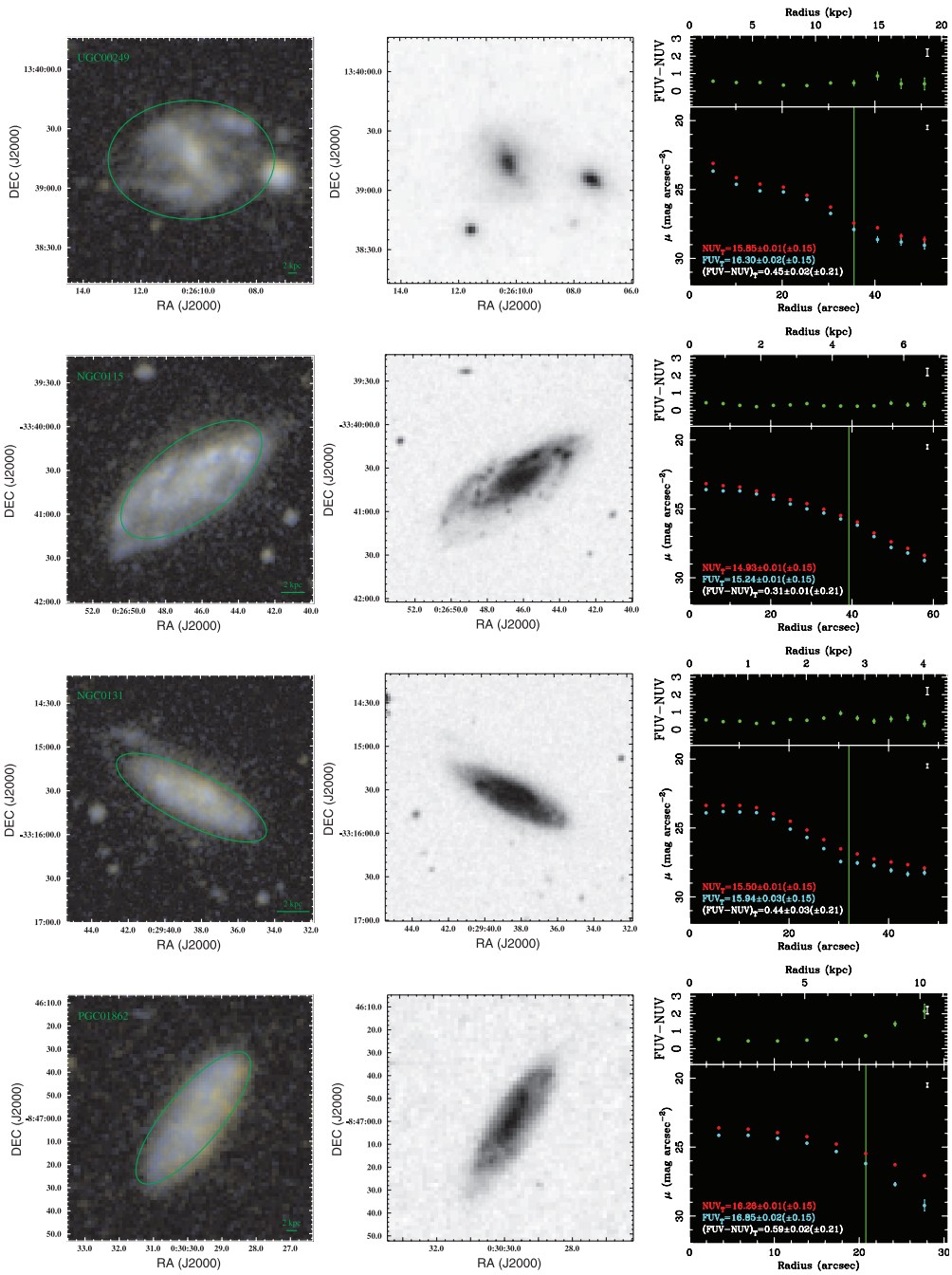

FIG. 3—*Continued*

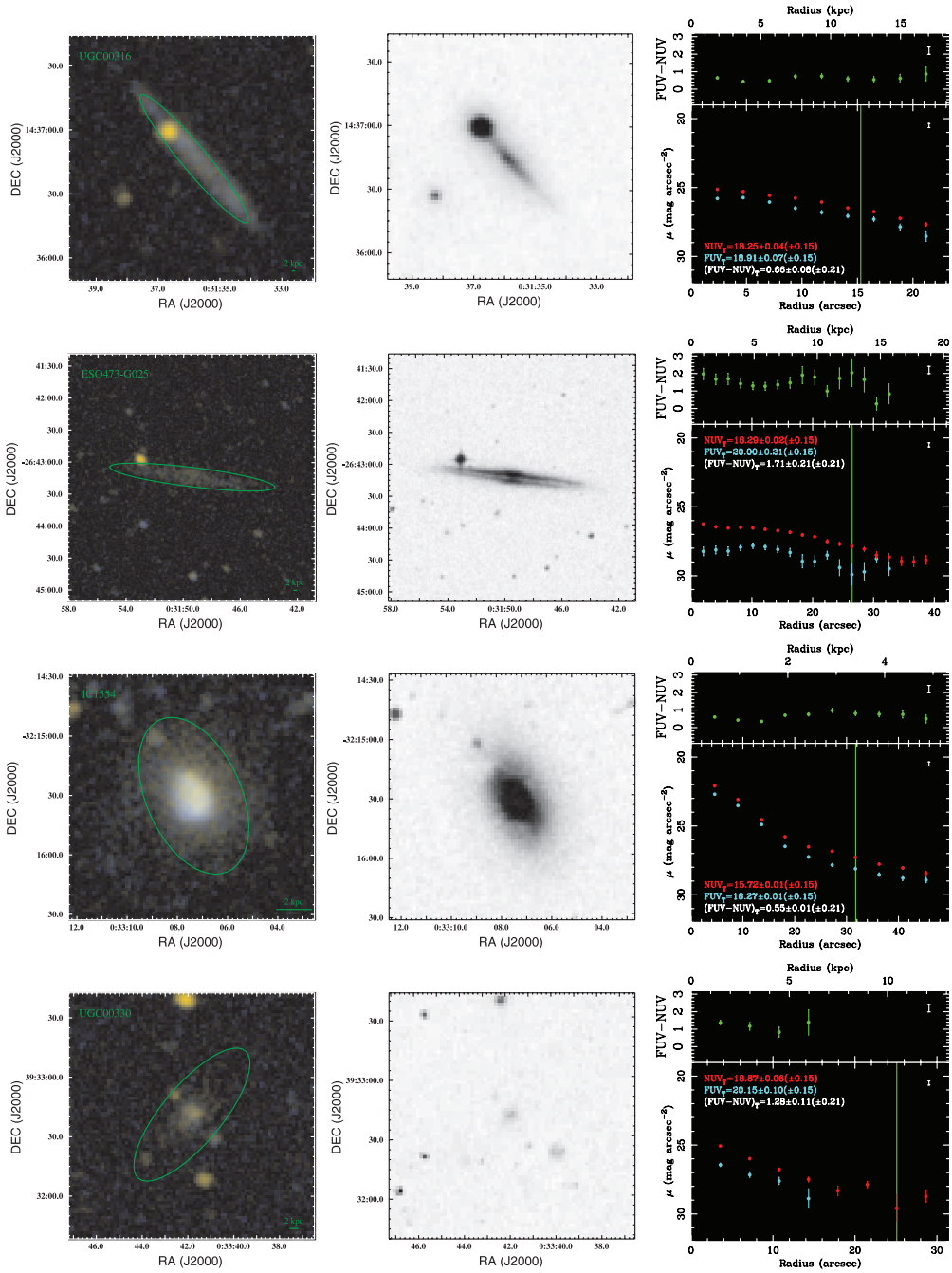

FIG. 3—*Continued*

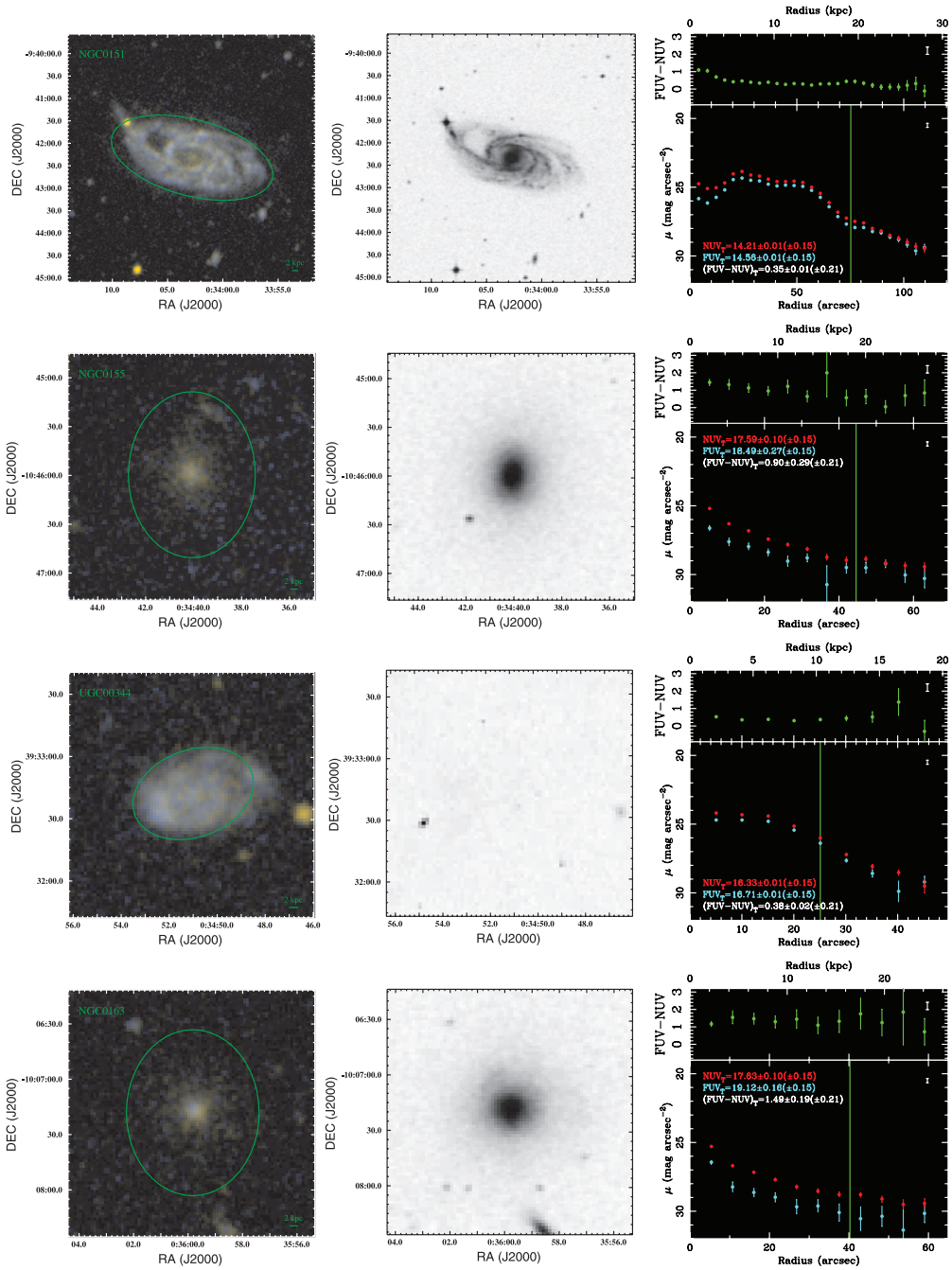

FIG. 3 — *Continued*

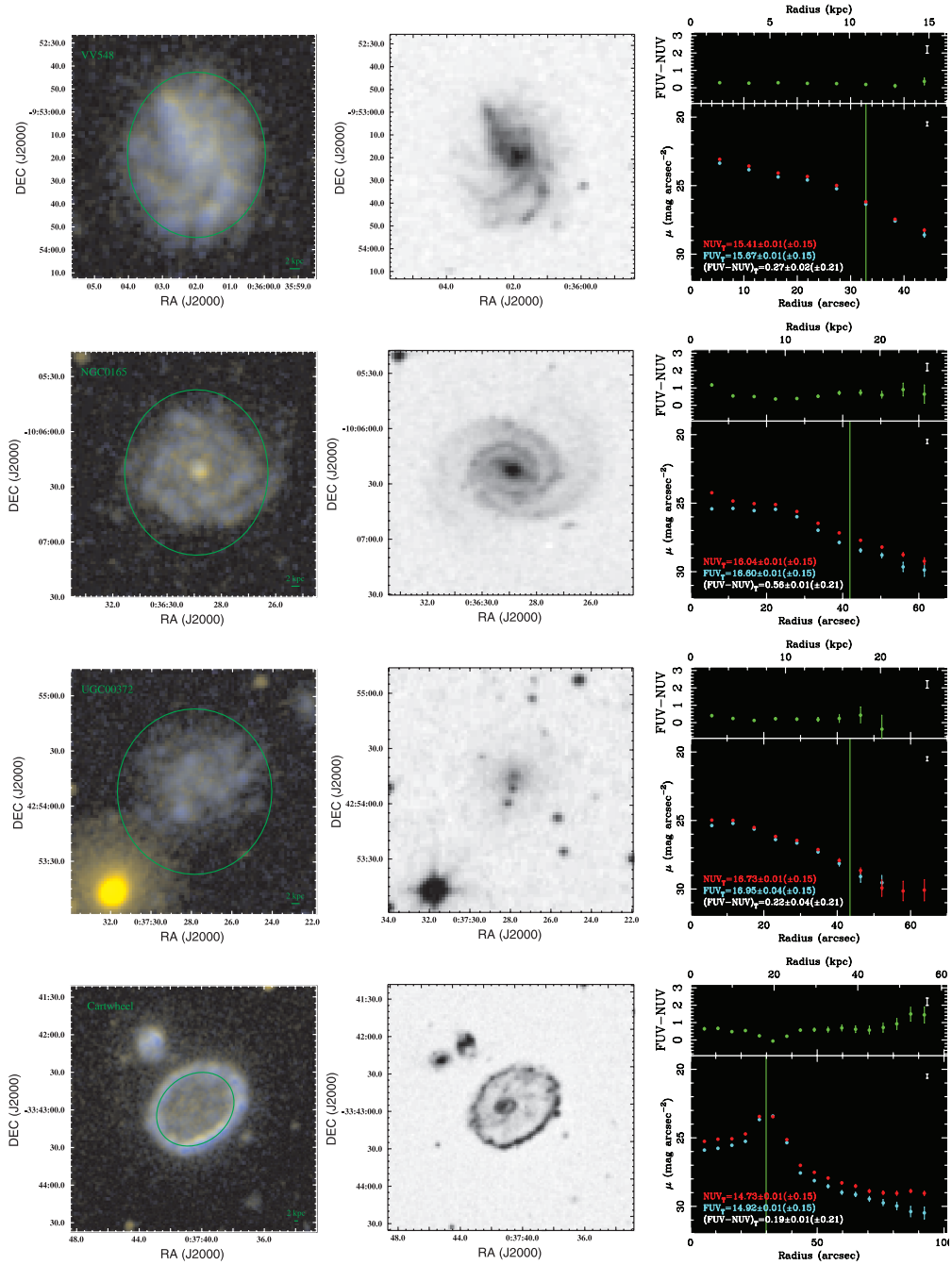

FIG. 3—*Continued*

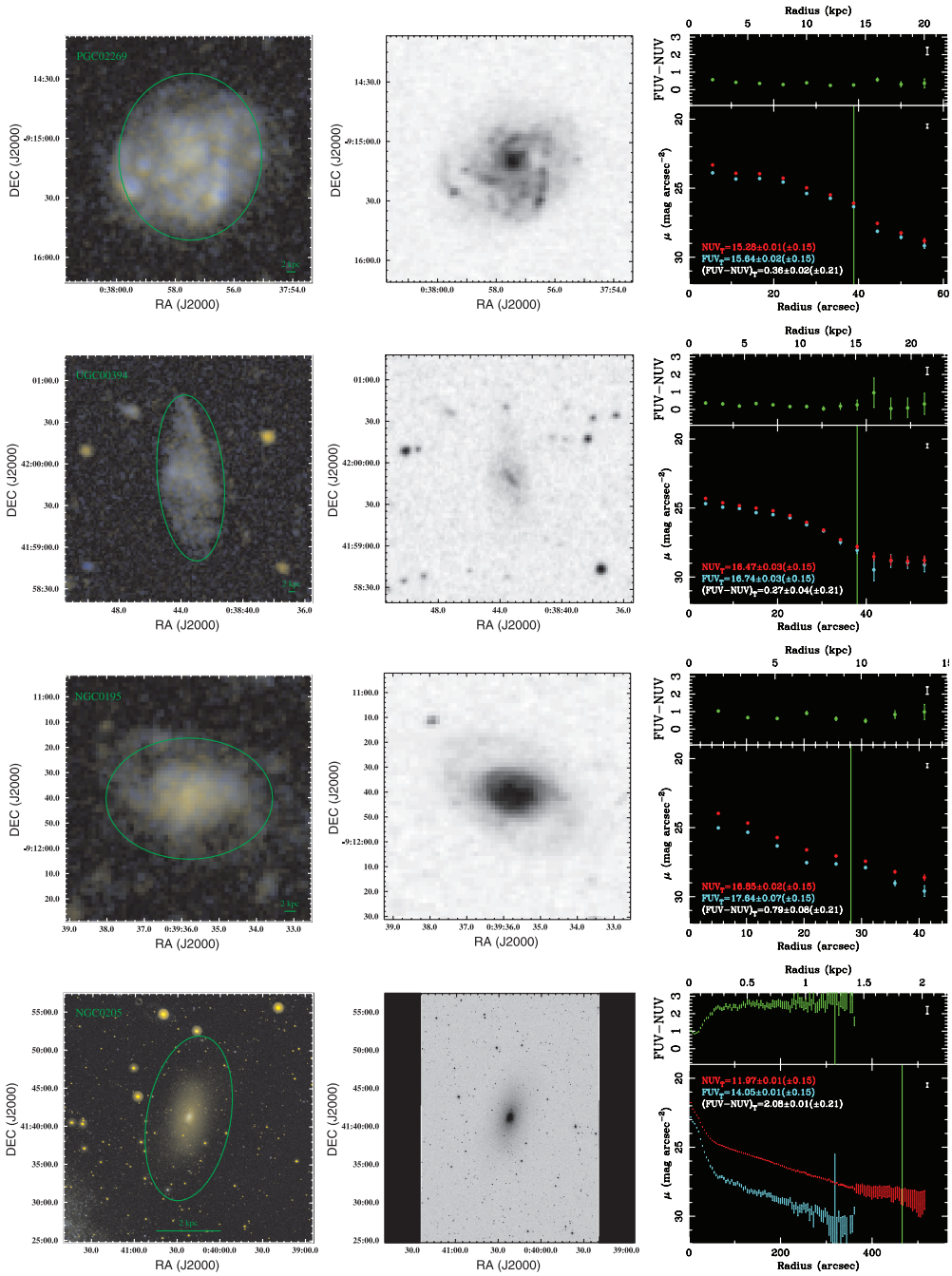

FIG. 3 — *Continued*

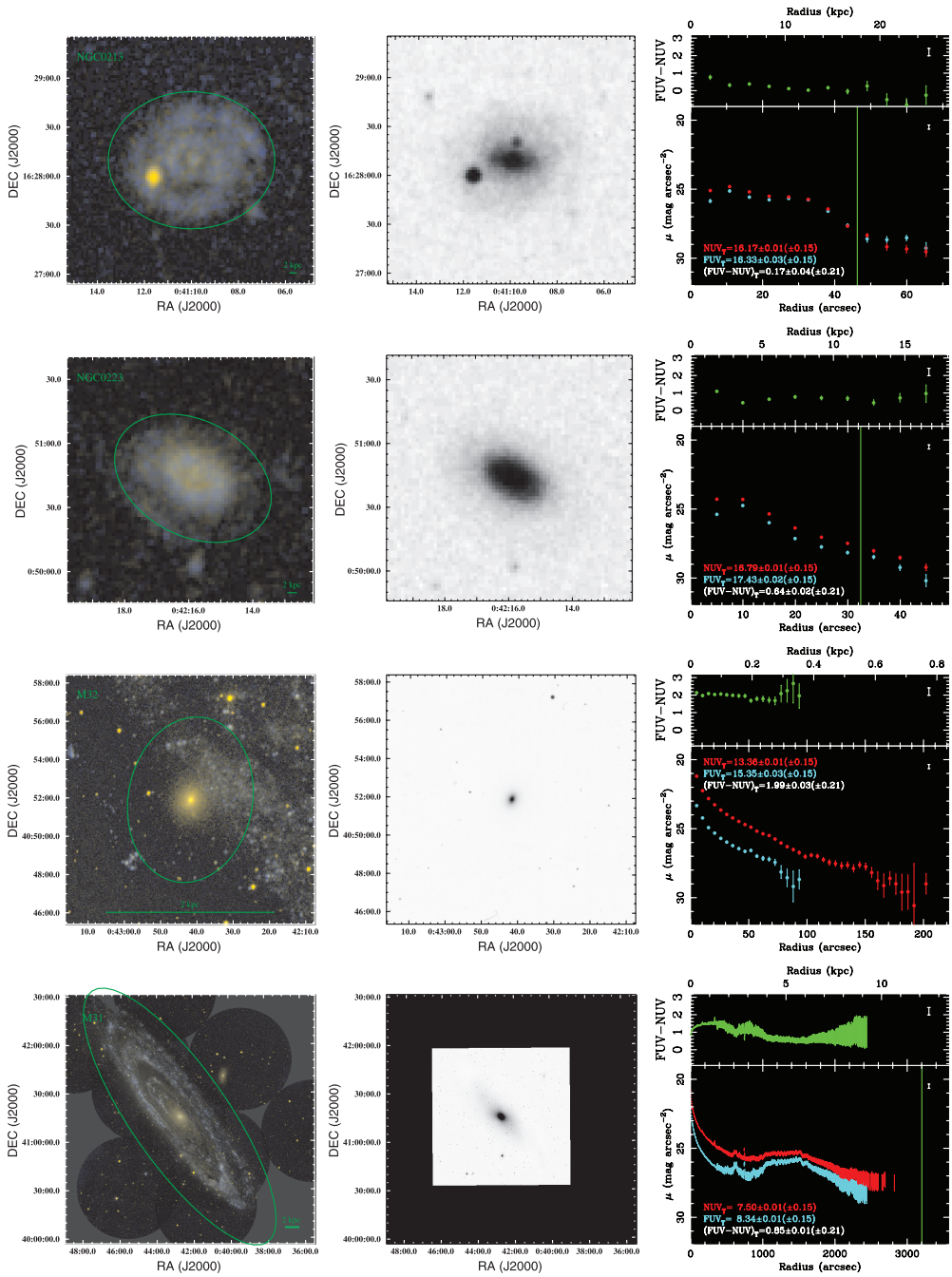

FIG. 3—*Continued*

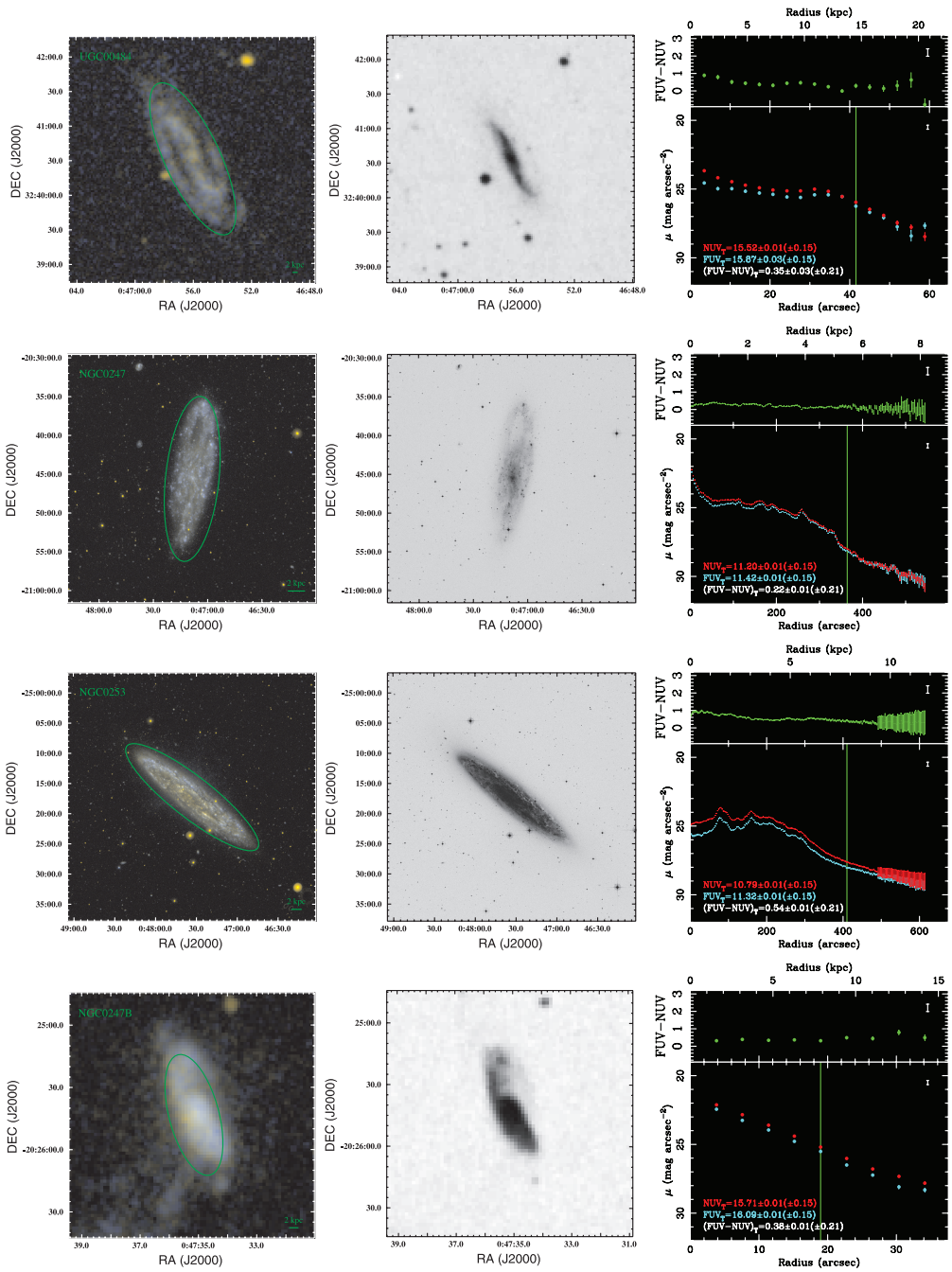

FIG. 3—*Continued*

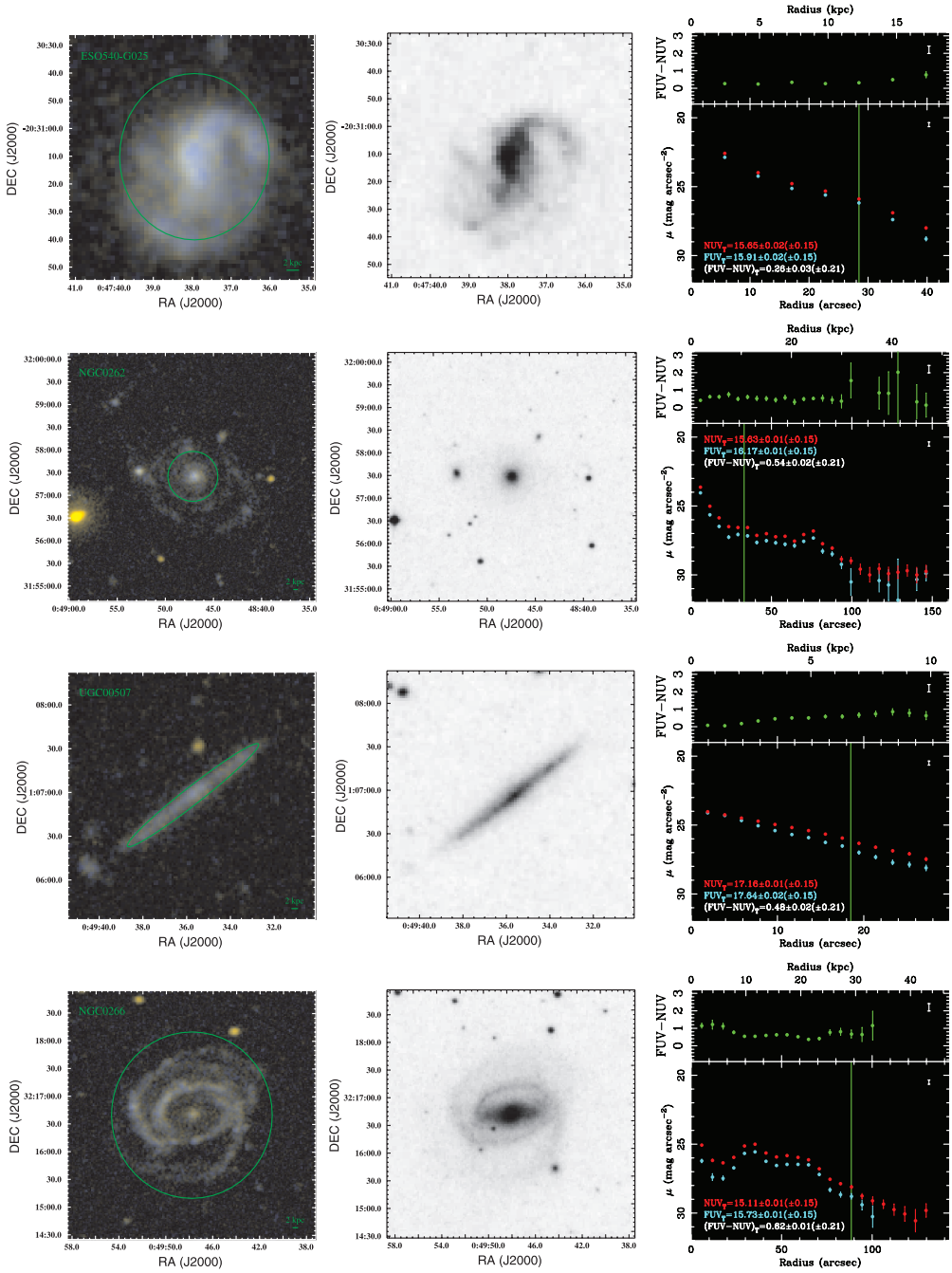

FIG. 3—*Continued*

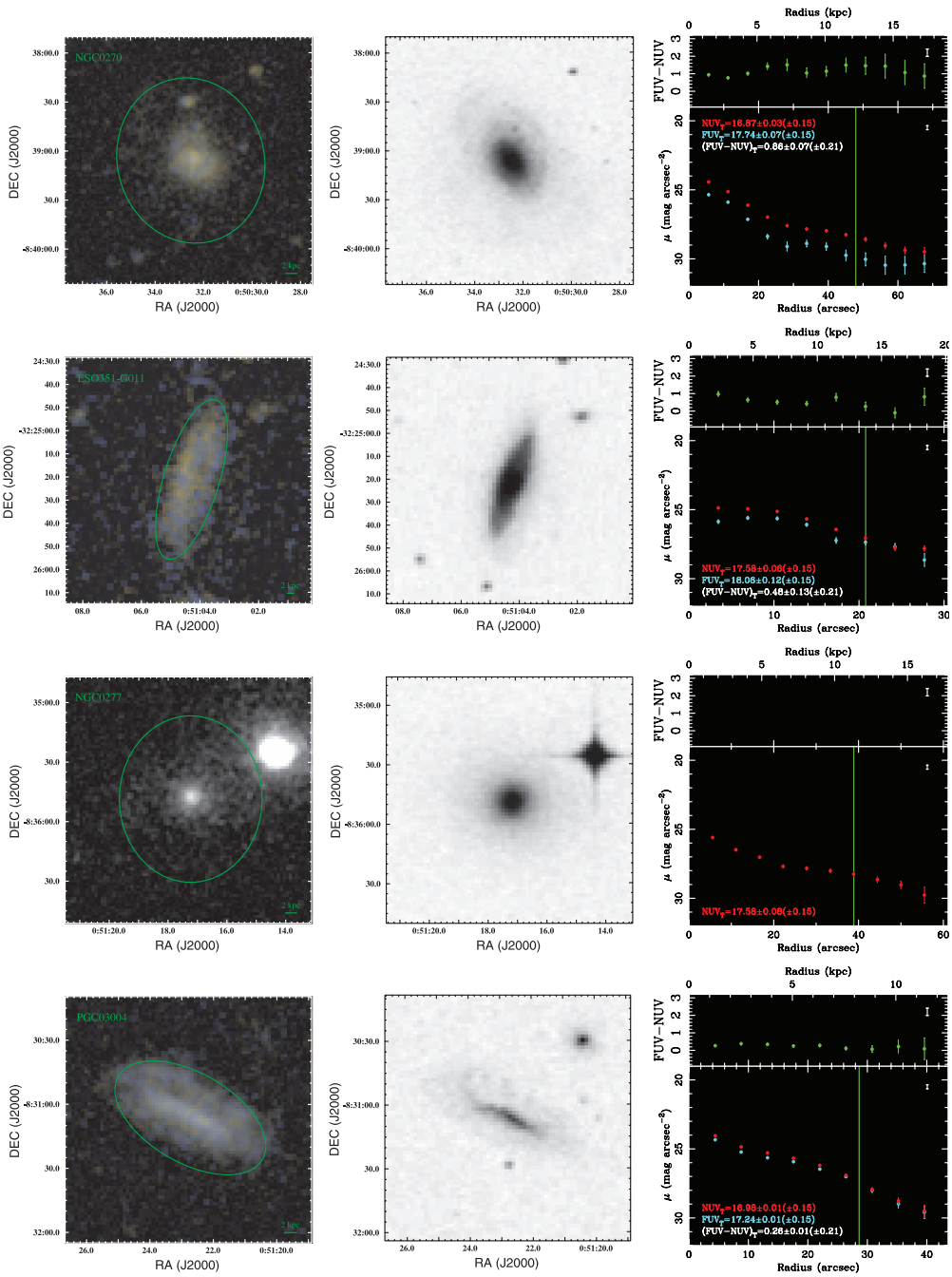

FIG. 3 — *Continued*

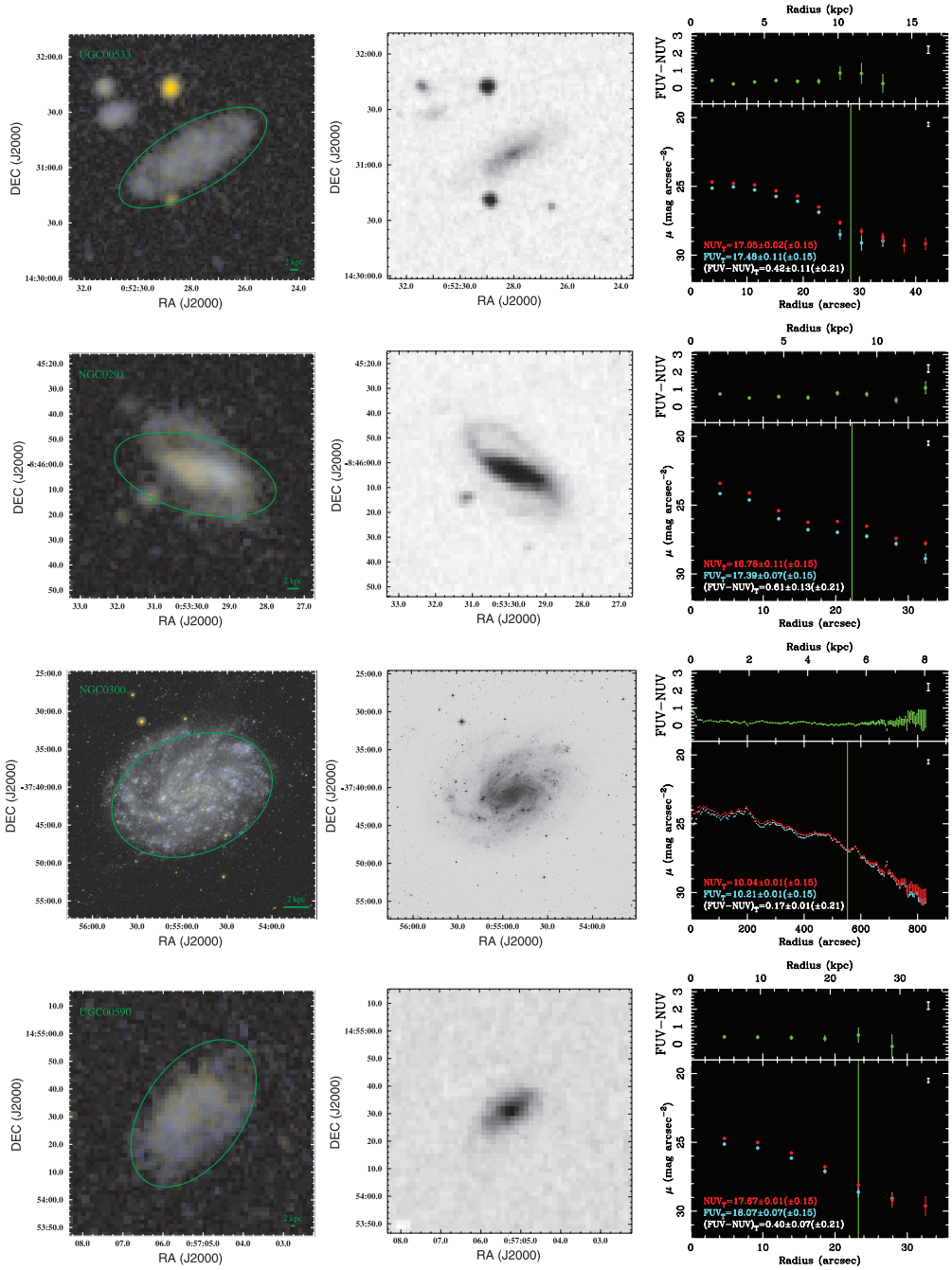

FIG. 3—*Continued*

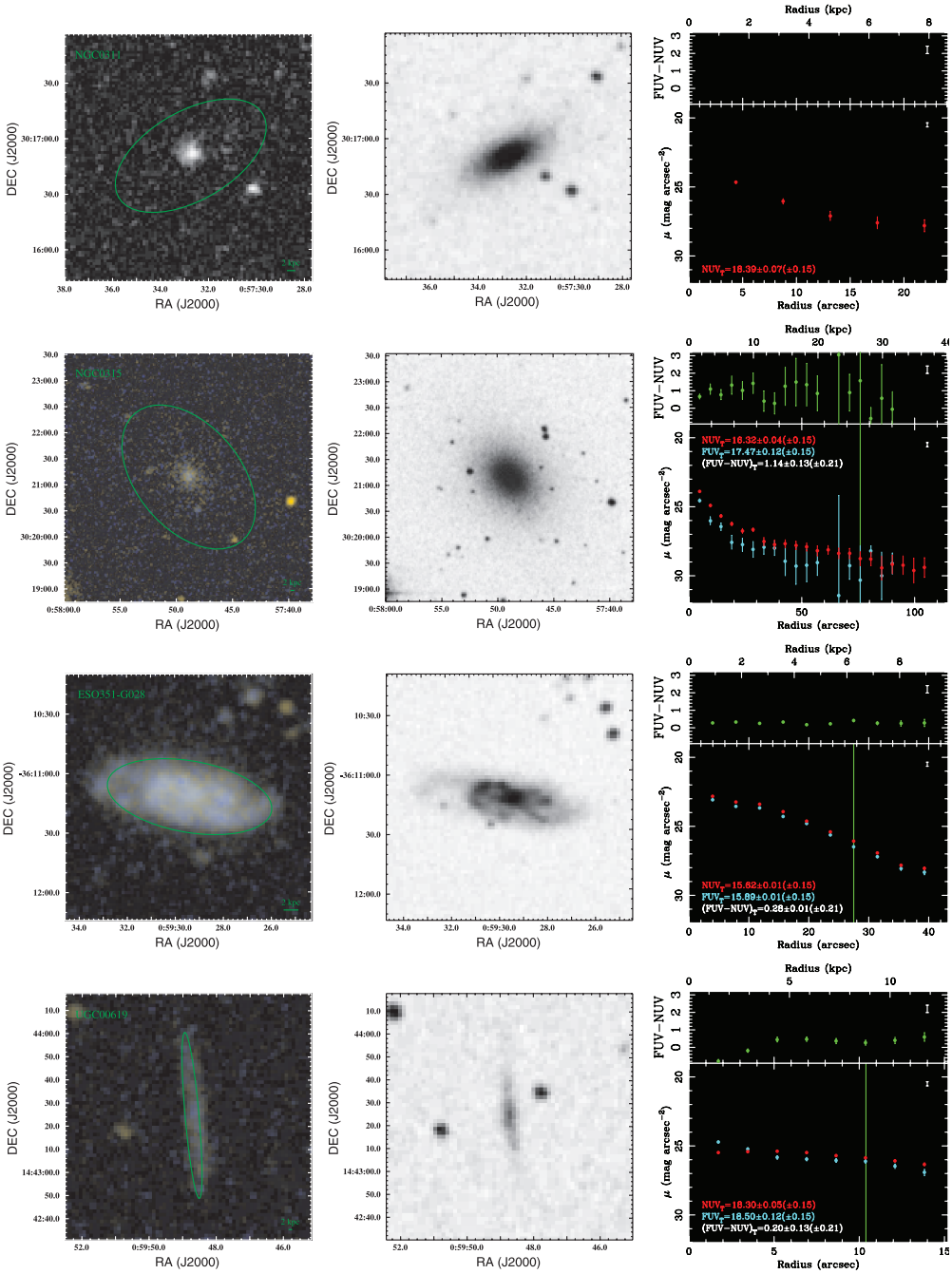

FIG. 3—*Continued*

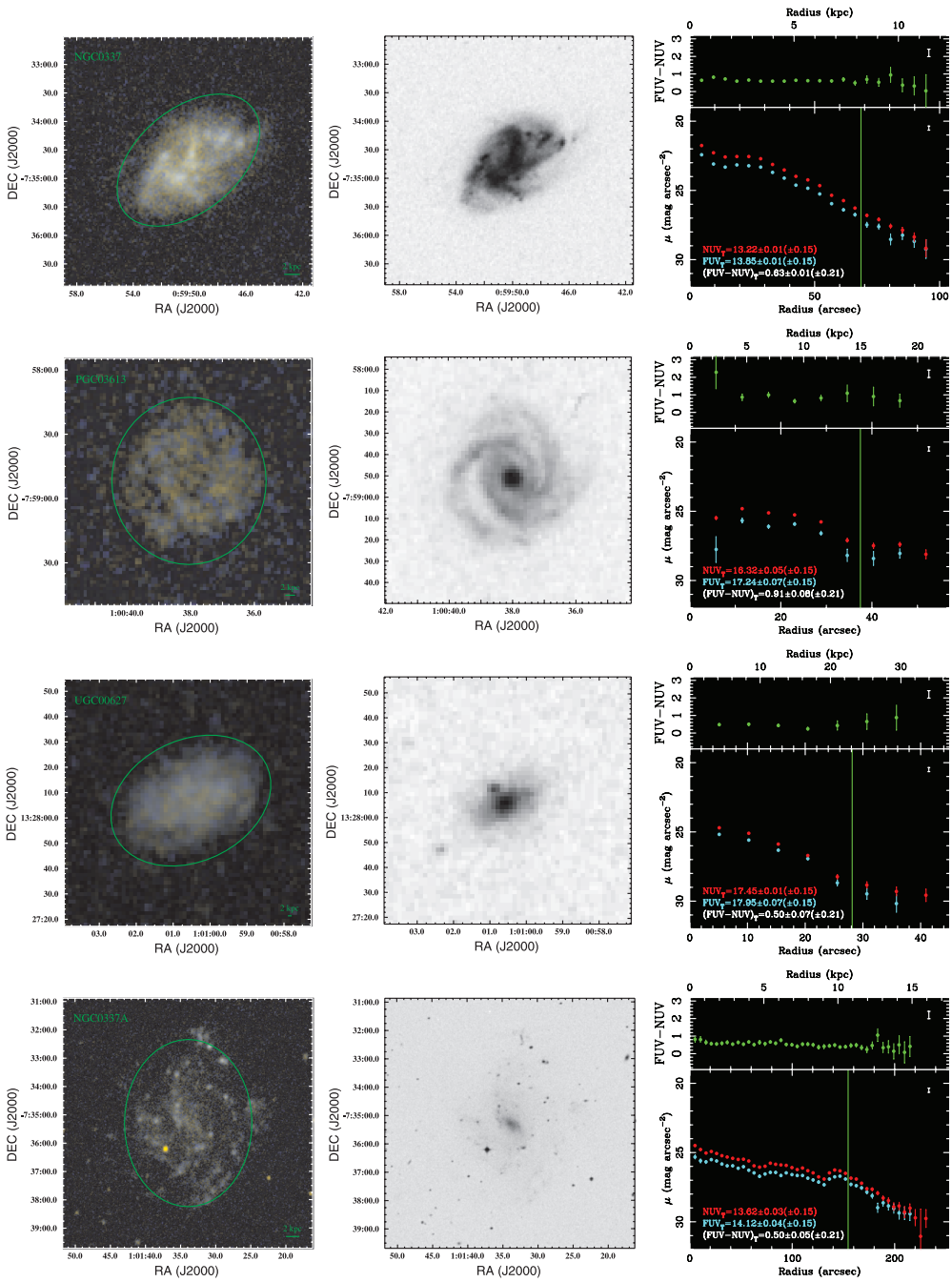

FIG. 3—*Continued*

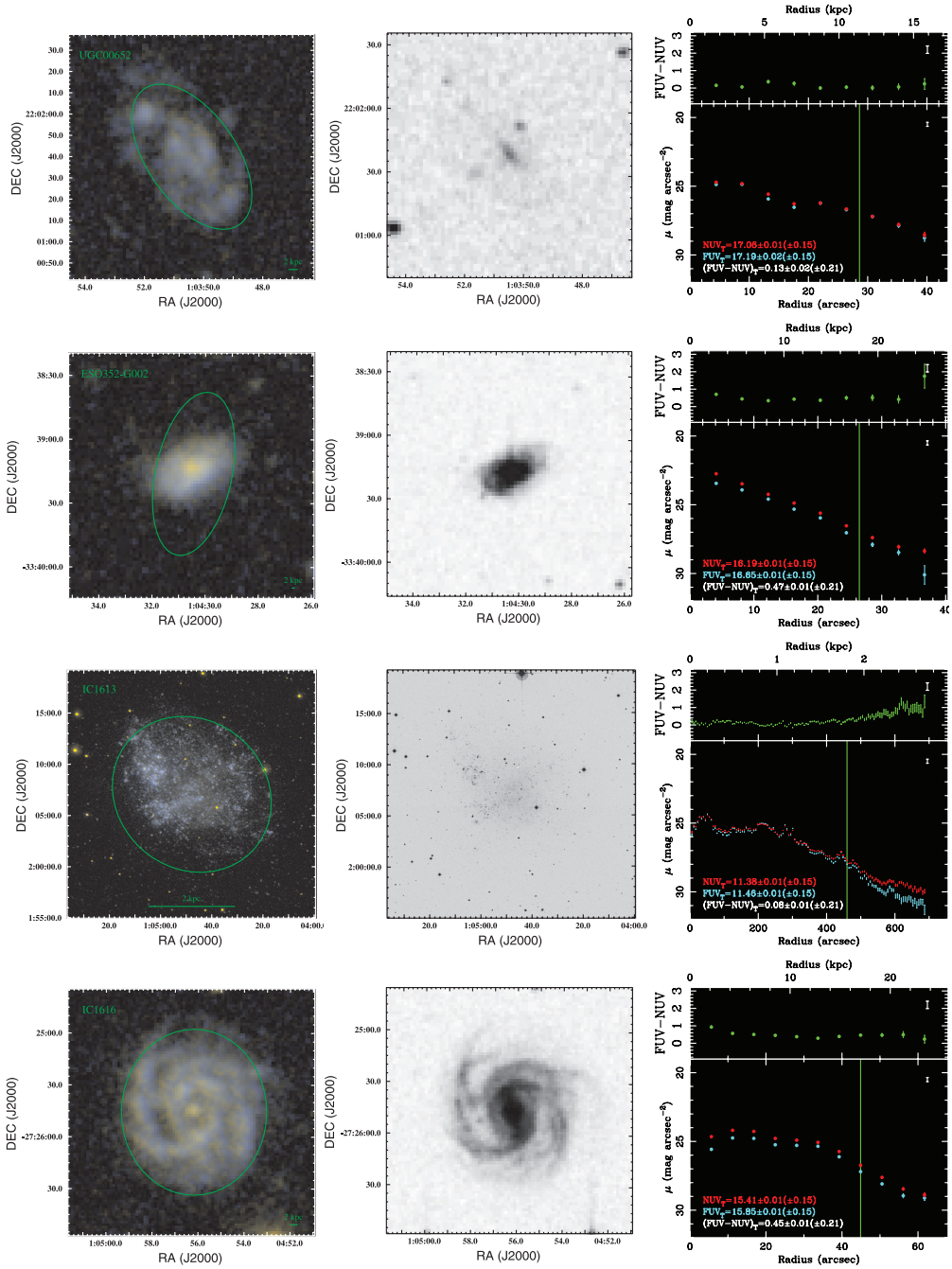

FIG. 3 — *Continued*

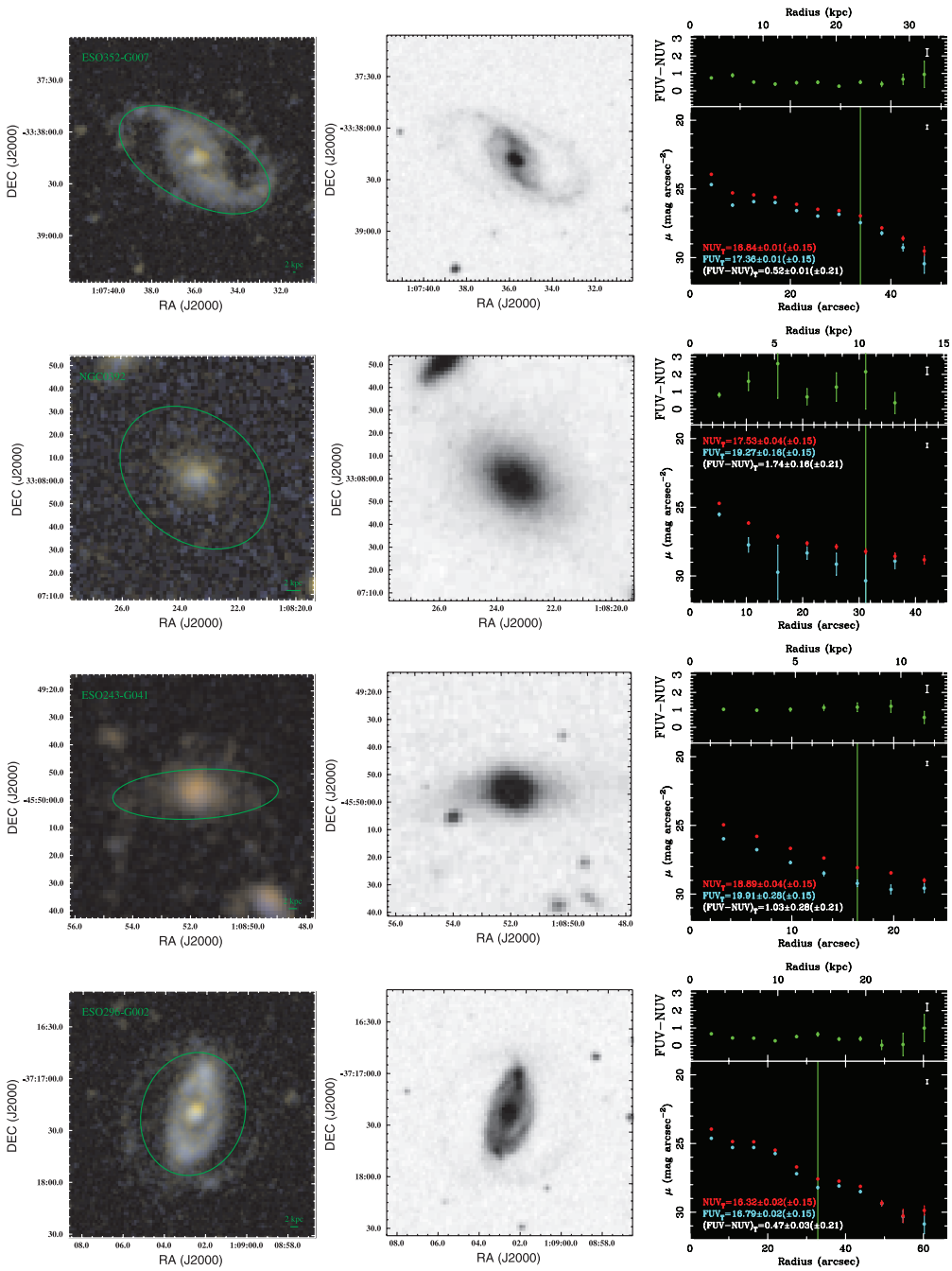

FIG. 3—*Continued*

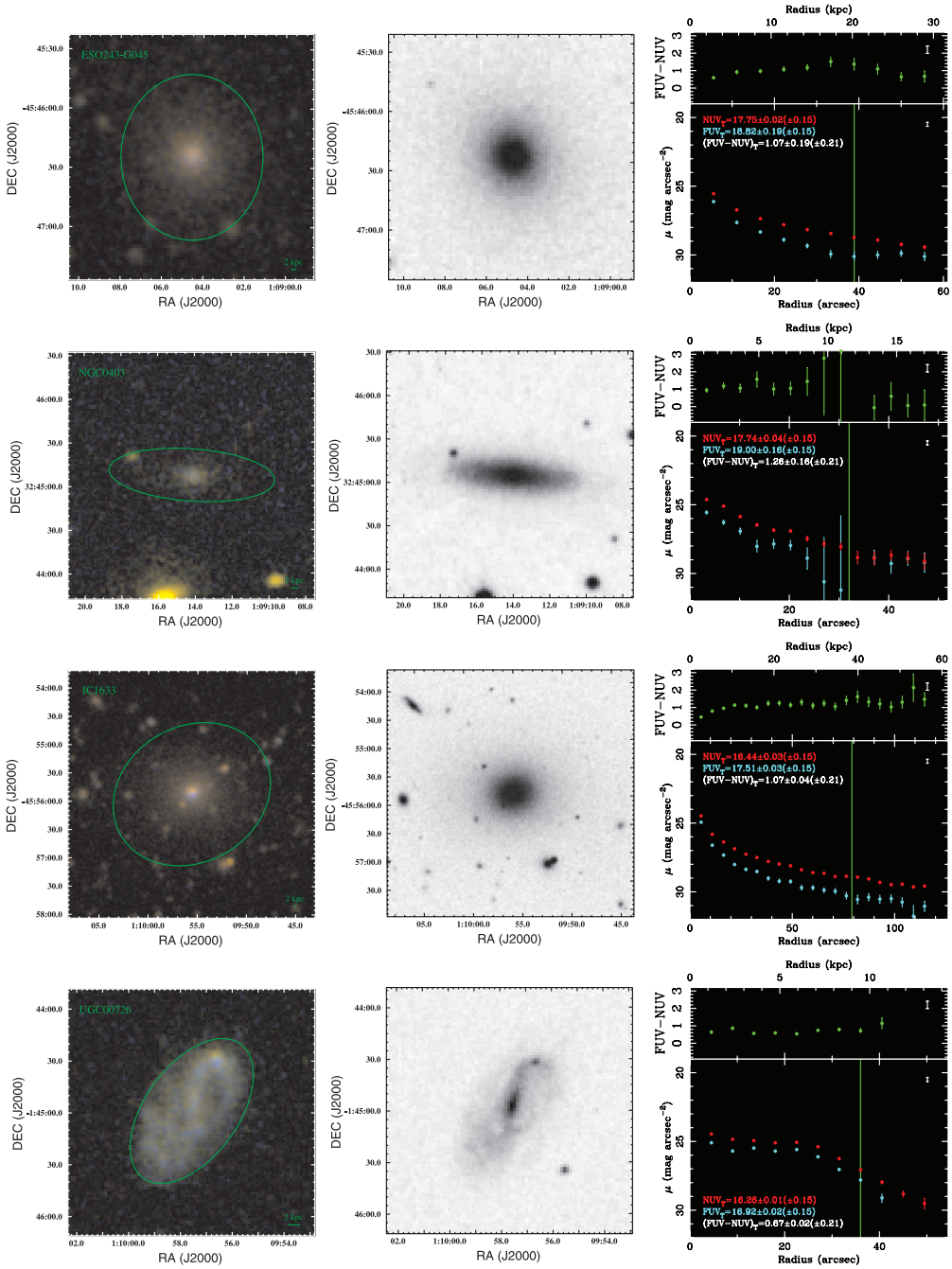

FIG. 3—*Continued*

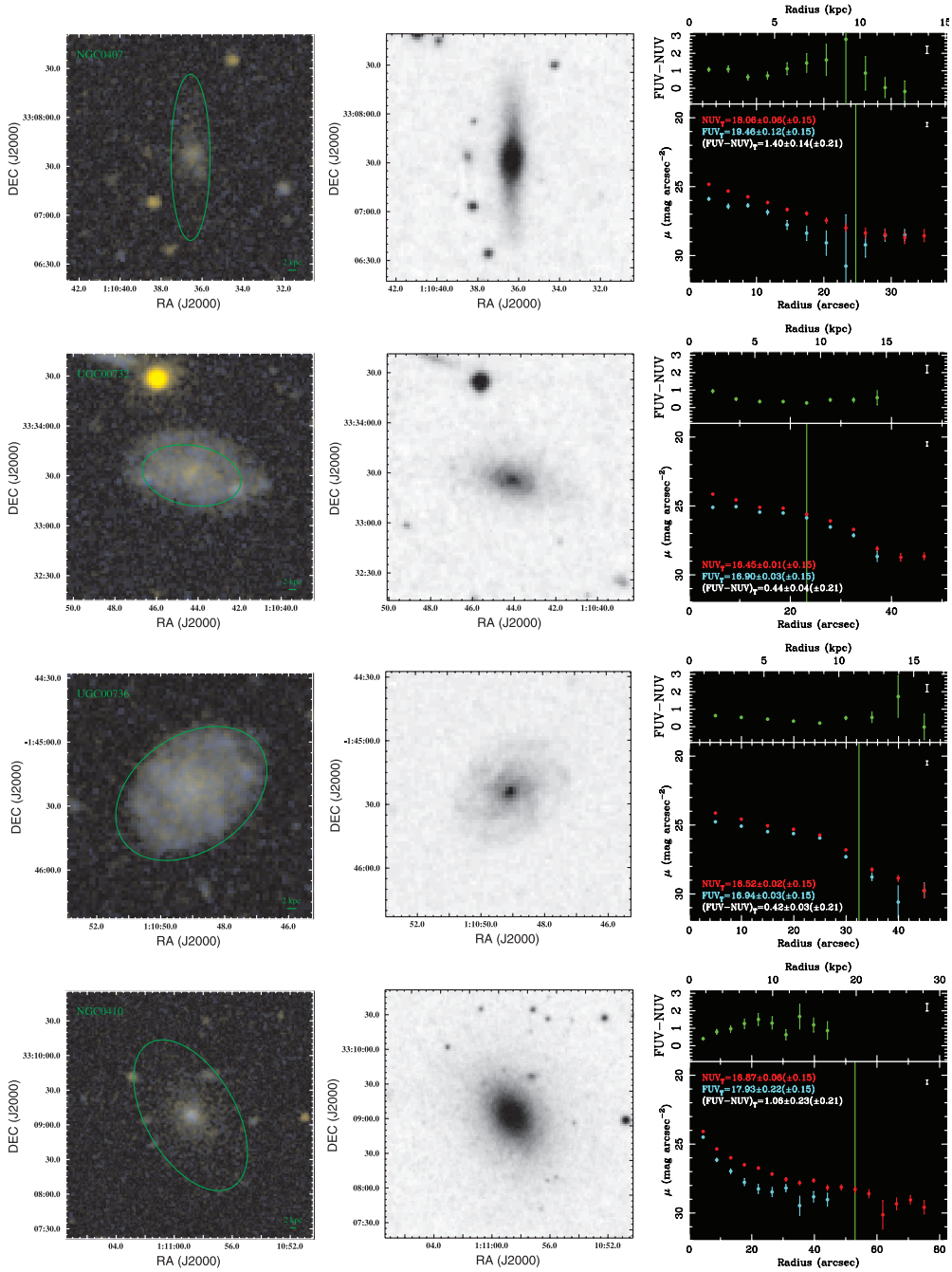

FIG. 3—*Continued*

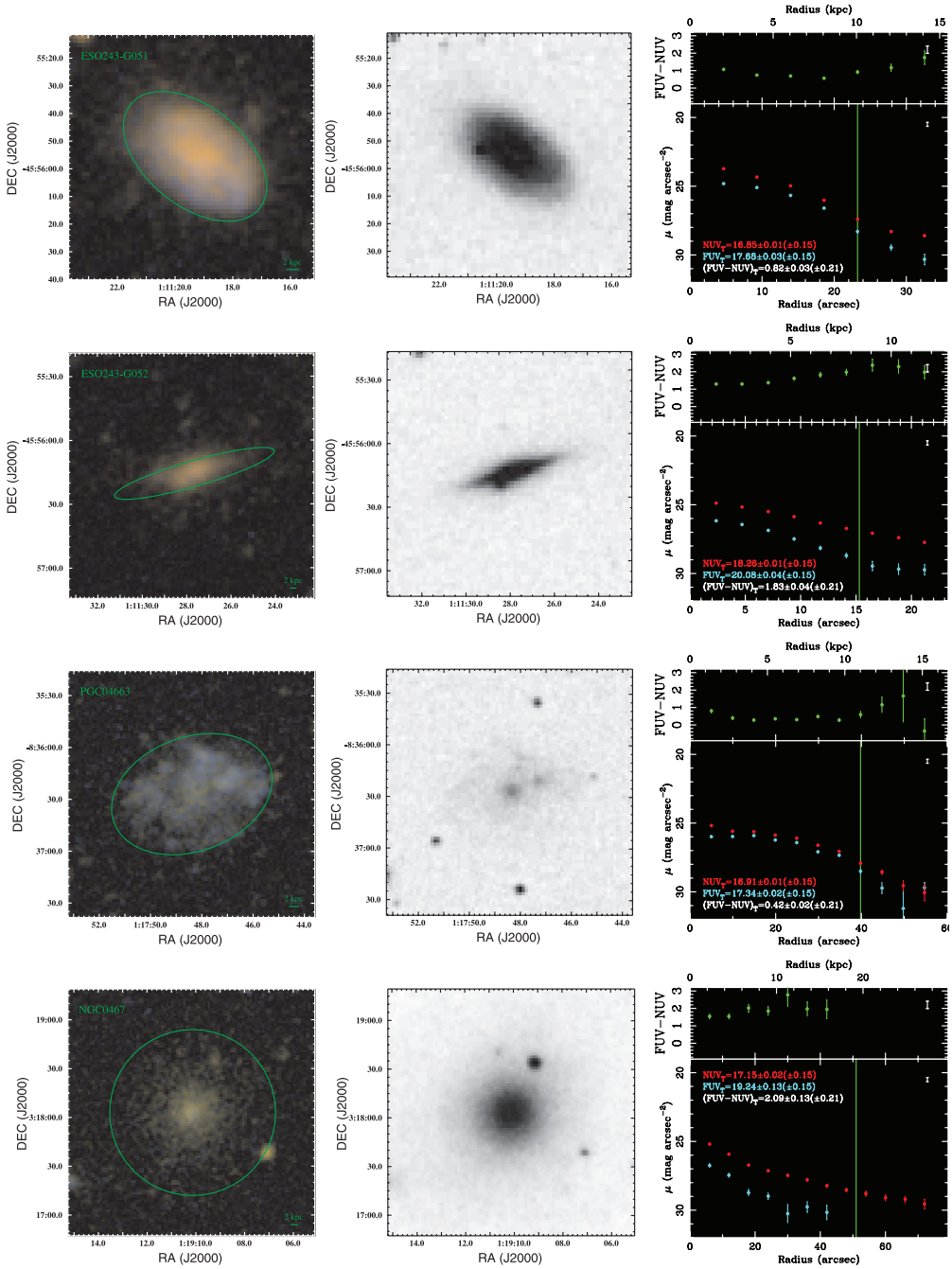

FIG. 3—*Continued*

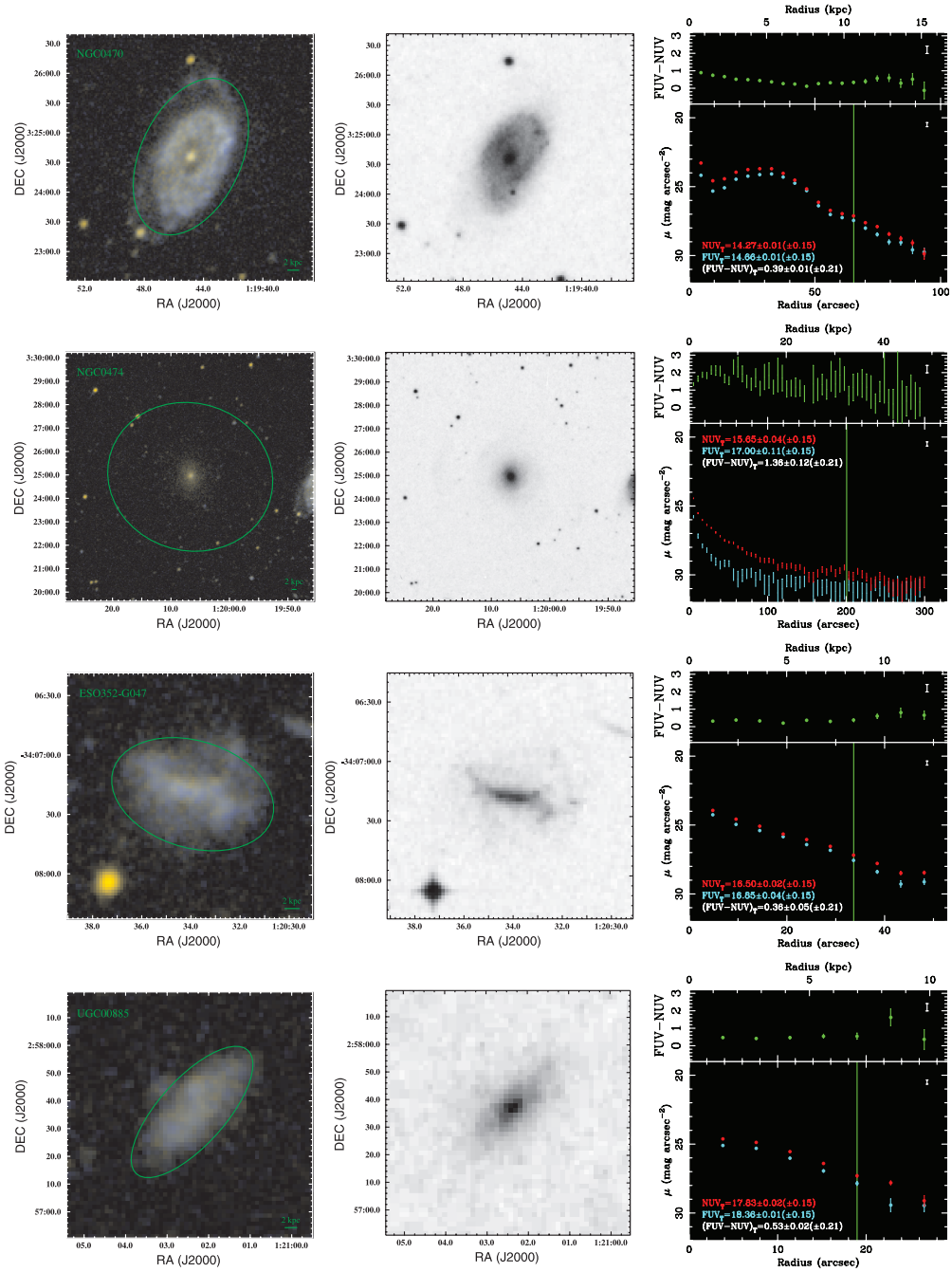

FIG. 3—*Continued*

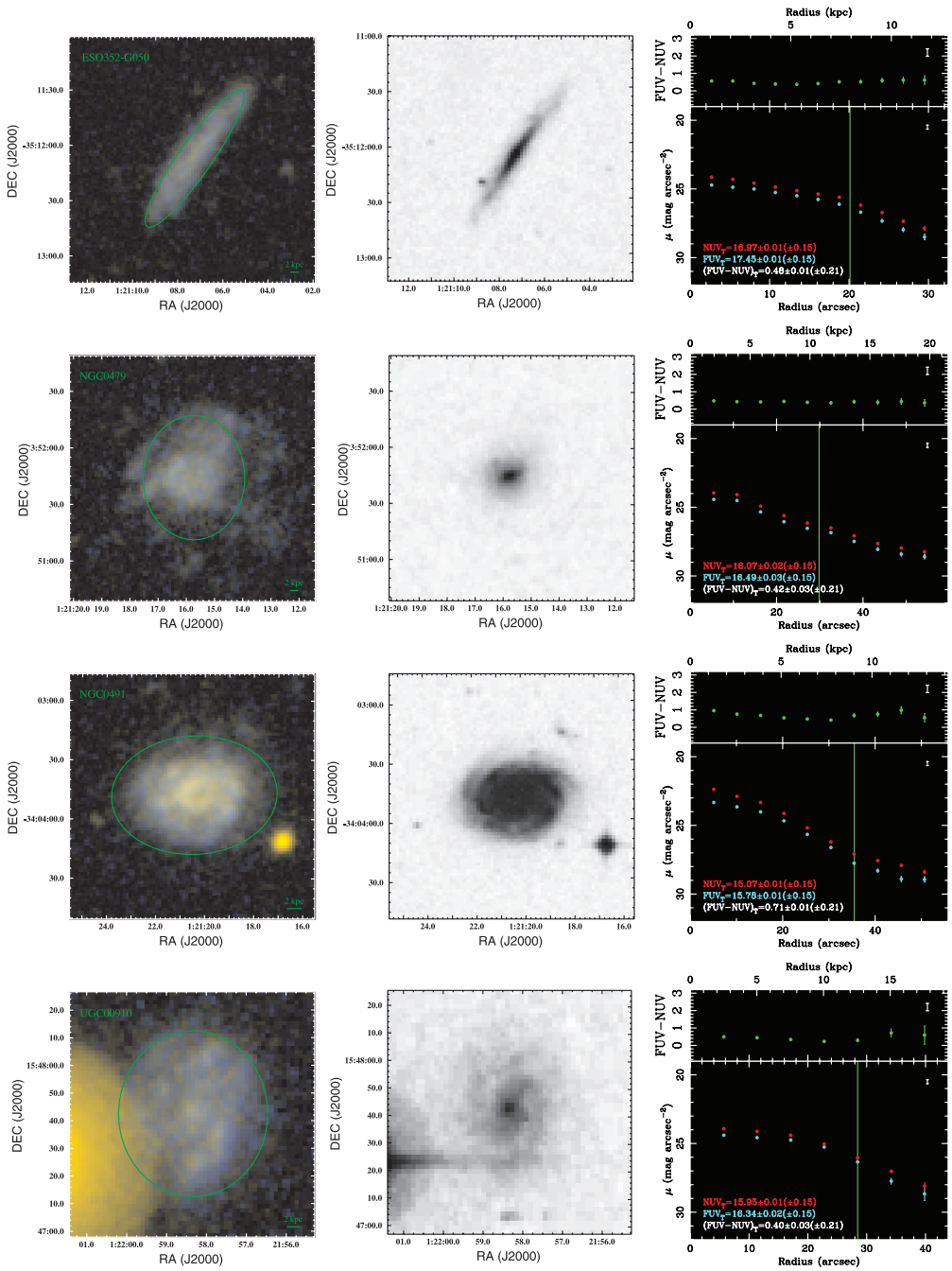

FIG. 3—*Continued*

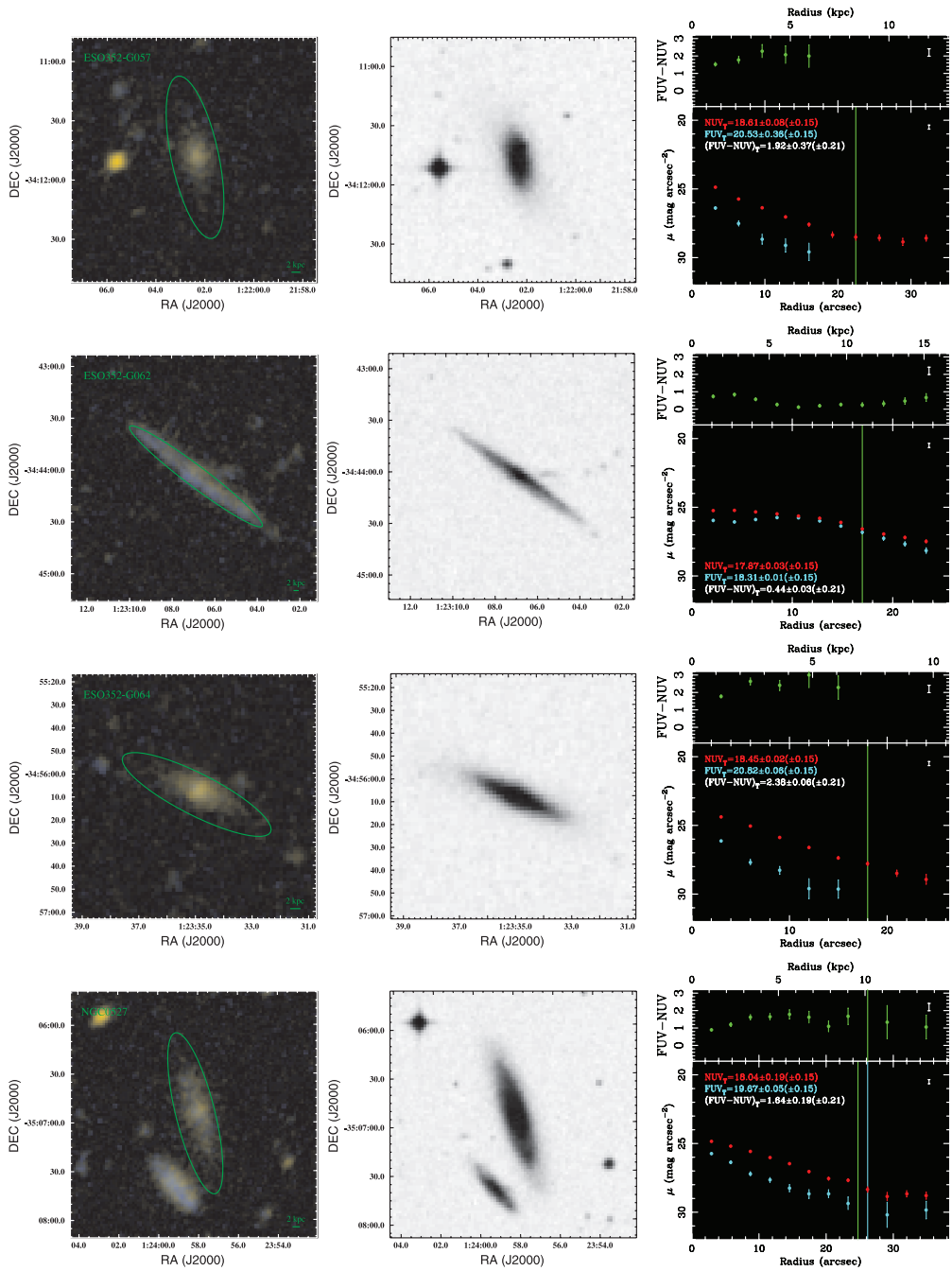

FIG. 3—*Continued*

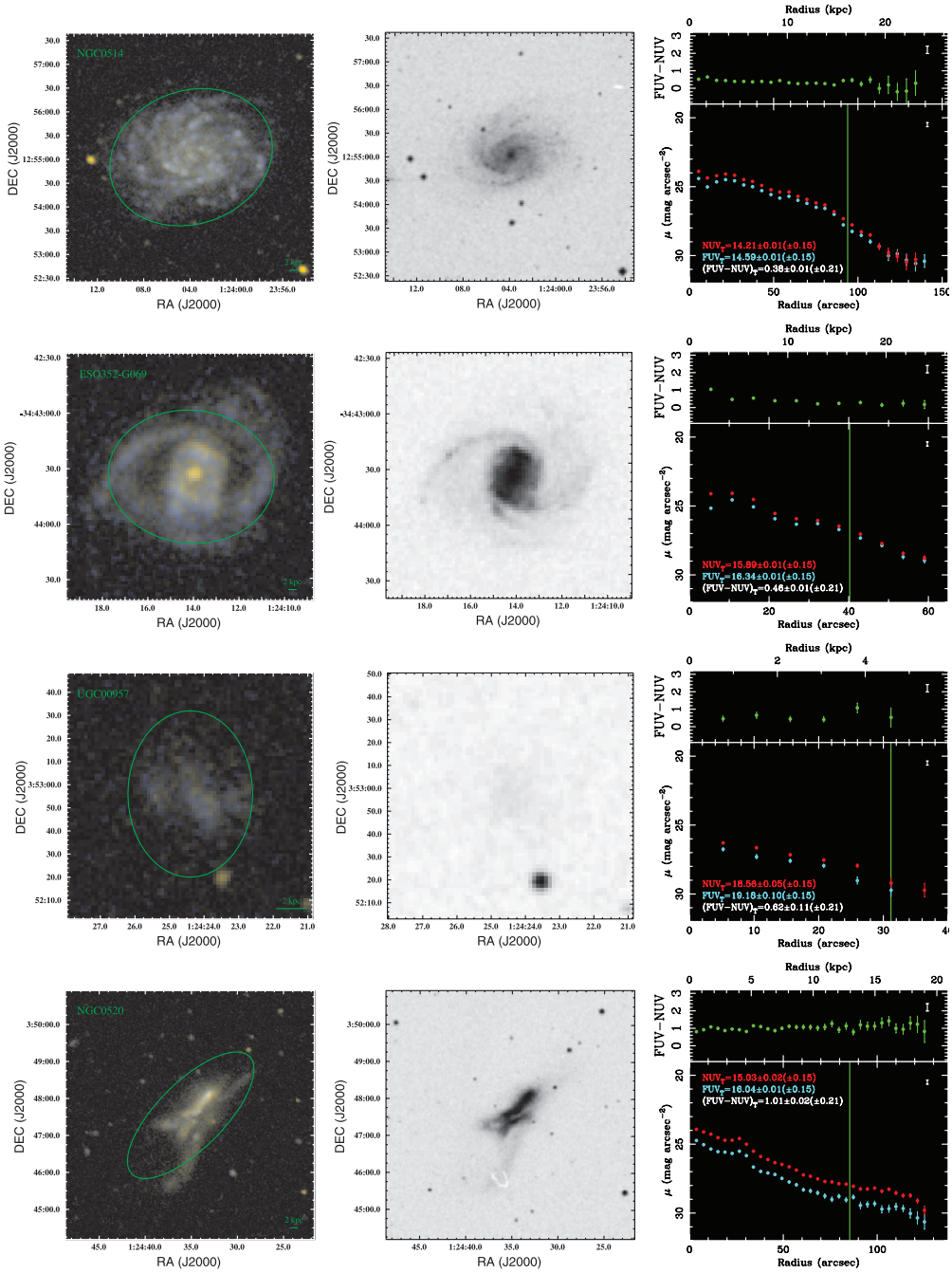

FIG. 3—*Continued*

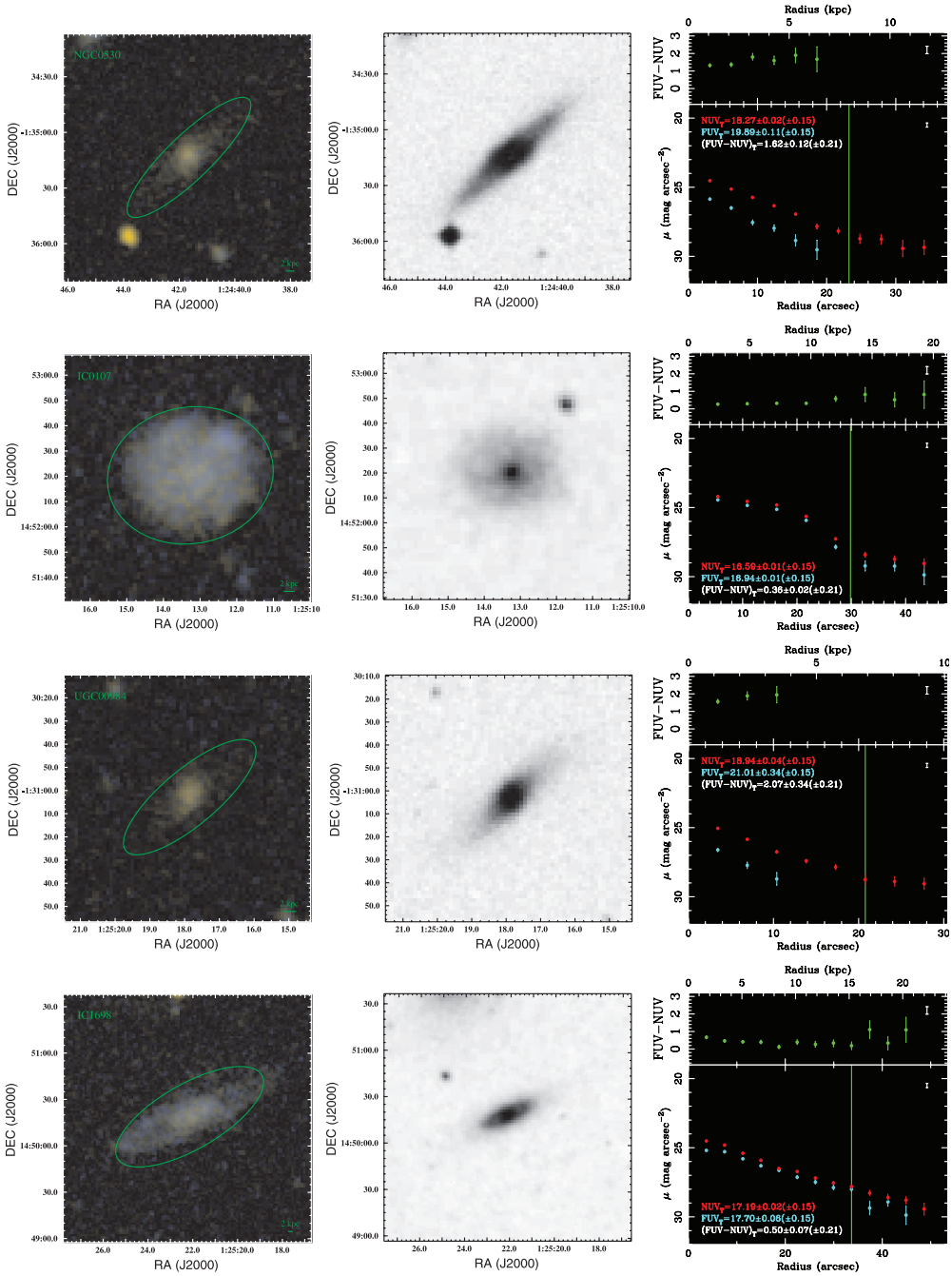

FIG. 3—*Continued*

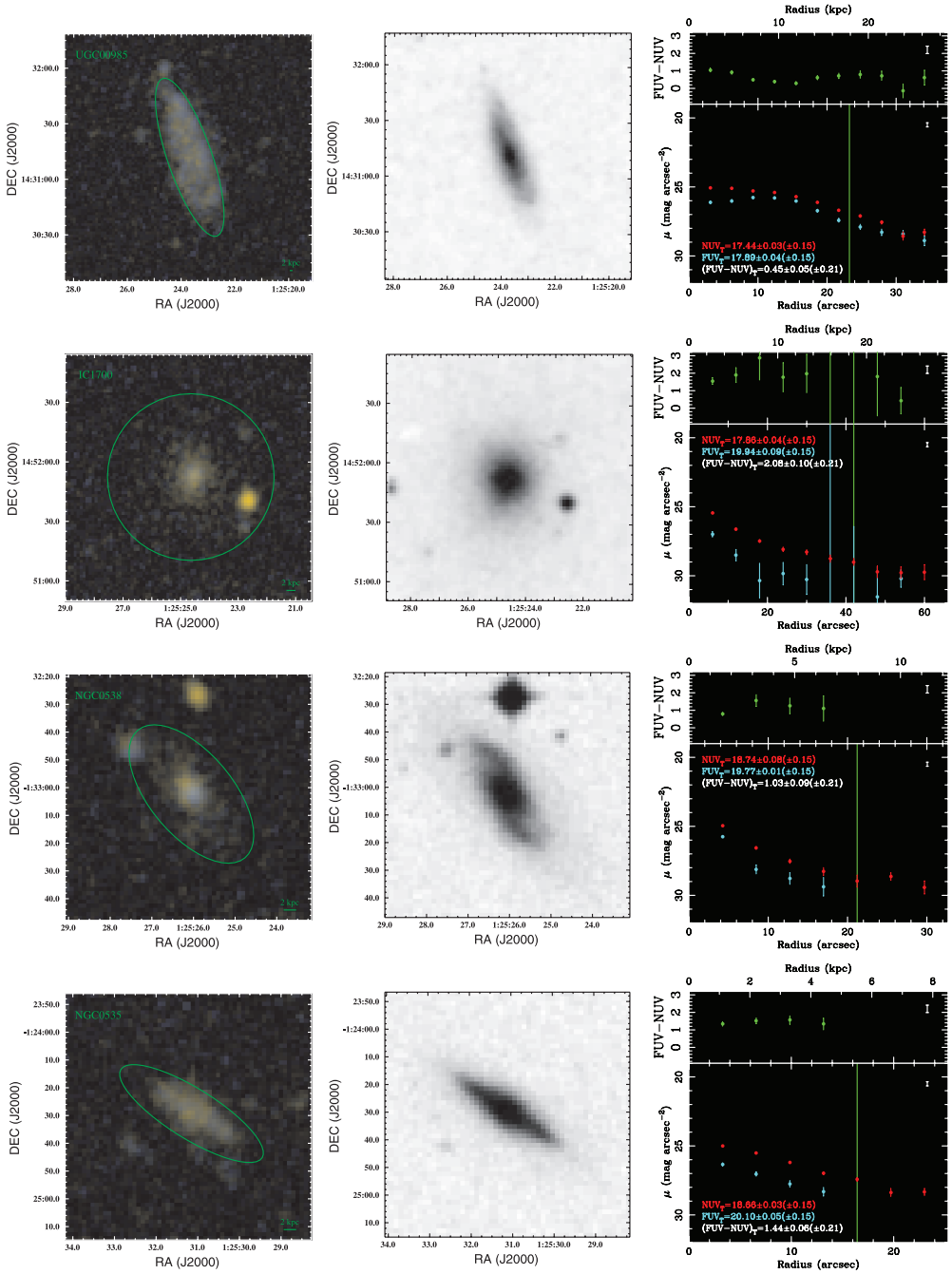

FIG. 3—*Continued*

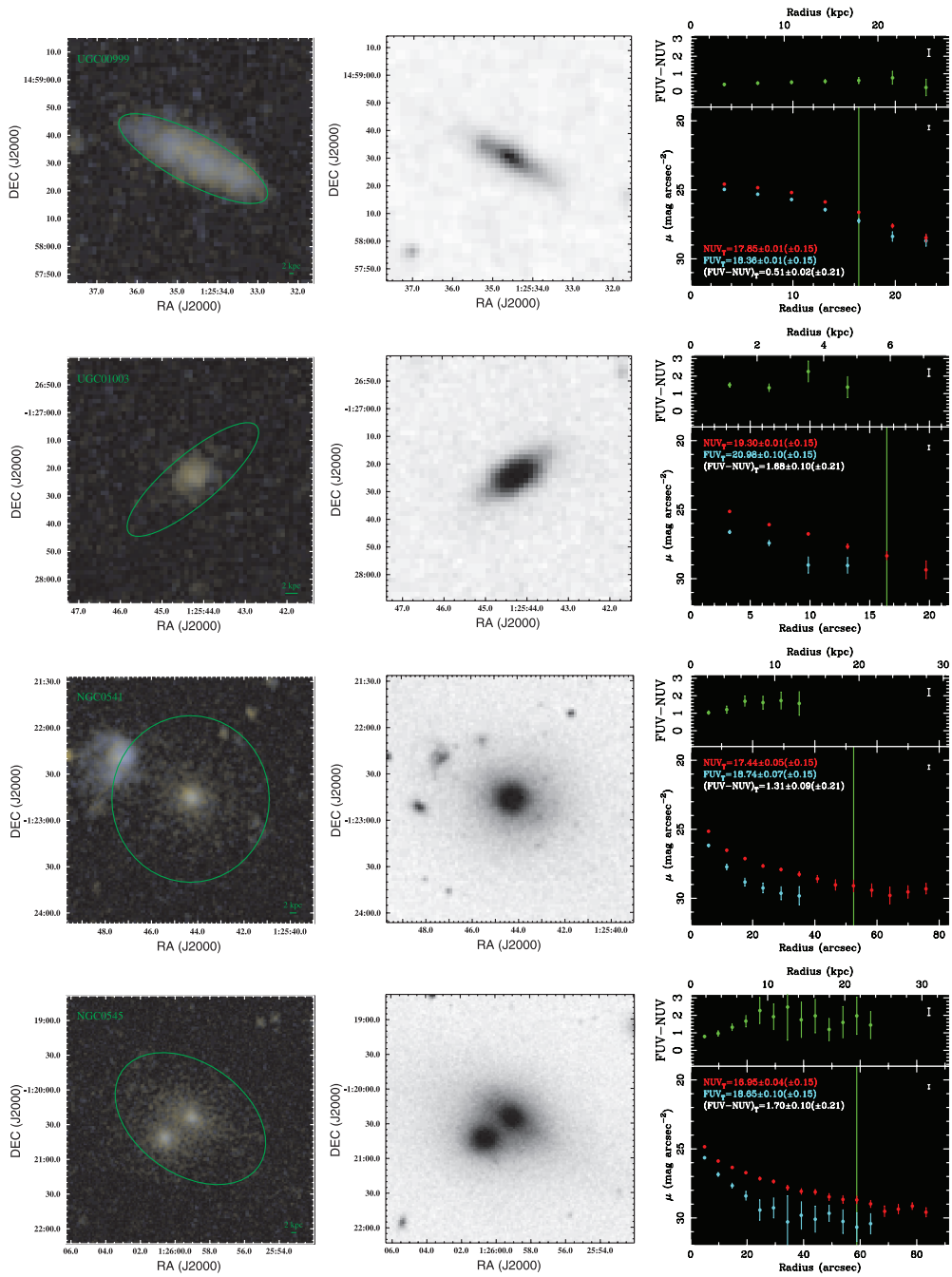

FIG. 3—*Continued*

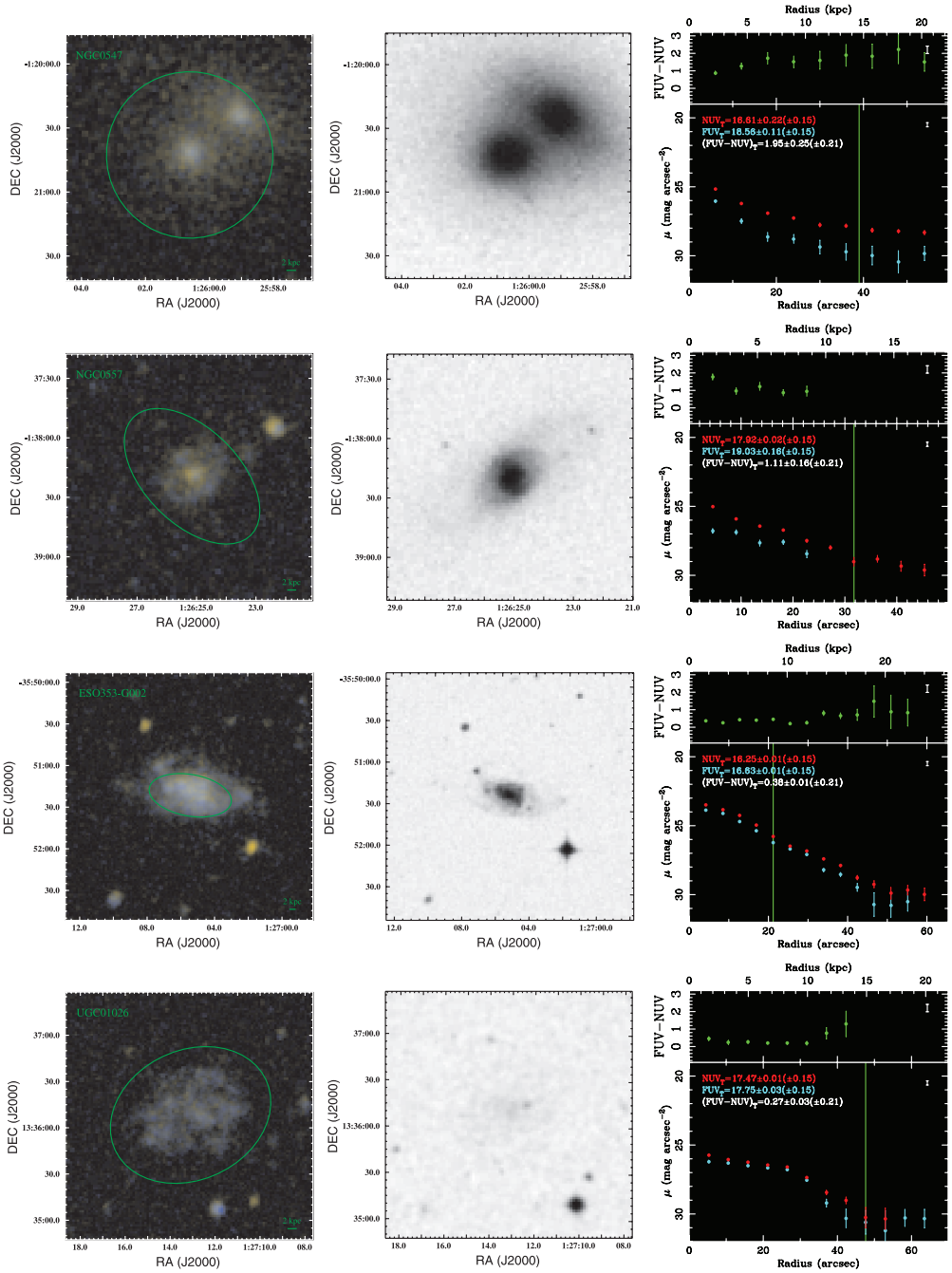

FIG. 3—*Continued*

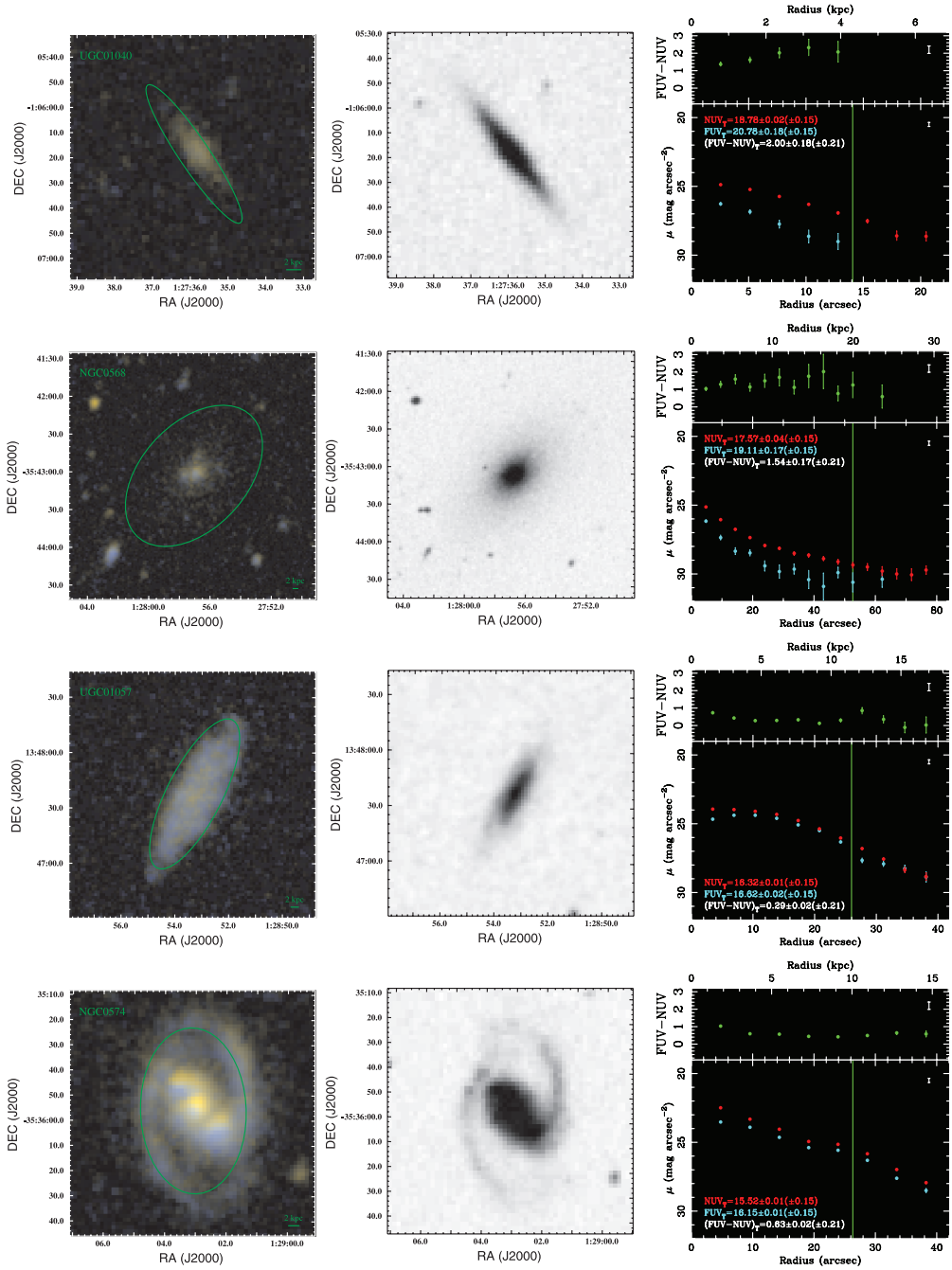

FIG. 3—*Continued*

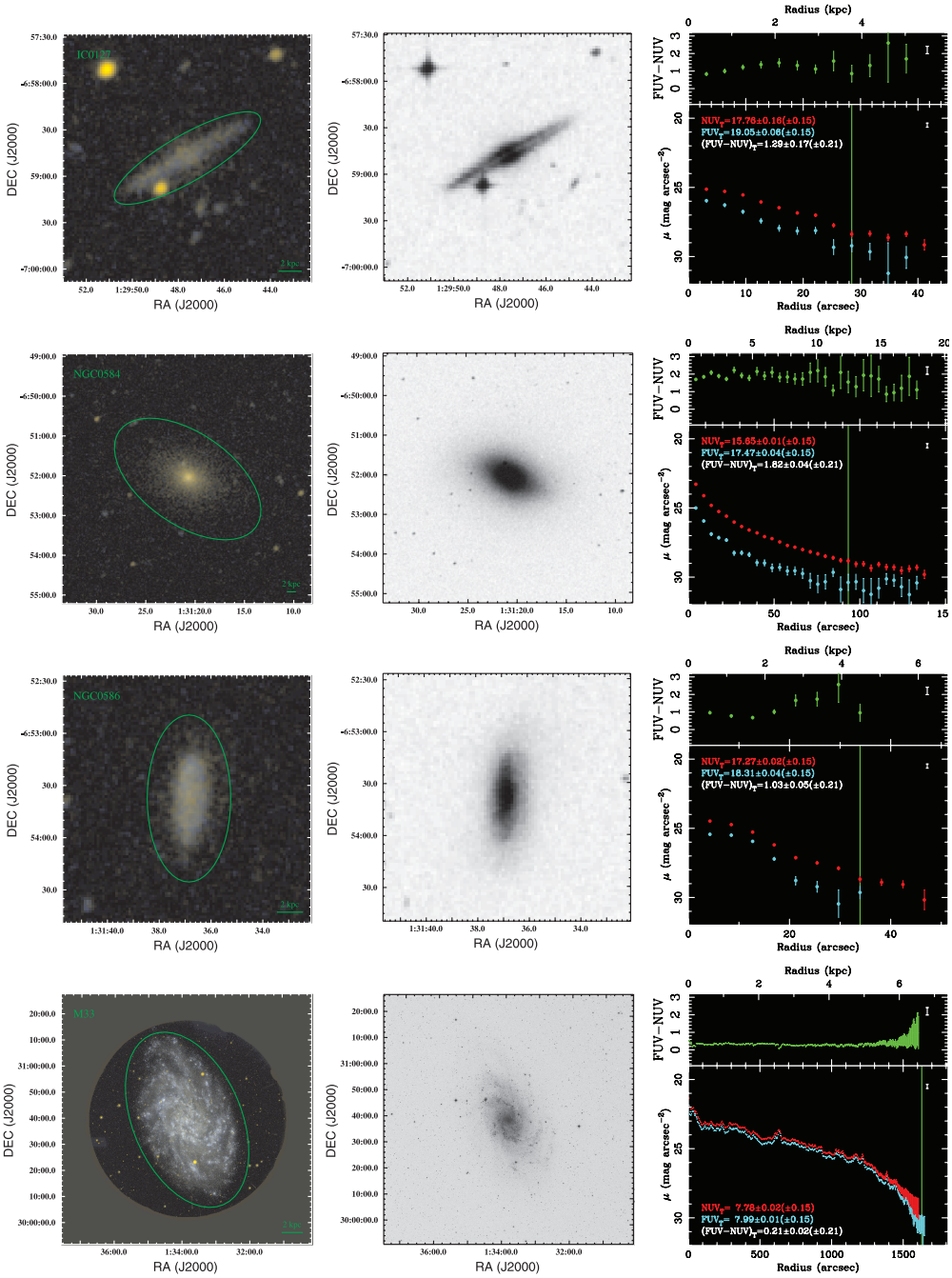

FIG. 3—*Continued*

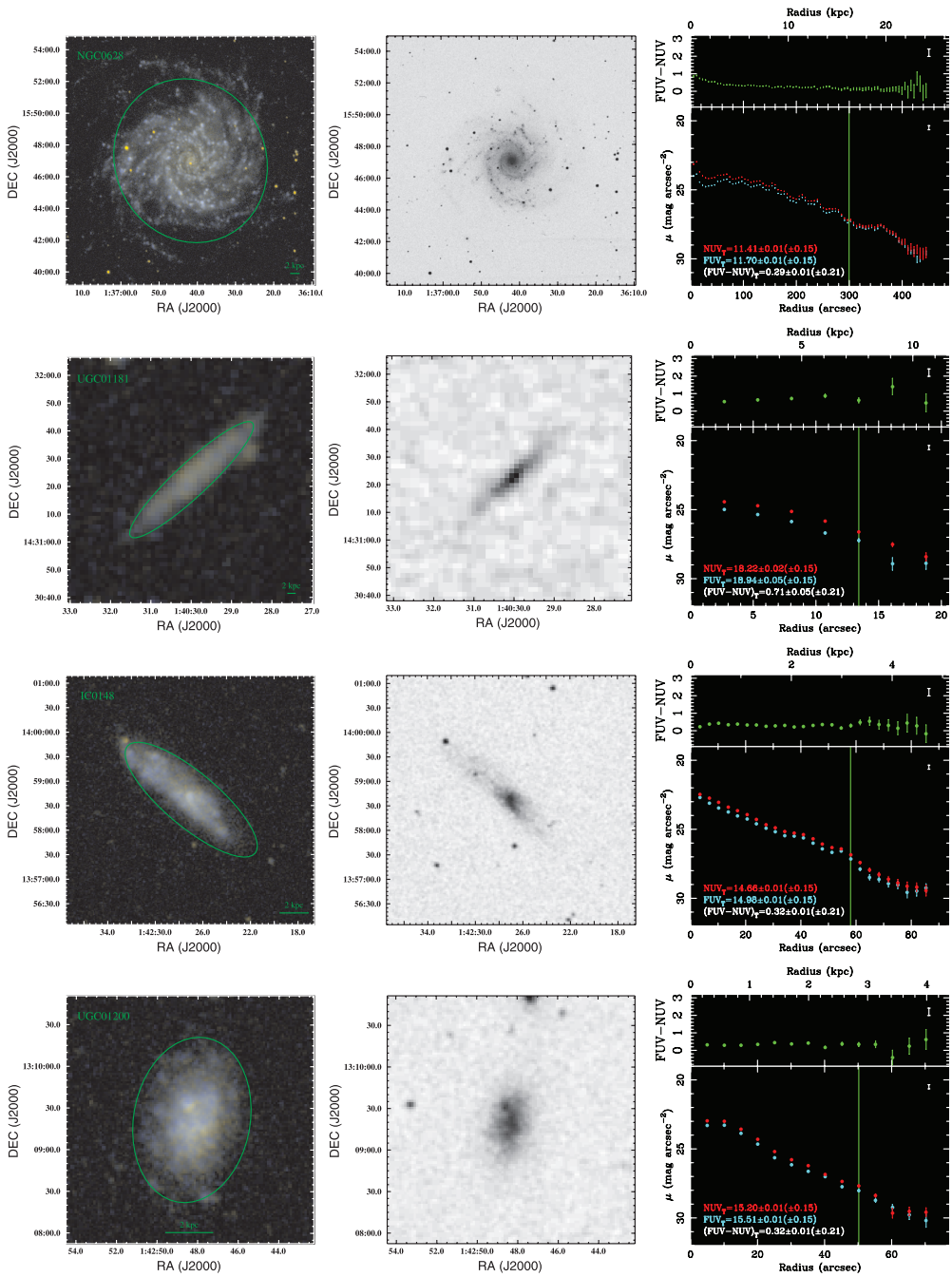

FIG. 3—*Continued*

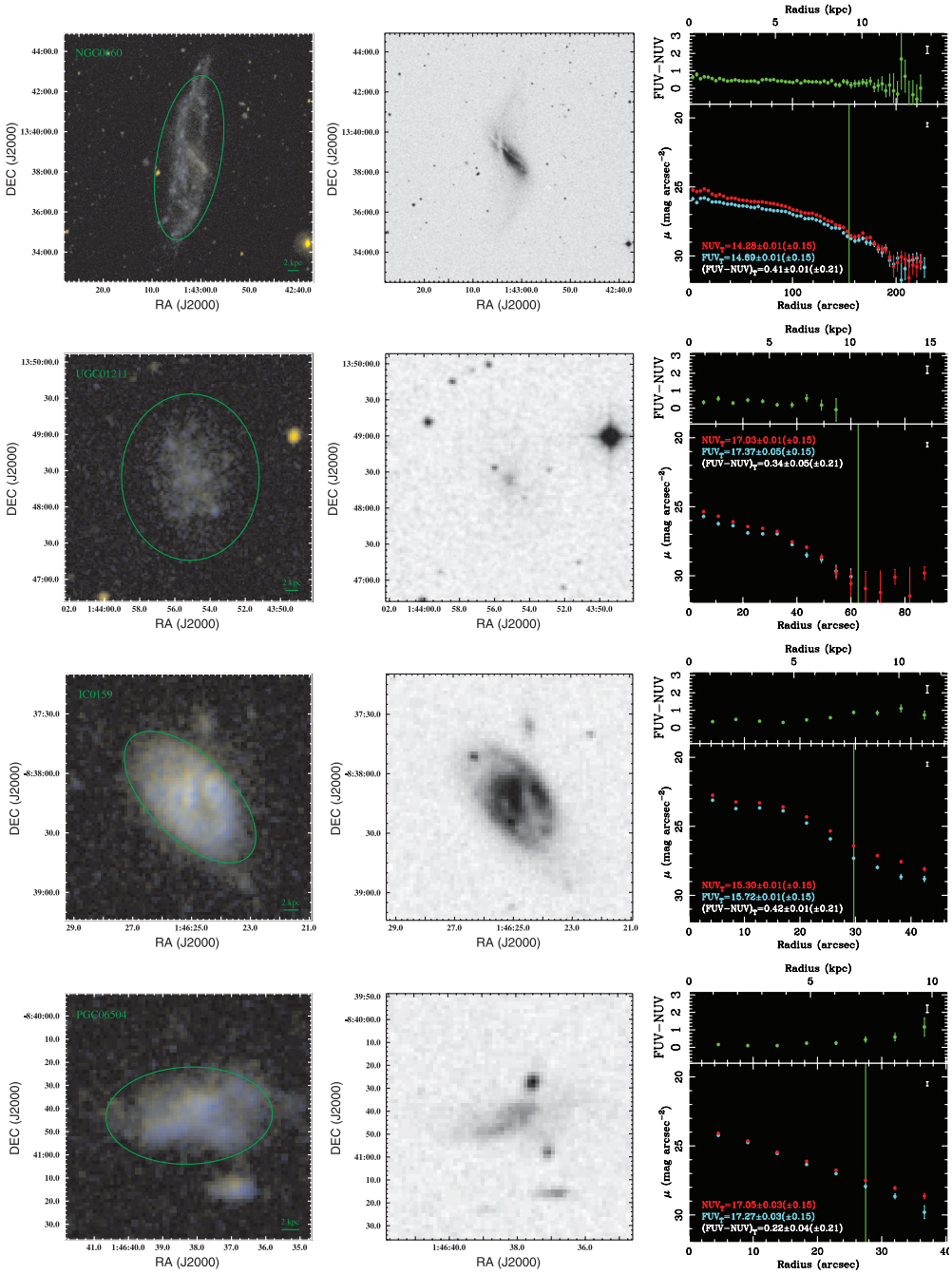

FIG. 3—*Continued*

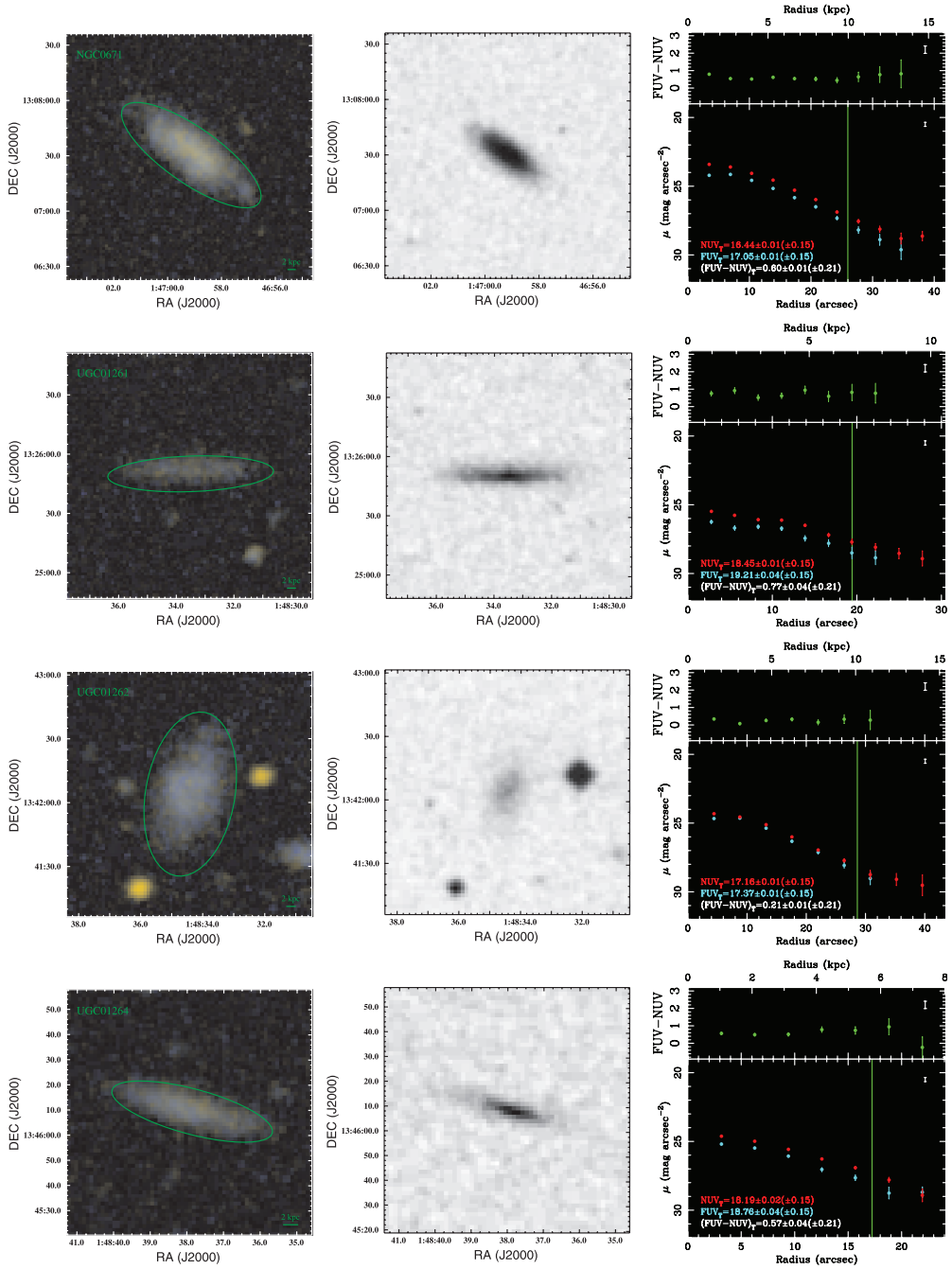

FIG. 3—*Continued*

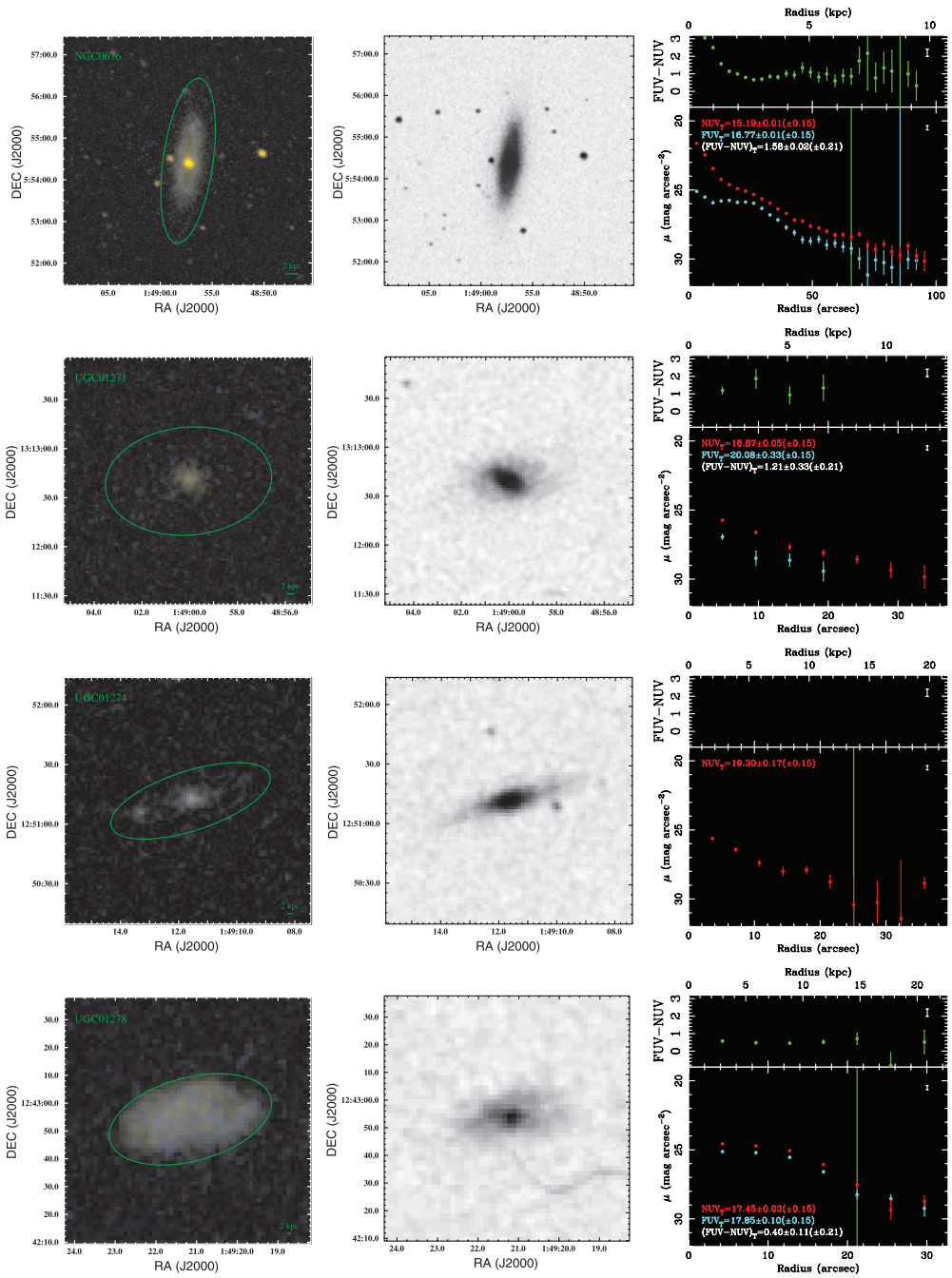

FIG. 3—*Continued*

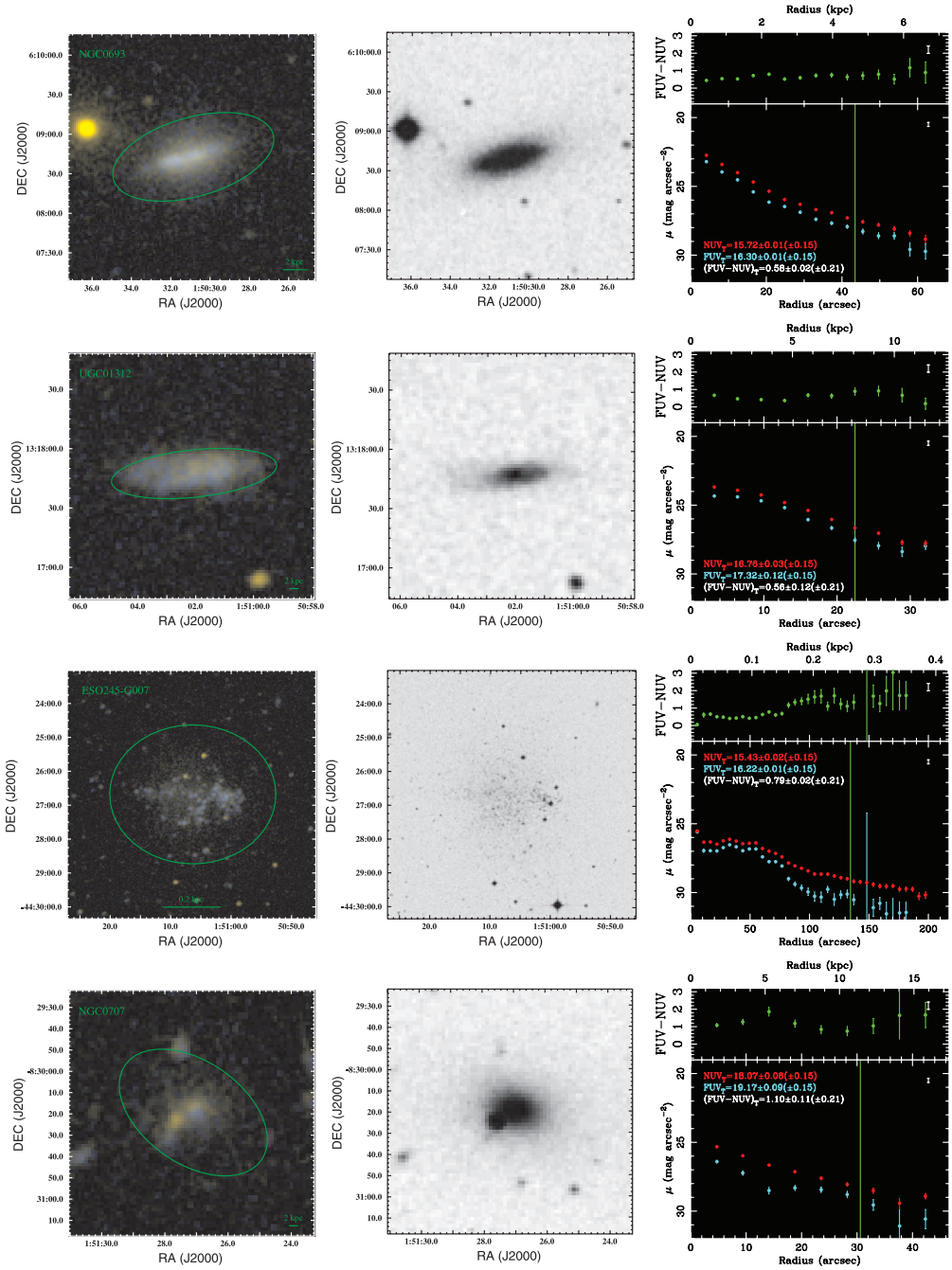

FIG. 3—*Continued*

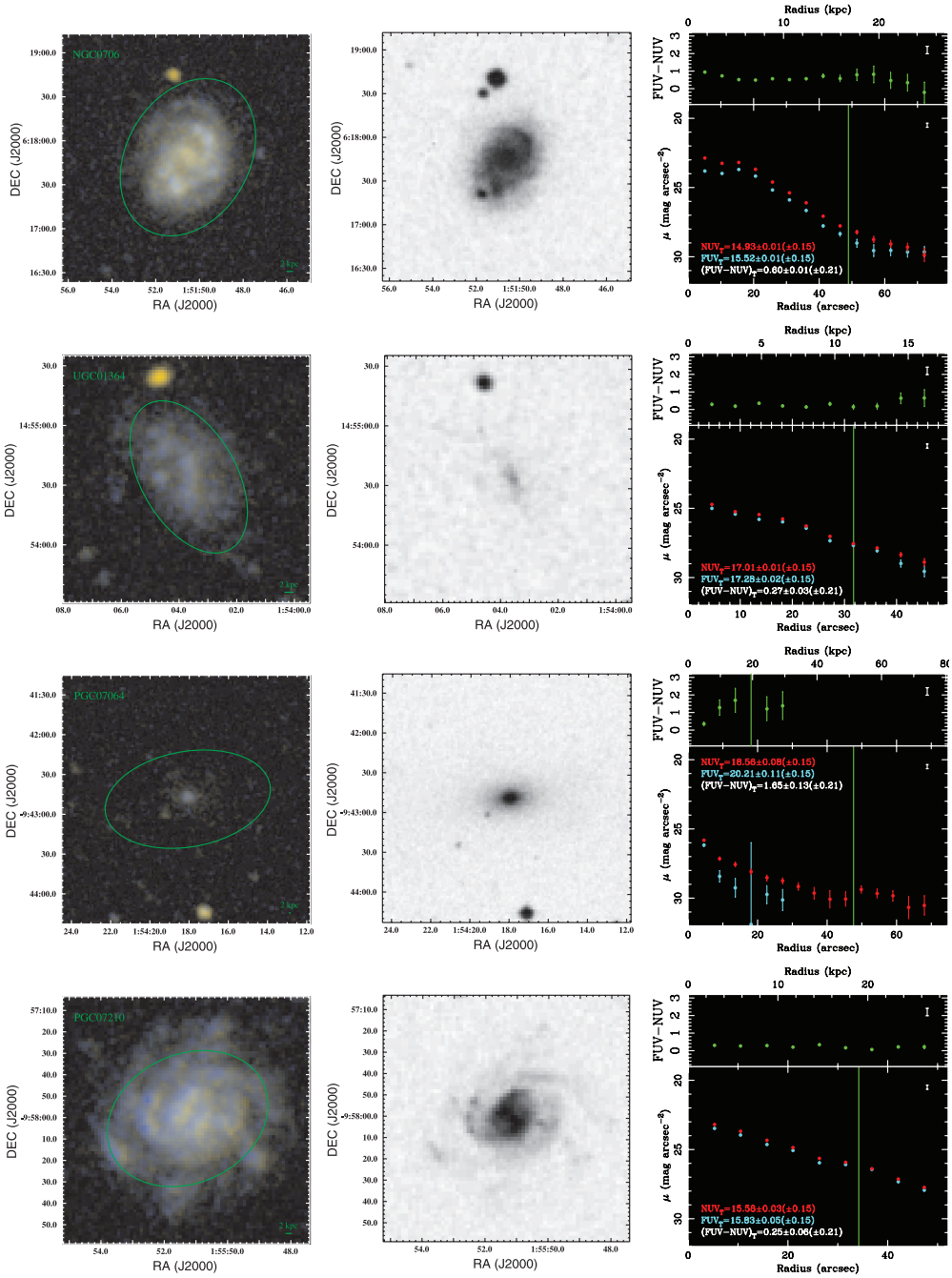

FIG. 3—*Continued*

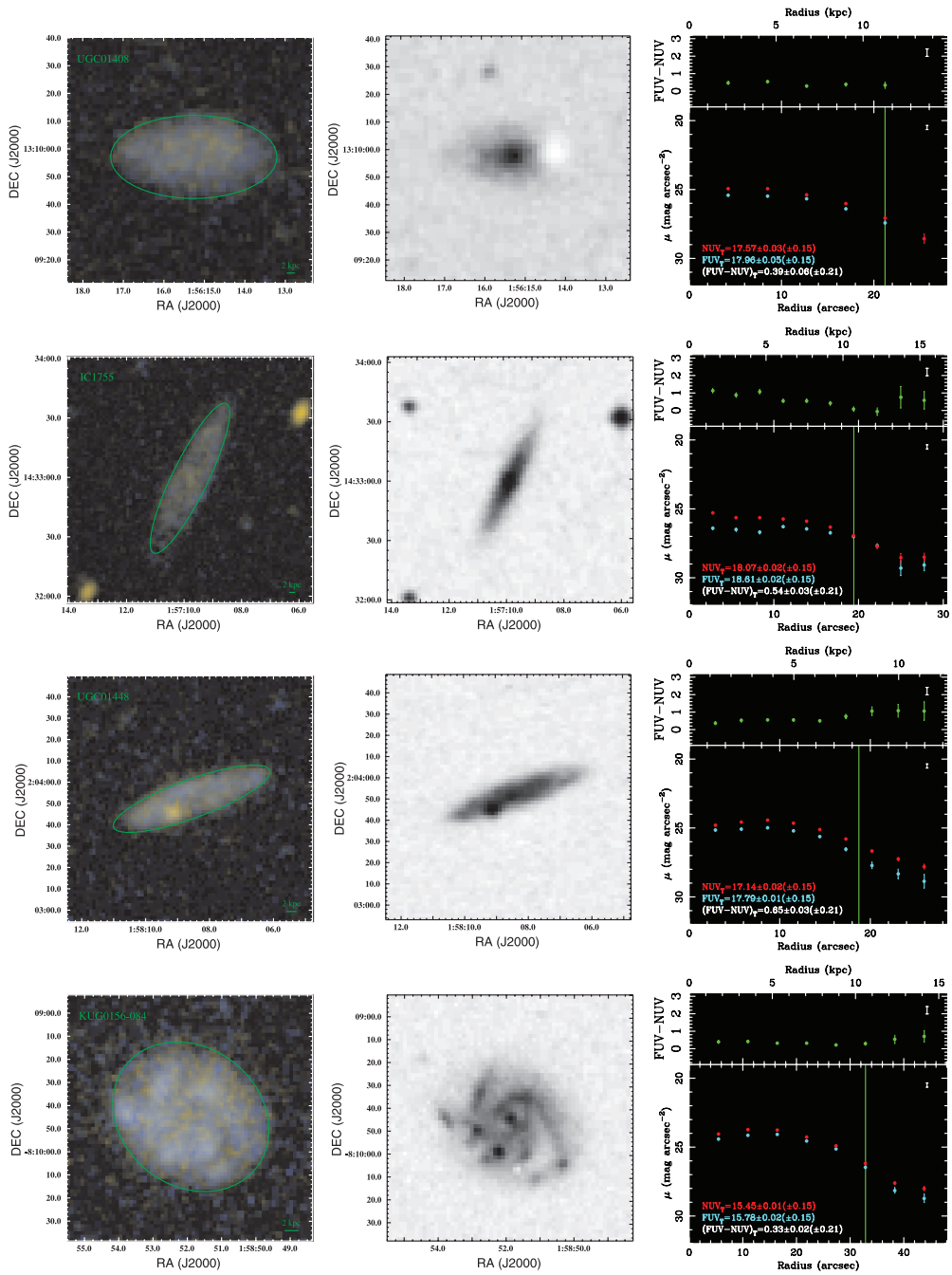

FIG. 3—*Continued*

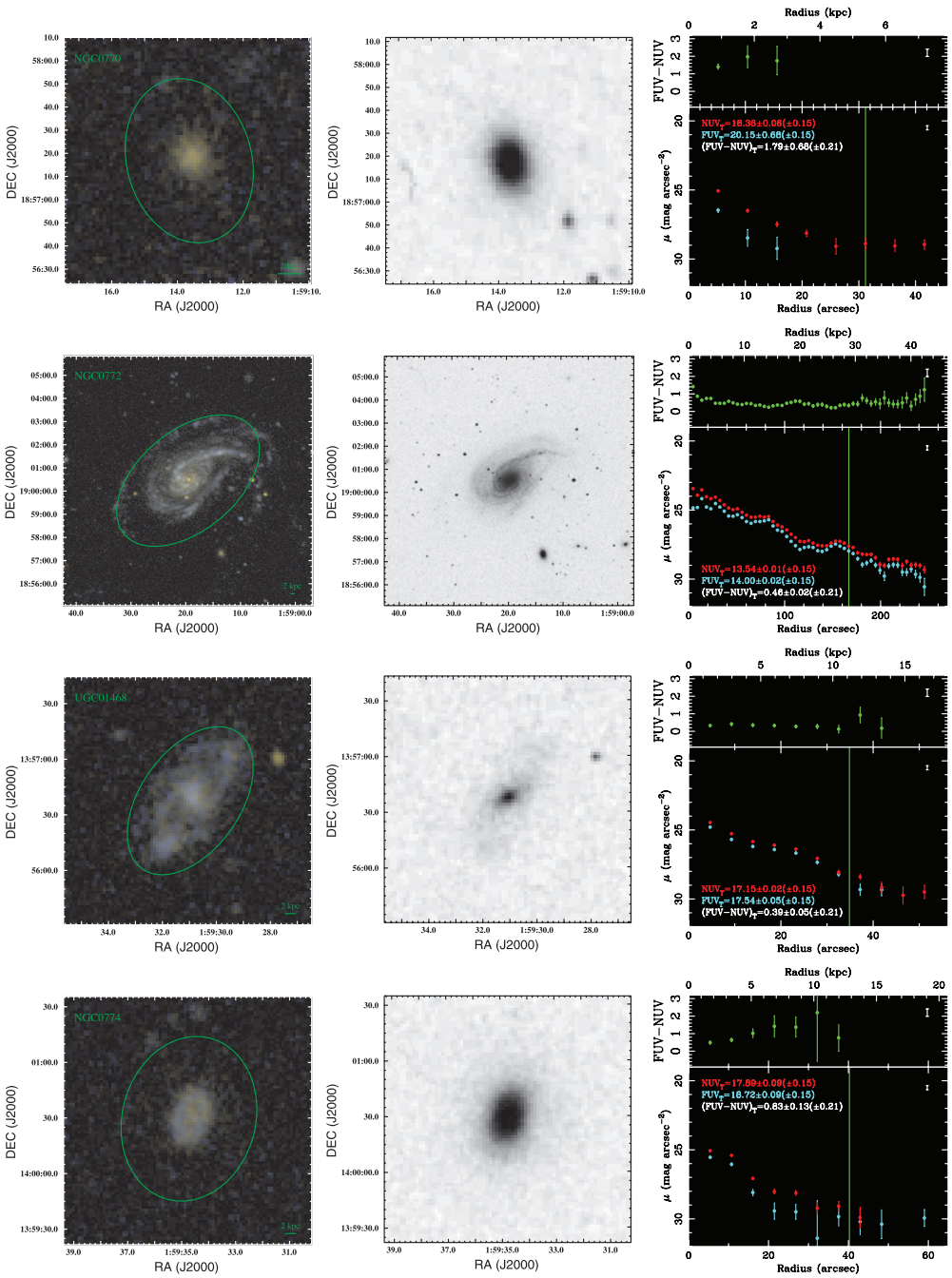

FIG. 3—*Continued*

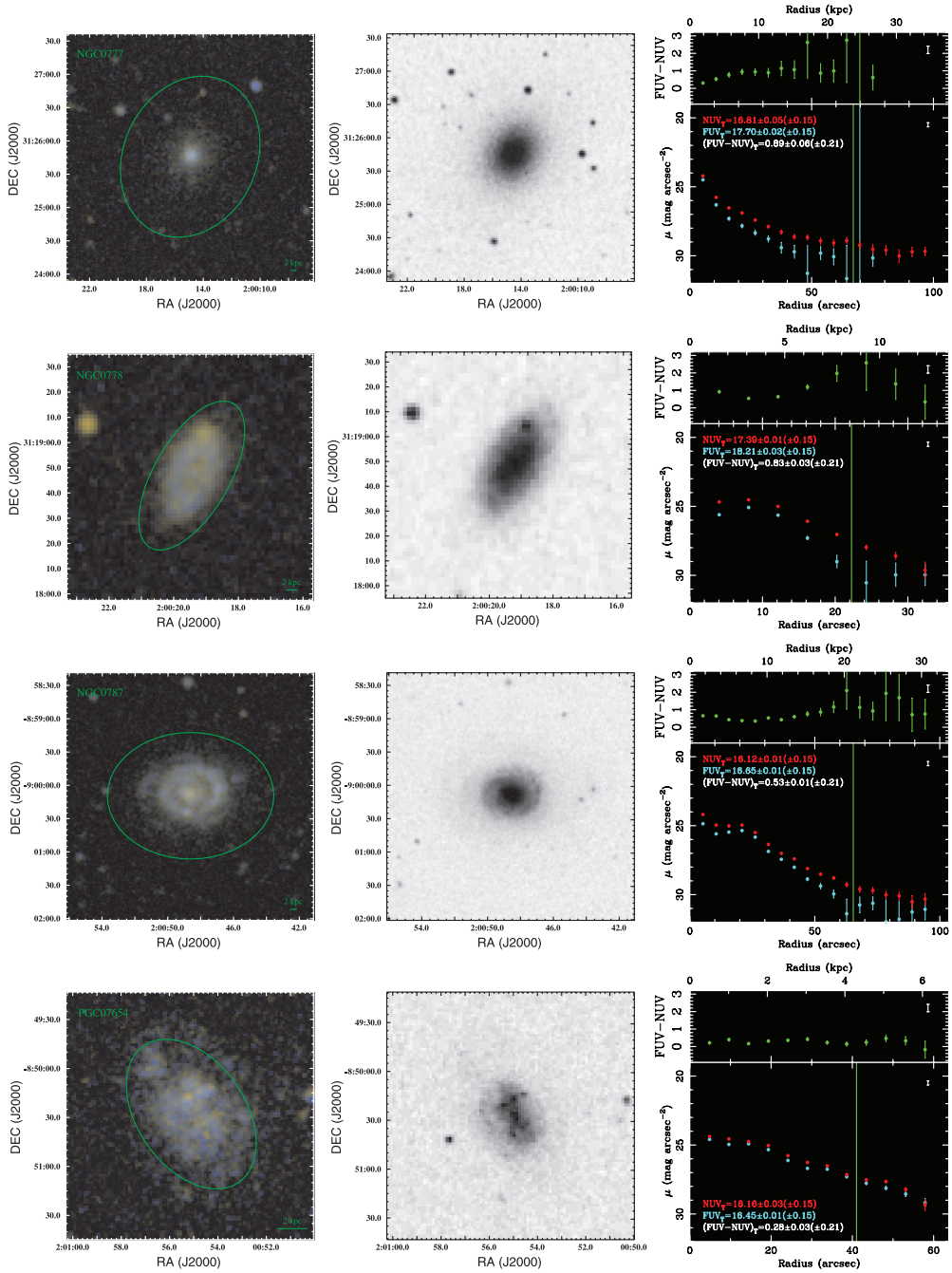

FIG. 3—*Continued*

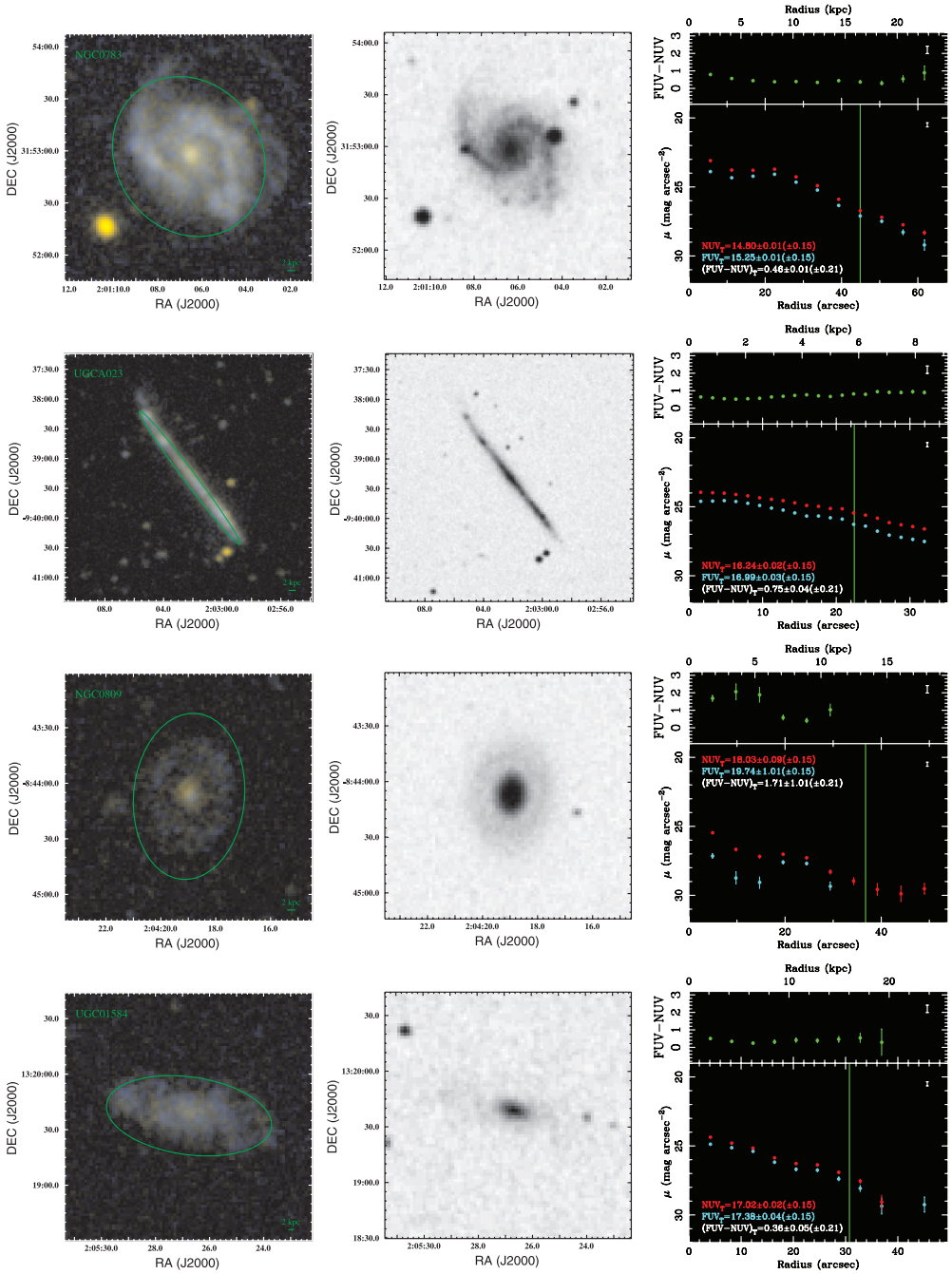

FIG. 3—*Continued*

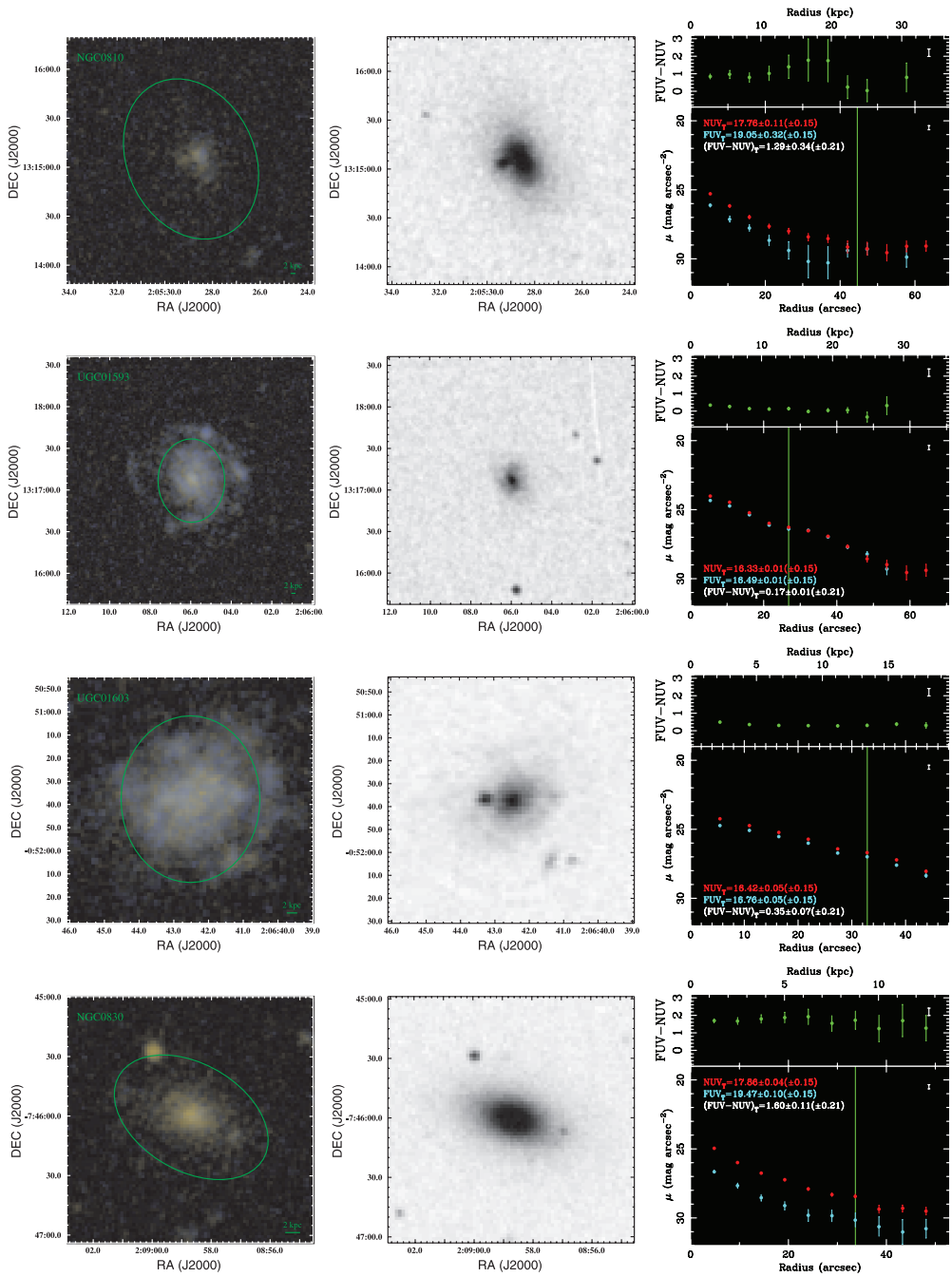

FIG. 3—*Continued*

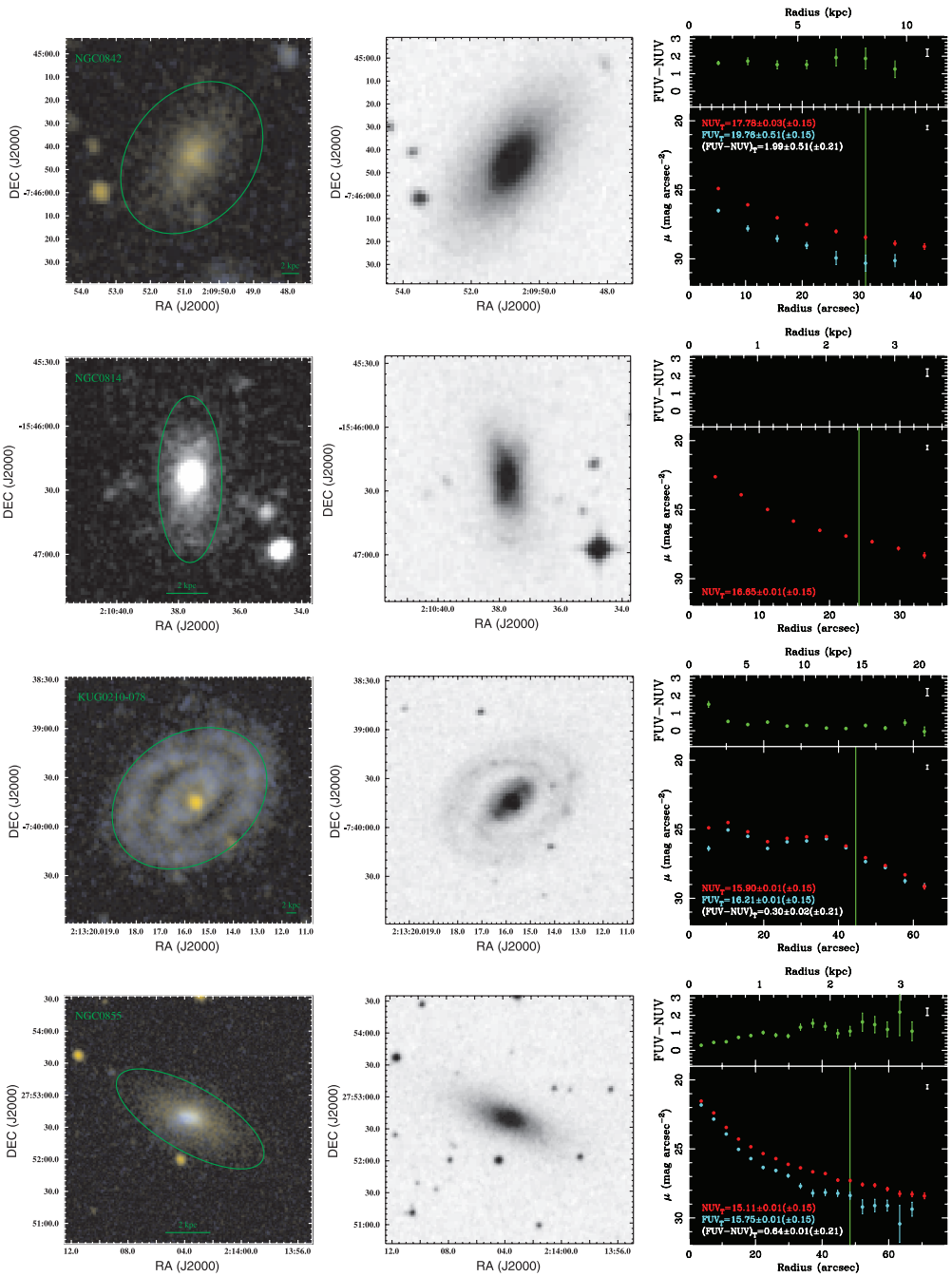

FIG. 3—*Continued*

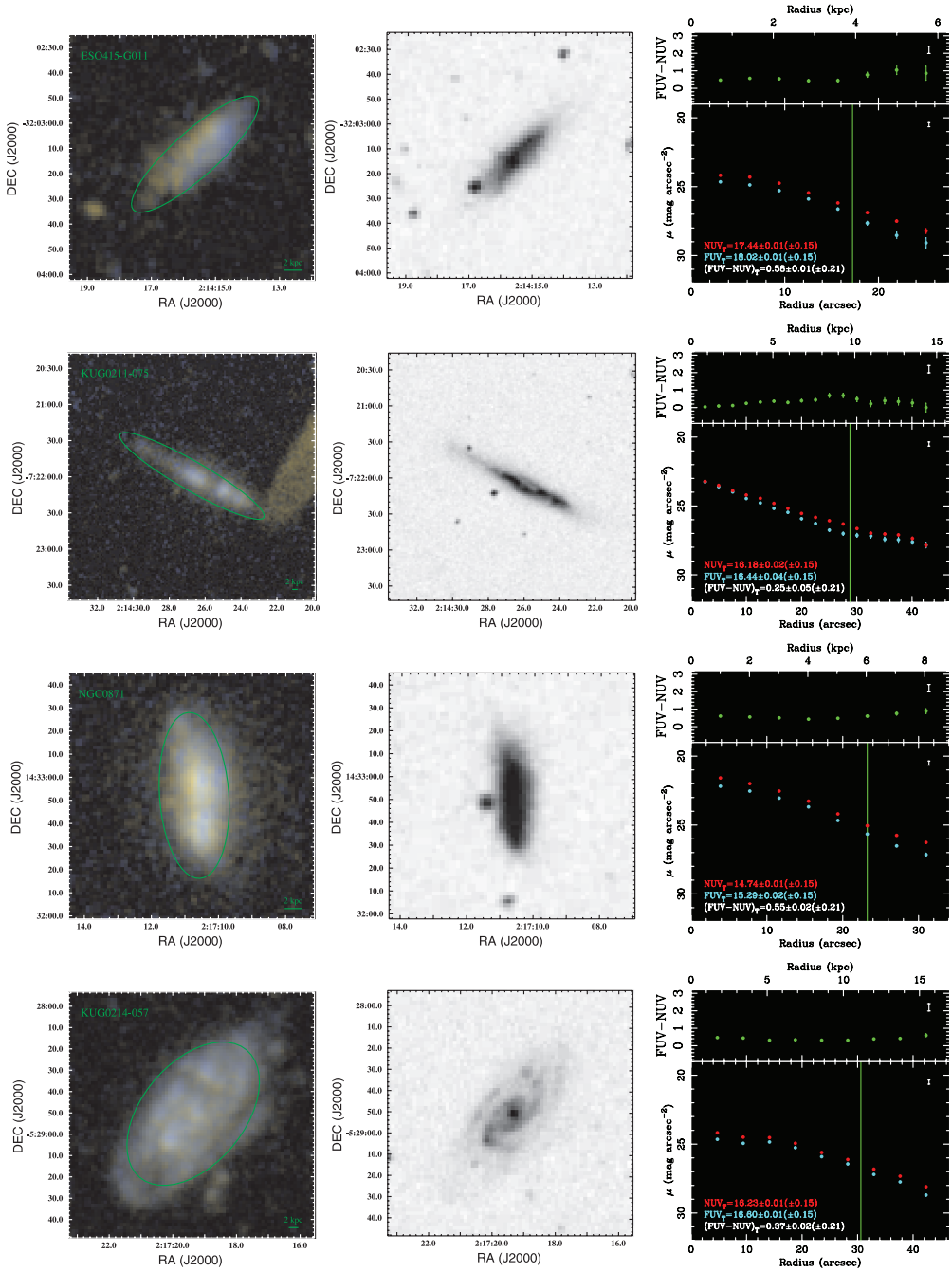

FIG. 3—*Continued*

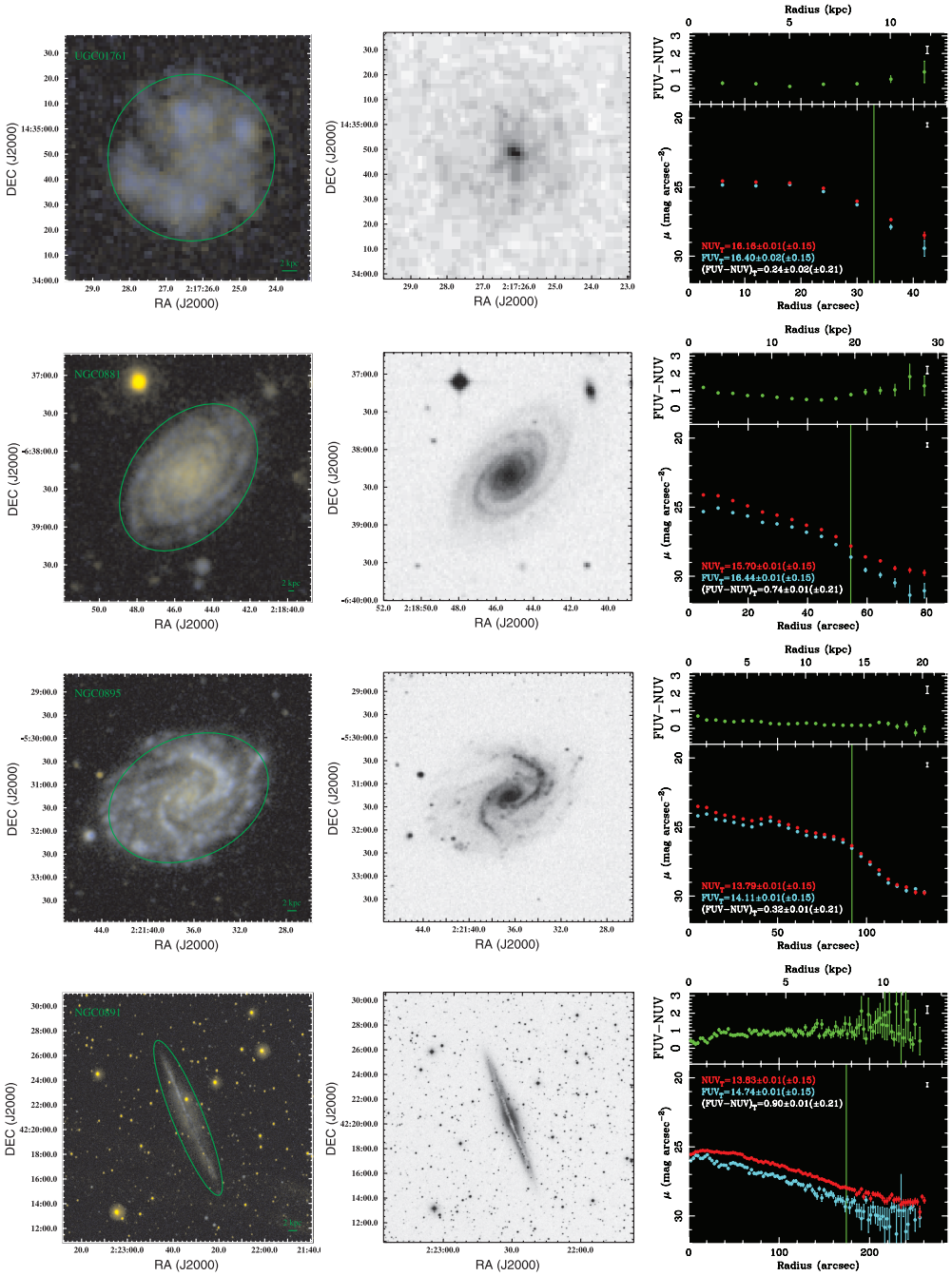

FIG. 3—*Continued*

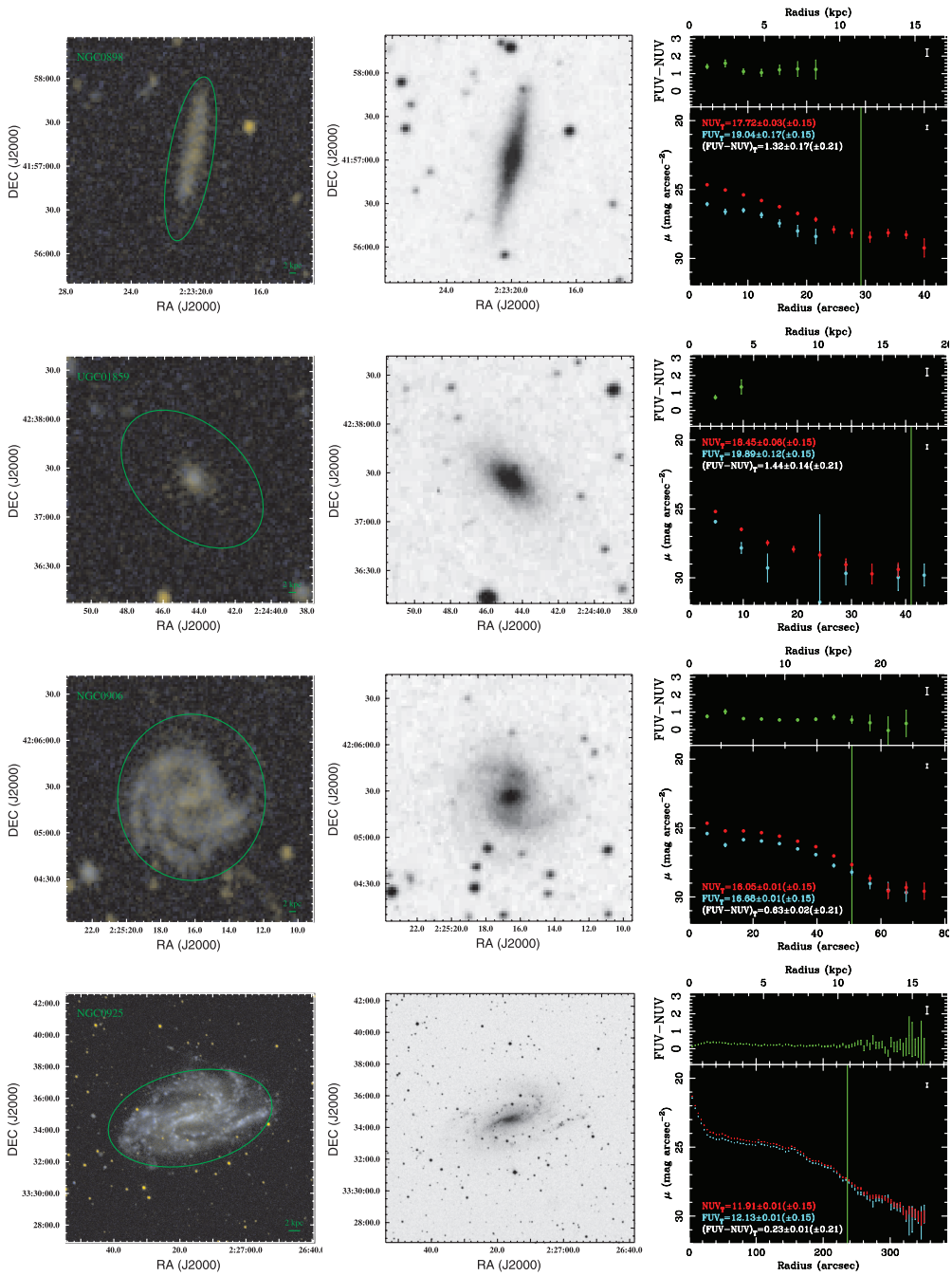

FIG. 3—*Continued*

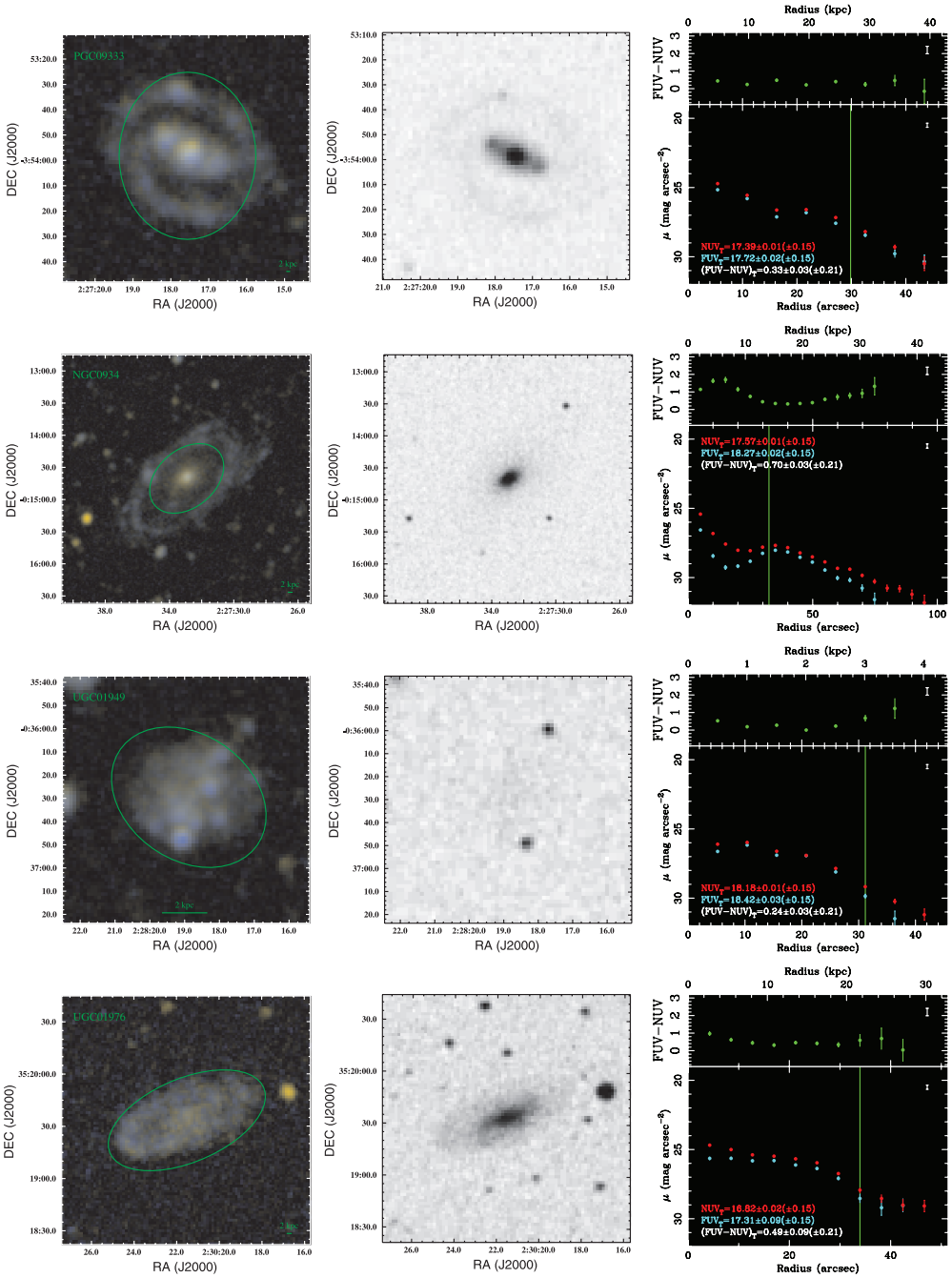

FIG. 3—*Continued*

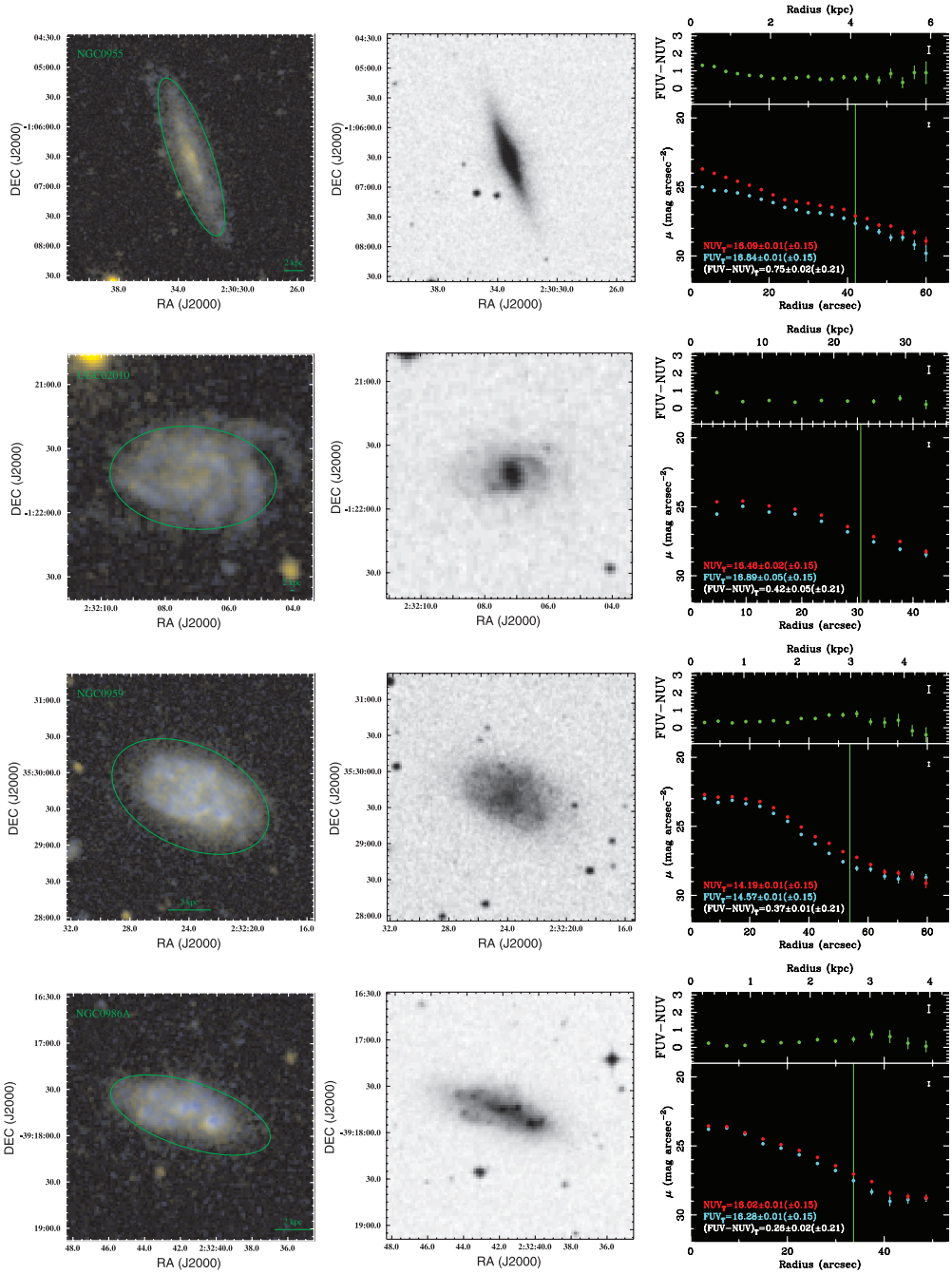

FIG. 3—*Continued*

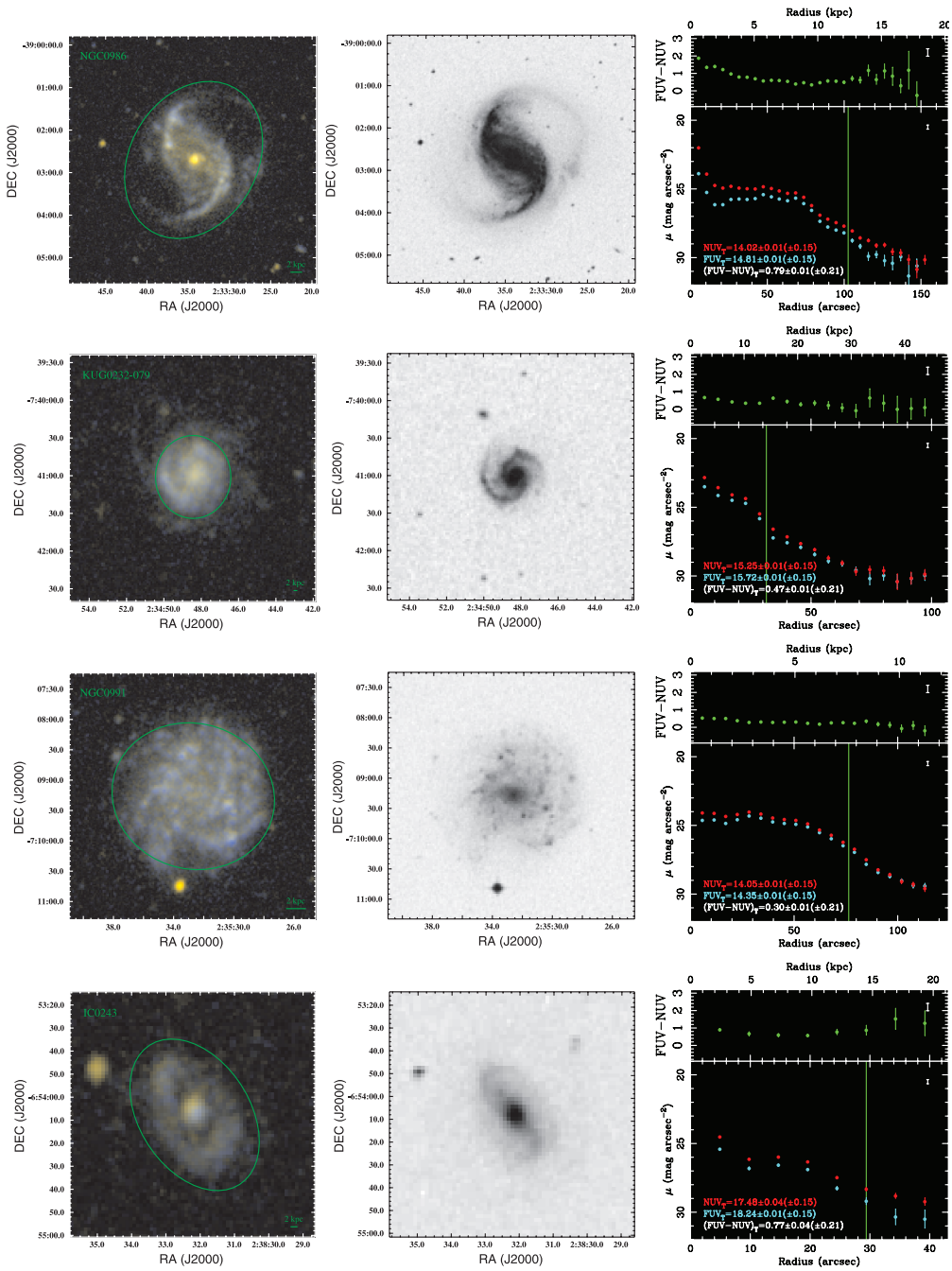

FIG. 3—*Continued*

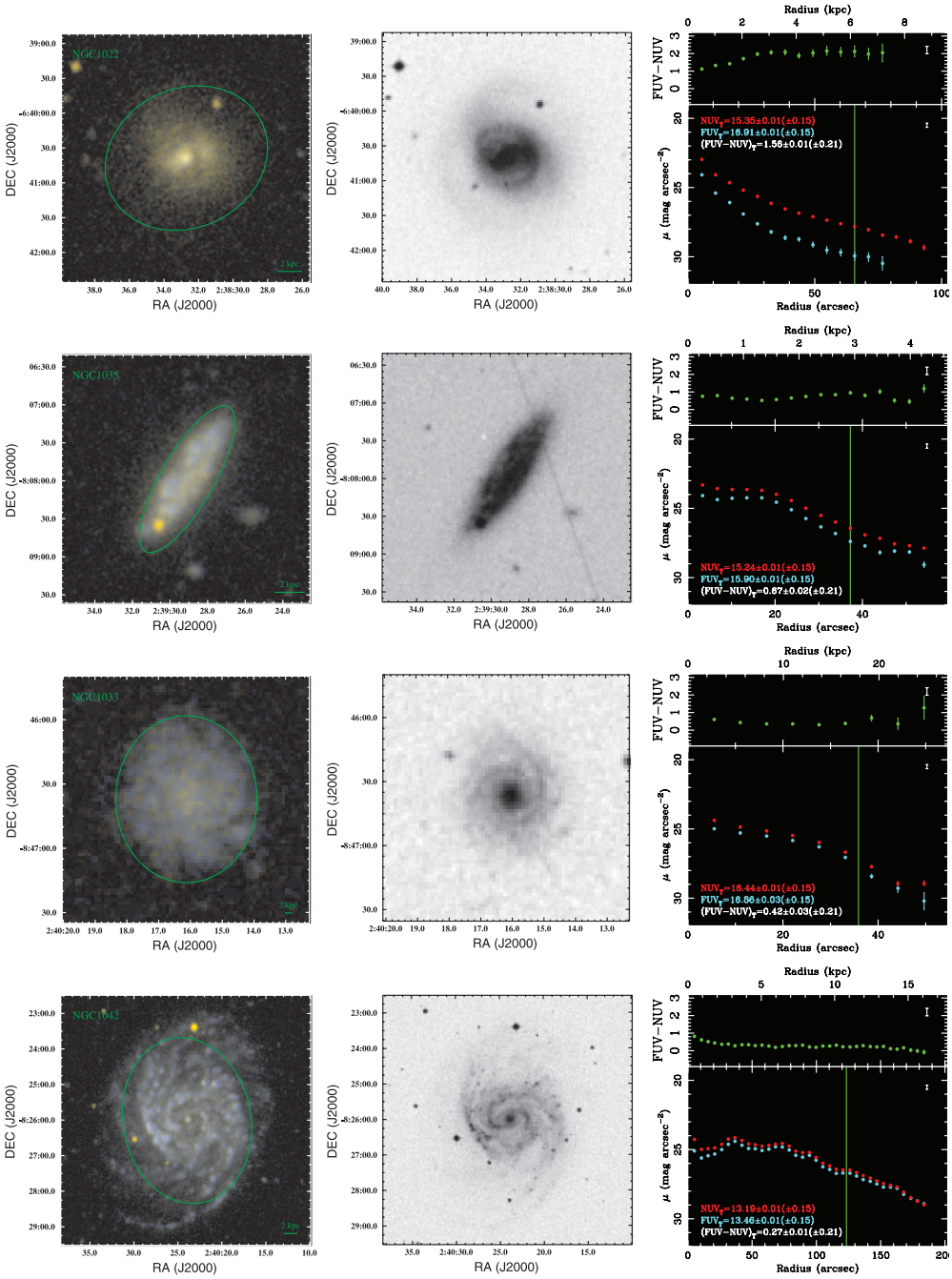

FIG. 3—*Continued*

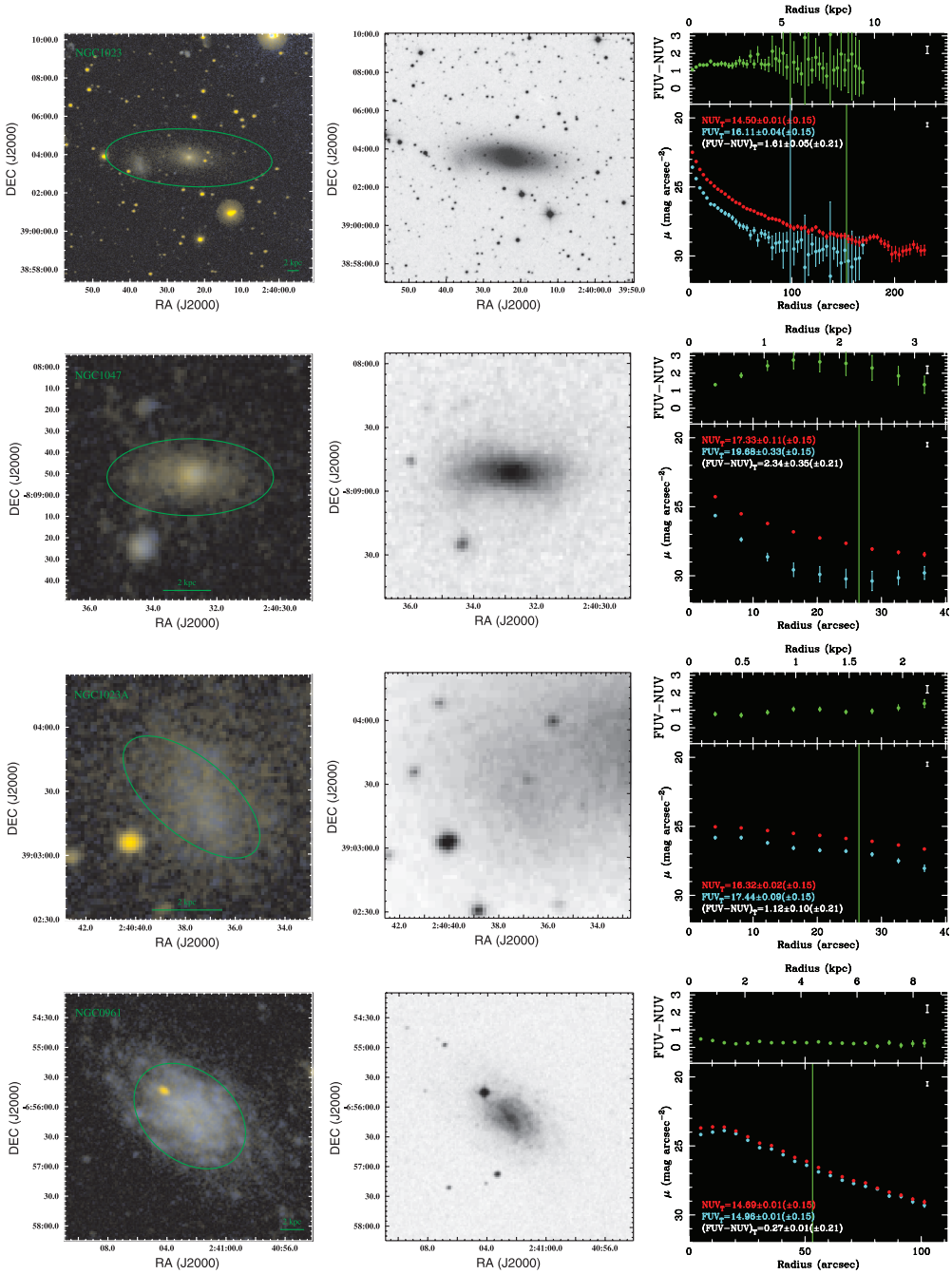

FIG. 3—*Continued*

TABLE 3
OBSERVED UV MAGNITUDES AND COLORS

OBJECT NAME (1)	ASYMPTOTIC MAGNITUDES AND COLOR			D25 MAGNITUDES AND COLOR			FOREGROUND EXTINCTION	
	FUV (mag) (2)	NUV (mag) (3)	FUV − NUV (mag) (4)	FUV (mag) (5)	NUV (mag) (6)	FUV − NUV (mag) (7)	$A_{FUV,MW}$ (mag) (8)	$A_{NUV,MW}$ (mag) (9)
WLM	12.76 ± 0.01	12.64 ± 0.01	0.13 ± 0.01	12.83 ± 0.01	12.72 ± 0.01	0.12 ± 0.01	0.29	0.30
NGC 7808	17.83 ± 0.03	17.11 ± 0.03	0.72 ± 0.04	17.86 ± 0.05	17.22 ± 0.02	0.64 ± 0.05	0.34	0.34
UGC 00017	17.24 ± 0.03	16.85 ± 0.01	0.39 ± 0.03	17.39 ± 0.02	17.03 ± 0.01	0.35 ± 0.03	0.38	0.38
PGC 00282	16.57 ± 0.04	16.31 ± 0.02	0.26 ± 0.04	16.64 ± 0.02	16.39 ± 0.01	0.25 ± 0.03	0.28	0.28
NGC 0024	14.20 ± 0.01	13.91 ± 0.01	0.29 ± 0.01	14.32 ± 0.01	14.03 ± 0.01	0.29 ± 0.01	0.16	0.16
UGC 00128	17.01 ± 0.04	16.83 ± 0.02	0.17 ± 0.04	17.15 ± 0.03	17.03 ± 0.02	0.11 ± 0.03	0.50	0.50
NGC 0055	10.30 ± 0.01	10.01 ± 0.01	0.29 ± 0.01	10.36 ± 0.01	10.07 ± 0.01	0.29 ± 0.01	0.10	0.10
Arp 256 NED 02	16.11 ± 0.01	15.68 ± 0.01	0.44 ± 0.02	16.37 ± 0.01	15.92 ± 0.01	0.46 ± 0.02	0.28	0.29
Arp 256 NED 01	16.13 ± 0.03	15.72 ± 0.04	0.43 ± 0.05	16.22 ± 0.01	15.83 ± 0.01	0.40 ± 0.02	0.28	0.29
UGC 00226	17.16 ± 0.02	16.83 ± 0.01	0.32 ± 0.03	17.25 ± 0.02	16.92 ± 0.01	0.32 ± 0.02	0.51	0.51

NOTES.—Col. (1): Galaxy name. Col. (2): Observed asymptotic FUV magnitude in AB scale. The errors quoted correspond to the error in the fit to the growth curve alone. The error in the FUV and NUV zero-point calibration is estimated to be ∼0.15 mag in each band. Col. (3): The same for the NUV. Col. (4): Observed asymptotic (FUV − NUV) color computed as the difference between col. (2) and col. (3). Cols. (5)–(7): The same as cols. (2)–(4) for the aperture magnitudes within the D25 ellipse. Col. (8): Foreground Milky Way extinction in the FUV band in magnitudes. Col. (9): Foreground Milky Way extinction in the NUV band in magnitudes. Table 3 is available in its entirety in the electronic edition of the *Astrophysical Journal Supplement*. A portion is shown here for guidance regarding its form and content.

respectively) that were used to compute the concentration indices C31 (de Vaucouleurs 1977) and C42 (Kent 1985) in both UV bands. These indices are defined as

$$\mathrm{C31} = \frac{r_{75}}{r_{25}}, \tag{1}$$

$$\mathrm{C42} = 5 \log\left(\frac{r_{80}}{r_{20}}\right). \tag{2}$$

4.4. *Morphological Classification of the UV Profiles*

We have visually classified the UV surface brightness profiles shown in Figure Set 3 according to their shape. Since most of the profiles (especially in spiral and irregular galaxies) show two distinct regions, our classification scheme uses two letters: the first letter describing the shape of the outer profile and the second one describing the shape of the inner region. In a few cases where we find an excess or depression associated with the nucleus of the galaxy we add a final suffix "n" (*nucleated*) or "h" (*hole*), respectively, to the corresponding morphological class. Also in galaxies showing obvious extended UV emission (XUV; Thilker et al. 2005; Gil de Paz et al. 2005b) the morphological class is preceded by the letter "x" (*extended*). The classes assigned are given in column (16) of Table 4. Those galaxies that are barely resolved by our *GALEX* observations have no such classes assigned. The codes used for the morphological classification of the outer region are "E" for exponential, "V" for a de Vaucouleurs profile, or "?" if there are not enough points in the outer profile to determine which of the two previous laws works best. In the case of the inner profile we use "E" or "V" if the profile is a smooth continuation of the corresponding outer profile or if there is a transition from a "E" profile in the outer parts to "V" in the inner regions, "F" for a flattening of the profile toward the inner regions, "D" for a profile falling in brightness toward the center, and finally, "R" for a profile moderately rising in brightness over what it would be expected from and inward extrapolation of the outer profile law. The letter describing the shape of the inner profile appears in lower case if the radial extension of the inner profile is significantly smaller than that of outer profile. In this scheme galaxies with pure de Vaucouleurs (exponential) profiles would be classified as VV (EE) type. Note that the majority of the galaxies in this Atlas are extracted from *GALEX* fields of similar depth (∼1 orbit) that were obtained as part of the Nearby Galaxies Survey (NGS) or the Medium-deep Imaging Survey (MIS). In the majority of the cases the same classification does apply to both the FUV and NUV profiles. In the few cases where the profiles differ enough to be placed in different classes we give first the FUV and then the NUV morphological class separated by a comma (e.g., NGC 1055, NGC 1386, NGC 1546).

4.5. *Corollary Data*

In order to compare the UV properties of the galaxies in this Atlas with those known from previous multiwavelength surveys we have compiled a large amount of corollary data on this sample (see Table 5). Of the 1034 galaxies in the Atlas a total of 871 (84%) have asymptotic *B*-band photometry available in RC3. We primarily used the B_T magnitude and only when B_T was unavailable we made use of the m_B magnitude instead. A total of 318 (393) galaxies also have asymptotic U (V) magnitudes published in RC3.

In addition we have also compiled integrated *JHK* magnitudes from 2MASS. In the first instance we adopted the JHK_{tot} magnitudes from the 2MASS Large Galaxy Atlas (LGA) of Jarrett et al. (2003). For those objects not in the 2MASS LGA we used the total JHK_{total} magnitudes given in the Final Release of the 2MASS Extended Source Catalog (XSC). A total of 853 galaxies in the Atlas had *K*-band data available.

The optical and near-infrared magnitudes given in Table 5 are observed values. The corresponding Galactic extinction-corrected magnitudes were derived using the color excesses given in Table 1 and the extinction law of Cardelli et al. (1989) for $R_V = 3.1$.

Finally, we compiled *IRAS* photometry using data from (in order of priority) Rice et al. (1988), J. Knapp (1994, private communication), the *IRAS* Point Source Catalog (PSC), and Moshir et al. (1990). A total of 459 galaxies had *IRAS* detections at both 60 and 100 μm. These two bands are required in order to estimate the total infrared emission of the galaxy and from it the total

TABLE 4

Foreground-Extinction–corrected UV Properties

	Asymptotic Magnitudes and Color			D25 Magnitudes and Color			$\log L$		Effective Radii		C31		C42		UV
Object Name	FUV (mag)	NUV (mag)	FUV − NUV (mag)	FUV (mag)	NUV (mag)	FUV − NUV (mag)	FUV (W)	NUV (W)	FUV (arcsec)	NUV (arcsec)	FUV	NUV	FUV	NUV	profile
(1)	(2)	(3)	(4)	(5)	(6)	(7)	(8)	(9)	(10)	(11)	(12)	(13)	(14)	(15)	(16)
WLM	12.47 ± 0.01	12.34 ± 0.01	0.13 ± 0.01	12.54 ± 0.01	12.42 ± 0.01	0.12 ± 0.01	33.93	33.80	90.89	92.77	2.11	2.15	1.97	2.08	EF
NGC 7808	17.49 ± 0.03	16.77 ± 0.03	0.72 ± 0.04	17.52 ± 0.05	16.88 ± 0.02	0.64 ± 0.05	36.13	36.24	...	...	...	...	...	...	EE
UGC 00017	16.86 ± 0.03	16.47 ± 0.01	0.39 ± 0.03	17.01 ± 0.02	16.65 ± 0.01	0.35 ± 0.03	34.44	34.42	31.81	32.48	2.32	2.52	2.37	2.61	EF
PGC 00282	16.29 ± 0.04	16.03 ± 0.02	0.26 ± 0.04	16.36 ± 0.02	16.11 ± 0.01	0.25 ± 0.03	36.83	36.76	14.55	14.43	...	...	...	...	ED
NGC 0024	14.04 ± 0.01	13.75 ± 0.01	0.29 ± 0.01	14.16 ± 0.01	13.87 ± 0.01	0.29 ± 0.01	35.15	35.09	35.98	36.16	2.74	2.73	2.71	2.71	Ef
UGC 00128	16.51 ± 0.04	16.33 ± 0.02	0.18 ± 0.04	16.65 ± 0.03	16.53 ± 0.02	0.12 ± 0.03	35.98	35.88	32.48	32.78	2.29	2.40	2.27	2.41	EFn
NGC 0055	10.20 ± 0.01	9.91 ± 0.01	0.29 ± 0.01	10.26 ± 0.01	9.97 ± 0.01	0.29 ± 0.01	35.46	35.40	155.54	149.95	2.80	2.87	2.79	2.79	EE
Arp 256 NED 02	15.83 ± 0.01	15.39 ± 0.01	0.44 ± 0.02	16.09 ± 0.01	15.63 ± 0.01	0.46 ± 0.02	36.73	36.73	11.48	11.36	...	...	...	...	Er
Arp 256 NED 01	15.85 ± 0.03	15.43 ± 0.04	0.43 ± 0.05	15.94 ± 0.01	15.54 ± 0.01	0.40 ± 0.02	36.72	36.71	...	...	...	...	...	...	ER
UGC 00226	16.65 ± 0.02	16.32 ± 0.01	0.33 ± 0.03	16.74 ± 0.02	16.41 ± 0.01	0.33 ± 0.02	36.05	36.00	...	...	...	...	...	...	...

Notes.—Col. (1): Galaxy name. Col. (2): Asymptotic FUV magnitude in AB scale corrected for Galactic extinction. The errors quoted correspond to the error in the fit to the growth curve alone. The error in the FUV and NUV zero-point calibration is estimated to be ∼0.15 mag in each band. Col. (3): The same for the NUV. Col. (4): Asymptotic (FUV − NUV) color computed as the difference between col. (2) and col. (3). Cols. (5)–(7): The same as cols. (2)–(4) for the aperture magnitudes within the D25 ellipse. Col. (8): Logarithm of the FUV luminosity in watts. Col. (9): The same for the NUV. Col. (10); Effective radii [equivalent radius of the ellipse including half of the total (asymptotic) light of the galaxy] in the FUV band measured in arcsec. Col. (11): The same for the NUV. Col. (12): C31 concentration index in the FUV. Col. (13): The same for the NUV. Col. (14): C42 concentration index in the FUV. Col. (15): The same for the NUV. Col. (16): Morphological class of the UV surface brightness profile (see text for details). Note that we only computed the effective radius and concentration index C31 (C42) for those galaxies whose radii containing 50% and 25% (20%), respectively, of the light were larger than $6''$. Table 4 is available in its entirety in the electronic edition of the *Astrophysical Journal Supplement*. A portion is shown here for guidance regarding its form and content.

TABLE 5

COROLLARY PHOTOMETRY DATA (OBSERVED VALUES)

	OPTICAL PHOTOMETRY			NEAR-INFRARED PHOTOMETRY			*IRAS* FLUXES			
OBJECT NAME (1)	*U* (mag) (2)	*B* (mag) (3)	*V* (mag) (4)	*J* (mag) (5)	*H* (mag) (6)	*K* (mag) (7)	12 μm (Jy) (8)	25 μm (Jy) (9)	60 μm (Jy) (10)	100 μm (Jy) (11)
WLM	...	11.03 ± 0.08	10.59 ± 0.09	...	...	...	<0.12	<0.20	0.32 ± 0.08	1.04 ± 0.26
NGC 7808	...	14.33 ± 0.13	13.48 ± 0.13	11.29 ± 0.03	10.65 ± 0.03	10.32 ± 0.04	0.11 ± 0.03	<0.21	0.37 ± 0.05	1.58 ± 0.21
UGC 00017	14.78 ± 0.23	14.80 ± 0.20	14.19 ± 0.22	...	...	...	...	...	...	...
PGC 00282	...	...	...	13.36 ± 0.06	12.76 ± 0.09	12.56 ± 0.13	<0.08	<0.18	0.28 ± 0.06	0.66 ± 0.15
NGC 0024	12.12 ± 0.13	12.19 ± 0.13	11.61 ± 0.13	9.71 ± 0.02	9.11 ± 0.03	8.95 ± 0.04	<0.13	0.16 ± 0.04	1.26 ± 0.14	3.59 ± 0.40
UGC 00128	...	...	...	...	...	...	...	...	...	...
NGC 0055	8.54 ± 0.06	8.42 ± 0.05	7.87 ± 0.06	6.98 ± 0.03	6.55 ± 0.04	6.25 ± 0.05	1.34 ± 0.20	6.25 ± 0.94	77.00 ± 11.60	174.00 ± 26.10
Arp 256 NED 02	...	...	13.60 ± 0.30	12.69 ± 0.05	12.35 ± 0.09	11.82 ± 0.09	...	...	...	...
Arp 256 NED 01	...	14.81 ± 0.13	14.33 ± 0.13	12.44 ± 0.03	11.70 ± 0.04	11.34 ± 0.05	...	...	...	...
UGC 00226	...	14.81 ± 0.18	...	12.96 ± 0.05	12.26 ± 0.08	11.95 ± 0.09	<0.09	<0.10	0.41 ± 0.05	1.11 ± 0.29

NOTES.—Col. (1): Galaxy name. Col. (2): Johnson-*U* integrated magnitude (in the Vega scale) published as part of RC3. Col. (3): The same for the Johnson-*B* band. Col. (4): The same for the Johnson-*V* band. Col. (5): 2MASS *J*-band total magnitude. Col. (6): The same for the *H* band. Col. (7): The same for the *K* band. Col. (8): Published 12 μm *IRAS* fluxes (in Jy) and upper limits. Col. (9): The same for the 25 μm fluxes. Col. (10): The same for the 60 μm fluxes. Col. (11): The same for the 100 μm fluxes. Table 5 is available in its entirety in the electronic edition of the *Astrophysical Journal Supplement.* A portion is shown here for guidance regarding its form and content.

energy budget by means of its comparison with the UV flux (see, e.g., Dale et al. 2001).

5. RESULTS

5.1. *Global Statistical Properties*

In Figure 4 we show the frequency histograms of the asymptotic FUV and NUV AB magnitudes, FUV luminosity and (FUV − NUV) (both asymptotic and at the D25 aperture) color. Heckman et al. (2005) have recently shown that galaxies with FUV luminosities brighter than 2×10^{10} $L_{\odot}$ (7.6×10^{36} W or $M_{\rm FUV} = -19.87$) (also known as ultraviolet-luminous galaxies or UVLGs) are extremely rare in our local universe. Their comoving space density is only $\sim 10^{-5}$ Mpc^{-3}, i.e., several hundred times lower than that of their $z = 3$ counterparts, the Lyman break galaxies (LBG). Indeed, only four galaxies in the Atlas (see Fig. 4*c*) would be classified as UVLGs: two active galactic nuclei, NGC 7469 and Mrk 501, and two actively star-forming interacting systems, the Cartwheel (see, e.g., Amram et al. 1998) and UGC 06697 (Gavazzi et al. 2001).

The color distribution of Figure 4*d* shows a pronounced peak at (FUV − NUV) $\simeq$ 0.4 mag and a long tail extending to very red colors. As we will show later, this red tail is, not unexpectedly, mostly populated by elliptical galaxies of intermediate mass that show little recent star formation activity and a weak UV upturn (see Boselli et al. 2005). This figure also shows the distribution of effective radii both in arcsec (Fig. 4*e*) and in kiloparsecs (Fig. 4*f*). The distribution of effective radii is very similar for the FUV and the NUV. Due to the limited spatial resolution of the *GALEX* data we only computed the effective radius of galaxies for which the semimajor axis of the ellipse including 50% of the light was larger than 6″ in radius. This fact, along with the lower limit in optical diameter (1′) imposed by the completeness of RC3, results in a paucity of compact galaxies and a relatively narrow distribution in apparent effective radius peaking at $\sim$15″. The distribution in physical size (Fig. 4*f*), on the other hand, is significantly wider with a peak around 5–6 kpc.

The distributions of the concentration indices C31 and C42 (Figs. 4*h* and 4*i*, respectively) are also very narrow with the galaxies being slightly more concentrated (i.e., larger values of C31 and C42) in the NUV than in the FUV (see Figs. 4*j* and 4*k* for a comparison between the value of these indices in the two bands). This is probably a consequence of the fact that in the NUV a significant fraction of the light in spiral galaxies still arises from within the bulge component, while in the FUV this contribution is in many cases negligible.

5.2. *Properties by Morphological Type*

The *GALEX* FUV and NUV observations presented here, along with the corresponding corollary data in the optical, NIR, and FIR provides us with an unprecedented set of multiwavelength data for a large population of galaxies in the local universe. One of the first questions that can be addressed using this sample concerns the relation between the qualitative (optical) morphology of these galaxies and more quantitative properties, such as colors, luminosities, total-infrared-to-UV ratios, etc. In Figure 5 we show the colors of the galaxies as a function of the blue-light morphological type as given by RC3. Figures 5*a* and 5*b* show that, although late-type spiral and irregular galaxies are somewhat bluer in $(B - V)$ and $(B - K)$ than ellipticals and early-type spirals, these colors are not unique to a given type. In particular, these colors cannot be used to unambiguously discriminate between different kinds of spiral galaxies nor even between elliptical/lenticular galaxies and spirals. As indicated by Roberts & Haynes (1994), the significant overlap in $(B - V)$ color between spiral galaxies of different types is mostly due to true variations in the optical colors and star-formation history of galaxies of same morphological type, not to misclassification or observational errors. The equivalent to the Figure 5*b* for late-type Virgo cluster galaxies was obtained by Boselli et al. (1997). These authors obtained a large overlap in $(B - K)$ color between different morphological types as well.

However, thanks to the extreme sensitivity of the FUV data to the presence of very low levels of recent star formation activity, the use of the (FUV − K) color turns out to be a very powerful discriminant between quiescent elliptical and lenticular galaxies, and star-forming spirals. In particular, an observed (FUV − K) color of 8.8 mag provides an excellent discrimination point between these two groups (see Fig. 5*c*). In this sense, of all the elliptical/lenticular galaxies in the Atlas with both FUV and K-band data available, only 23% of them show a (FUV − K) color bluer than this threshold. It is worth noting that significant a fraction of these are known to host some residual star formation activity (e.g., NGC 3265, Condon et al. 2002; NGC 0855, Wiklind et al. 1995) or are low-luminosity ellipticals with obvious star formation activity like NGC 1510 (Marlowe et al. 1999). Spiral and irregular galaxies with (FUV − K) colors redder than this value only represent 9% of the total.

Although with significantly degraded discriminating capabilities compared to the (FUV − K) color, the (NUV − K) is also well correlated with the morphological type (see Fig. 5*d*). The same can be said about the (FUV − NUV) color, where a cutoff at (FUV − NUV) = 0.9 mag provides a relatively clean separation of elliptical/lenticular galaxies from spirals (Fig. 5*e*). The fraction of elliptical/lenticular galaxies with (FUV − NUV) color bluer than 0.9 mag (and both FUV and NUV magnitudes available) is 18%, while the percentage of spiral and irregulars redder than this value is only 12%. Note that in this case the far left lower corner of the diagram may be populated both by ellipticals with residual star formation and also by elliptical galaxies with a strong UV upturn (Deharveng et al. 2002 and references therein). The best linear fits derived for the correlation of observed colors with the morphological type for spirals and irregulars (types T > -0.5) are

$$(\mathrm{FUV} - K) = 7.97 - 0.48 \times \mathrm{T}; \quad \sigma = 1.36 \text{ mag}; \tag{3}$$

$$(\mathrm{NUV} - K) = 7.07 - 0.40 \times \mathrm{T}; \quad \sigma = 1.14 \text{ mag}; \tag{4}$$

$$(\mathrm{FUV} - \mathrm{NUV}) = 0.854 - 0.066 \times \mathrm{T}; \quad \sigma = 0.32 \text{ mag}. \tag{5}$$

These relations are shown in Figures 5*c*, 5*d*, and 5*e*. Note that, although the rms of the fit for the (FUV − NUV) color is smaller than for (FUV − K) this is purely a consequence of the much smaller dynamic range of the (FUV − NUV) color (1 mag) compared with the (FUV − K) color ($\sim$6 mag) (see Fig. 5*c*). The corresponding best fits in the type T versus color diagrams are (only galaxies with types T < 13 are considered)

$$\mathrm{T} = 11.2\text{–}1.28 \times (\mathrm{FUV} - K); \quad \sigma = 2.4 \text{ (units of T)}; \tag{6}$$

$$\mathrm{T} = 12.1\text{–}1.62 \times (\mathrm{NUV} - K); \quad \sigma = 2.5 \text{ (units of T)}; \tag{7}$$

$$\mathrm{T} = 8.4\text{–}8.5 \times (\mathrm{FUV} - \mathrm{NUV}); \quad \sigma = 3.0 \text{ (units of T)}. \tag{8}$$

These fits are valid only for colors (FUV − K) < 8.8 mag, (NUV − K) < 7.9 mag, and (FUV − NUV) < 0.9 mag, respectively.

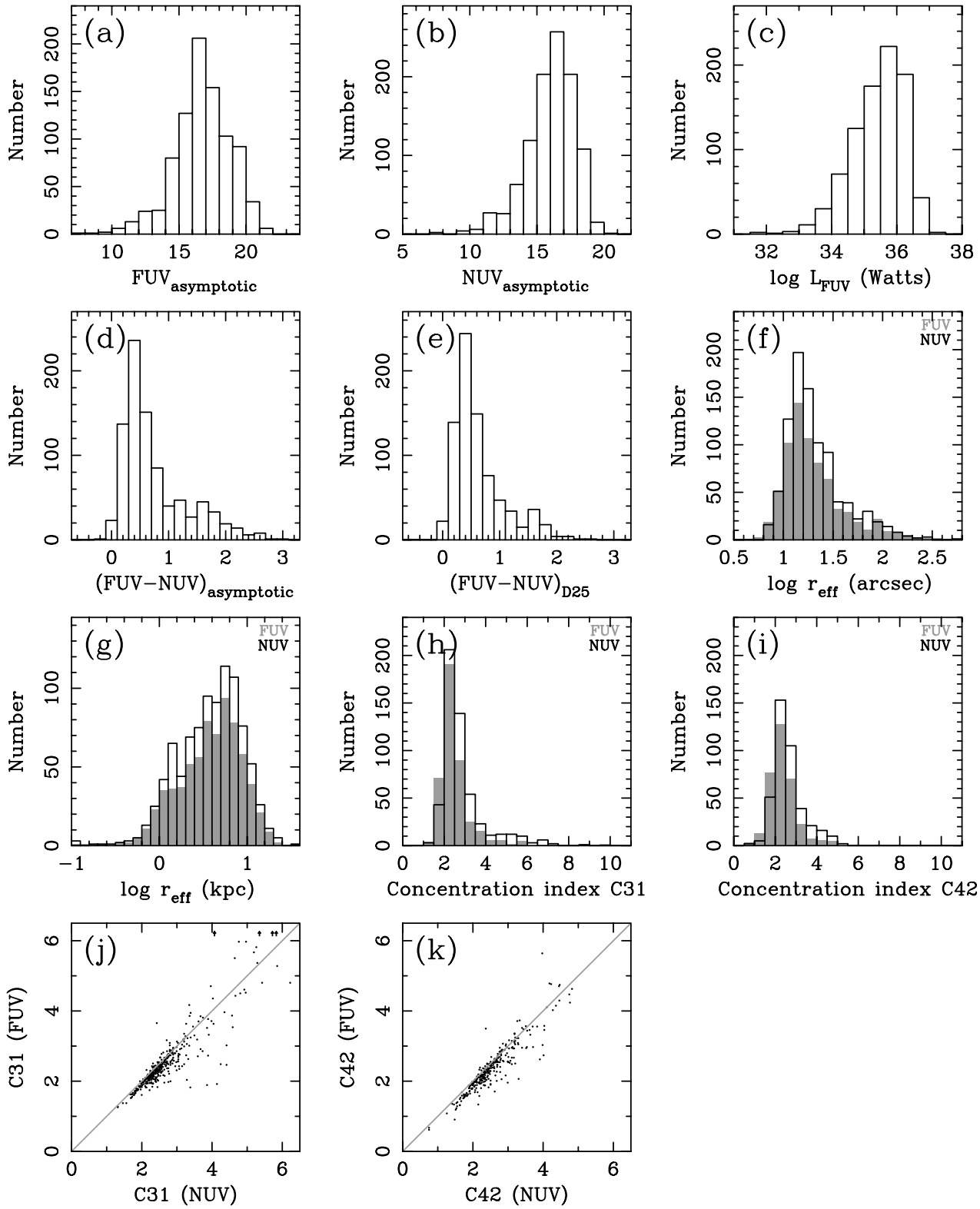

FIG. 4.— UV properties of the galaxies in the Atlas. (*a*) Frequency histogram of apparent asymptotic FUV magnitudes (AB scale). (*b*) Apparent asymptotic NUV magnitudes. (*c*) FUV luminosity in watts computed as νF_ν (see Buat et al. 2005). (*d*) (FUV − NUV) color. (*e*) (FUV − NUV) color inside the D25 ellipse. (*f*) Effective radius (in arcsec) of the galaxies in the FUV (*gray-shaded histogram*) and NUV (*outlined histogram*). (*g*) The same with the radius in kpc. (*h*) FUV (*gray-shaded histogram*) and NUV (*outlined histogram*) C31 concentration index. (*i*) The same for the C42 concentration index. (*j*) Comparison of the FUV and NUV C31 concentration indices. (*k*) The same for the C42 concentration index.

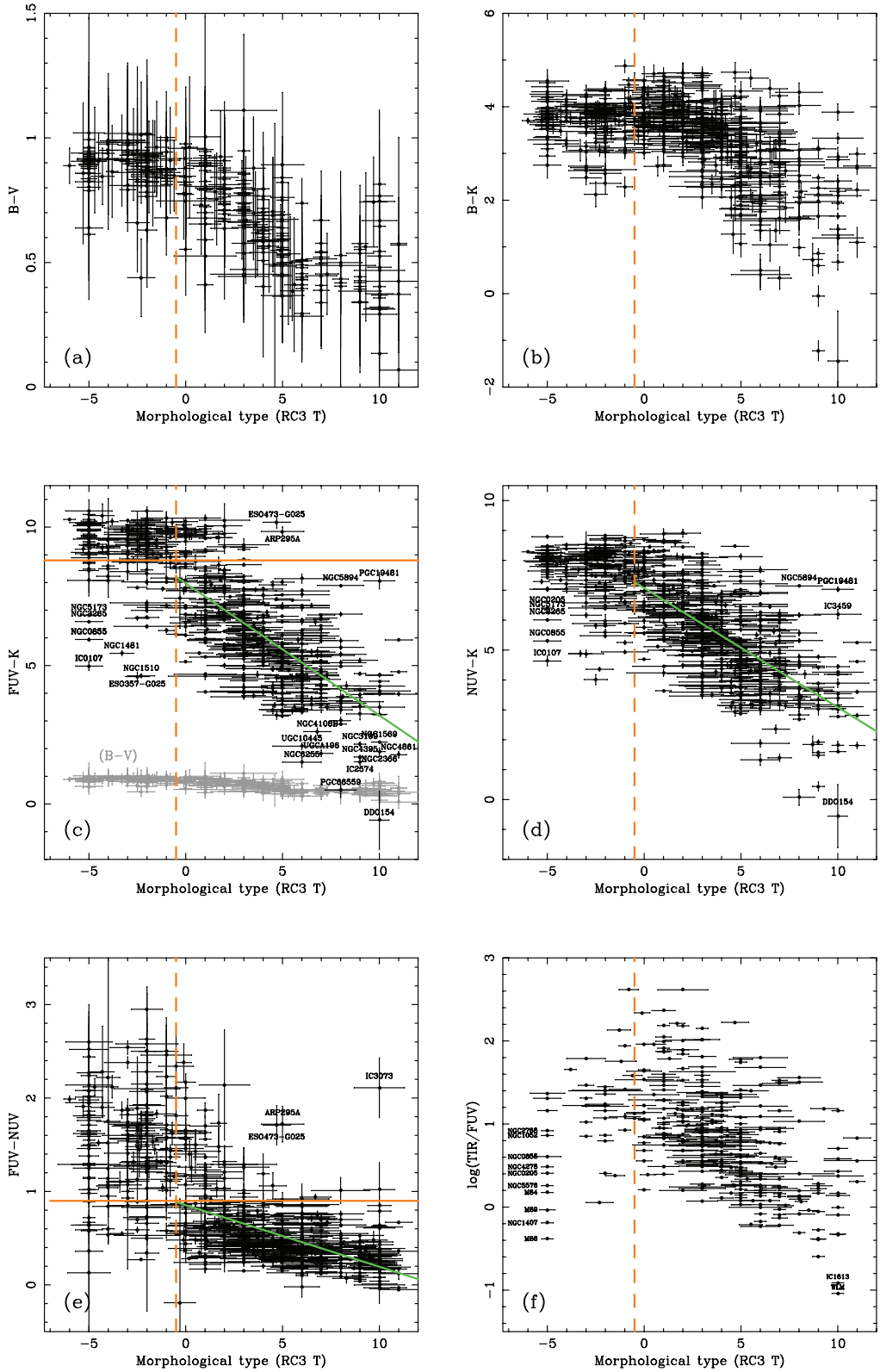

FIG. 5.—Variation in the observed colors and total-infrared (TIR) to FUV ratio of the galaxies in the Atlas with the morphological type (T). (*a*) $(B-V)$ vs. the morphological type for elliptical/lenticular ($T < -0.5$), spiral ($-0.5 \leq T < 9.5$), and irregular/compact galaxies ($T \geq 9.5$). The separation between elliptical/lenticular and the rest is shown by a vertical dashed line. (*b*) The same for $(B-K)$. Note the small segregation in color between the different types when the $(B-V)$ or $(B-K)$ colors are used. (*c*) The same for $(FUV-K)$. The segregation between ellipticals/lenticulars and spirals (*horizontal solid line*) and even between different kind of spiral galaxies is now remarkable. For comparison purposes we show (in the same scale) the range in $(B-V)$ color span by the galaxies in the sample (see panel *a*). (*d*) The same for $(NUV-K)$. (*e*) The same for the $(FUV-NUV)$ color. Note that FUV and NUV magnitudes are in AB scale and optical and NIR magnitudes are in the Vega system. Green lines represent the best linear fit to the data for types $T = -0.5$ or later (i.e., spiral galaxies). (*f*) The same for the TIR-to-FUV ratio (see Buat et al. 2005).

Finally, in Figure 5*f* we compare the total-infrared (TIR) to FUV ratio with the morphological type of the galaxies in the Atlas. The TIR flux was derived using the parameterization of the TIR-to-FIR ratio given by Dale et al. (2001), where FIR is computed from the 60 and 100 μm *IRAS* fluxes as in Lonsdale et al. (1985). The flux in the FUV is expressed in units of νF_ν (see Buat et al. 2005). In the case of spiral and irregular galaxies, for which both the UV and infrared emission are ultimately due to young massive stars, this ratio provides a well-defined estimator of the dust attenuation in the UV (Buat et al. 2005; Cortese et al. 2006). Given the sensitivity limits of the *IRAS* catalog and the low dust content of elliptical and lenticular galaxies the number of these galaxies detected in both the 60 and 100 μm *IRAS* bands is only 49 out of the 225 ellipticals in the Atlas. Figure 5*f* shows that late-type spirals and irregulars tend to show, on average, a lower TIR-to-FUV ratio and consequently smaller attenuation in the UV than that derived for early-type spirals.

5.3. *Color-Magnitude and Color-Color Diagrams*

Although morphology is certainly related with the way galaxies form and evolve, especially when the properties of elliptical and spiral galaxies are compared, the luminosity and even more the mass (either the luminous or total mass) is thought to be the main driving force of the evolution of galaxies through the history of the universe. In this sense, the analysis of color-magnitude diagrams (CMDs) has traditionally provided a fundamental tool for understanding galaxy evolution.

Figures 6*a* and 6*b* show the CMDs in $(\mathrm{FUV}-K)-M_K$ and $(\mathrm{NUV}-K)-M_K$. At the top of these diagrams we find the "red sequence" populated primarily by elliptical and lenticular galaxies (*dots*). In the case of the $(\mathrm{NUV}-K)-M_K$ CMD the red sequence shows a clear slope with lower luminosity galaxies showing bluer colors, especially below $M_K > -23$ mag. A similar behavior is seen when optical or optical-NIR colors are used, both locally and at high redshift (Gladders & Yee 2005). This is commonly explained in terms of lower metal abundances (thus bluer colors) of the stellar populations in low-mass ellipticals as compared to the more massive (higher metallicity) systems (Gladders et al. 1998 and references therein). In the case of the $(\mathrm{FUV}-K)-M_K$ CMD, on the other hand, the distribution of the $(\mathrm{FUV}-K)$ color is rather flat over a range of almost 7 mag in absolute magnitude. The explanation for this different behavior can be found in Figure 6*c*. Here the (FUV − NUV) gets systematically redder as we move to lower luminosities. This is opposite to what is seen in any other colors, and it is probably a consequence of a weaker UV upturn in intermediate-mass ellipticals than in the most luminous and massive ones (see Boselli et al. 2005). Note that, due to the stronger UV upturn toward the centers of elliptical galaxies (Ohl et al. 1998; Rhee et al. 2008, in preparation), the asymptotic colors do not probably show the full strength of the UV upturn in the way aperture colors like those obtained from the analysis of *IUE* spectra do (Burstein et al. 1988).

Dwarf elliptical galaxies have *K*-band absolute magnitudes that are typically fainter than $M_K = -21$ mag. Unfortunately, not many of these more extreme low-luminosity ellipticals are found in the Atlas. This is mainly because dwarf ellipticals in Virgo (where most of the studies on dE have been carried out to date) are typically smaller than $1'$ in size, placing them outside the selection limit imposed on the Atlas. Nevertheless, a recent study by Boselli et al. (2005) suggests that residual star formation might play a leading role in the interpretation of the UV emission from dE galaxies, which would explain their behavior in the CMD (i.e., similar to the behavior seen in low-mass star-forming galaxies). The tendency for the most luminous ellipticals to show bluer (FUV − NUV) colors is even more clear when the FUV-band absolute magnitude is considered (see Fig. 6*e*). However, if the *B*-band luminosity is used, the (FUV − NUV) color seems to be independent of luminosity.

Regarding the properties of spiral (*triangles*) and irregular galaxies (*asterisks*) in these plots we find that the majority of these galaxies are concentrated in a "blue sequence" with high-luminosity spirals (which also tend to be of earlier types) being redder than low-mass spirals and irregular/compact galaxies. This is true for all the observed $(\mathrm{FUV}-K)$, $(\mathrm{NUV}-K)$, and (FUV − NUV) colors (Figs. 6*a*, 6*b*, and 6*c*). There are two mechanisms that may lead to the observed behavior. First, low-luminosity galaxies are known to have lower metallicities (both in the stars and in the gas) than more luminous ones (Salzer et al. 2005 and references therein). This implies that the amount of dust (and reddening of the colors) in low-luminosity galaxies should be lower than in luminous ones.

The $(\mathrm{FUV}-K)$ [$(\mathrm{NUV}-K)$] color is found to span a range of 5 mag (4 mag) in spiral and irregular galaxies of different types and luminosities with a mean value of 5.9 mag (5.4 mag). The corresponding 1 σ of the distribution is 1.7 mag (1.4 mag). On the other hand, the dispersion in the A_{FUV} (A_{NUV}) derived is only 1.0 mag (0.8 mag) (see below). Since the $A_{\mathrm{FUV}}/(A_{\mathrm{FUV}}-A_K)$ [$A_{\mathrm{NUV}}/(A_{\mathrm{NUV}}-A_K)$] total-to-selective extinction ratio is always between 1.0 and 1.1 for any attenuation law considered, dust extinction alone is not able to explain the dispersion in the observed $(\mathrm{FUV}-K)$ [$(\mathrm{NUV}-K)$] color, neither its dependence on luminosity or morphological type.

It is now widely accepted that the star formation history of galaxies depends strongly on their stellar or total mass. Low-mass galaxies show relatively flat star formation histories, while more massive systems have shorter timescales of formation (e.g., Gavazzi et al. 1996, 2002; Gavazzi & Scodeggio 1996; Boselli et al. 2001). By virtue of this phenomenon, sometimes simplistically referred to as "down-sizing" (see Cowie et al. 1996), low-mass galaxies should be on average bluer in these colors than more massive galaxies. In this sense, we know that the typical stellar mass of a star-forming galaxy in the local universe is $\sim 1.3 \times 10^{10}\, M_\odot$ (Pérez-González et al. 2003; Gil de Paz et al. 2000a), i.e., more than 5 times less massive than an L^* galaxy in the NIR (Cole et al. 2001; Kauffmann et al. 2003).

Since we have information about the TIR emission for a large fraction of these galaxies, we can compute the attenuation in the FUV and NUV from the observed TIR-to-FUV ratio using the recipes published by Buat et al. (2005). The mean and 1 σ FUV (NUV) attenuation of the sample of spiral and irregular galaxies in the Atlas is 1.8 ± 1.0 mag (1.3 ± 0.8 mag). The internal-extinction–corrected (FUV − NUV) color is plotted in Figure 6*d* as a function of the *K*-band absolute magnitude. The solid (dashed) line shown in this plot represents the best weighted (nonweighted) fit to the data

$$(\mathrm{FUV}-\mathrm{NUV})_0 = 0.1083 + 0.00371 \times M_K; \quad \sigma = 0.054 \text{ mag (weighted)}; \tag{9}$$

$$(\mathrm{FUV}-\mathrm{NUV})_0 = 0.0942 + 0.00299 \times M_K; \quad \sigma = 0.055 \text{ mag (nonweighted)}. \tag{10}$$

Although there is a small tendency for the galaxies to show redder UV colors at lower luminosities and later types, we do not exclude the possibility that the intrinsic (FUV − NUV) color

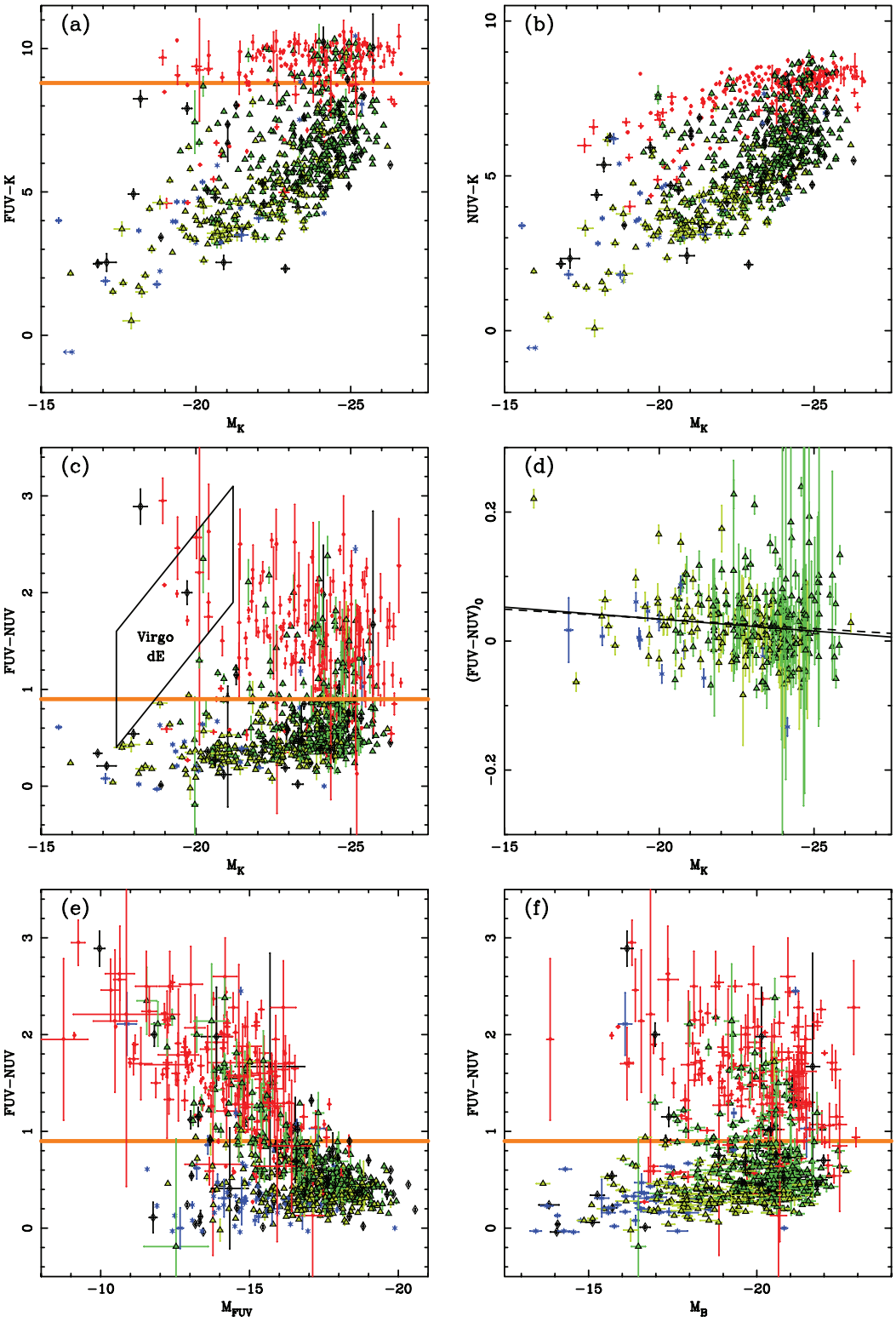

FIG. 6.— Color-magnitude diagrams (CMDs) of the Atlas galaxies. Red dots are elliptical / lenticular galaxies, dark green triangles are early-type spirals ($T < 5$), light green triangles are late-type spirals ($T \geq 5$), blue asterisks are irregular and compact galaxies, and black diamonds are galaxies currently lacking morphological classification. (*a*) (FUV $-$ *K*) $-$ M_K CMD. Spiral and irregular galaxies show a systematic bluing as we move to galaxies of lower mass. Elliptical / lenticular galaxies, on the other hand, show a very small change in the (FUV $-$ *K*) color with the *K*-band absolute magnitude (i.e., stellar mass) of the galaxy. (*b*) (NUV $-$ *K*) $-$ M_K CMD. In this case, however, lower mass ellipticals are also systematic bluer than more massive ones. (*c*) (FUV $-$ NUV) $-$ M_K CMD. This plot shows that the behavior observed in the elliptical galaxies in previous diagrams seems to be the consequence of a much fainter UV upturn (best traced by the FUV $-$ NUV color) in low-luminosity ellipticals than in massive ones. In this plot we show the position occupied by dwarf elliptical galaxies in Virgo (Boselli et al. 2005). Dwarf elliptical galaxies fainter than $M_K < -21$ mag start to show the effects of recent star formation both on their (FUV $-$ NUV) and UV-optical colors (see Boselli et al. 2005 for more details). (*d*) (FUV $-$ NUV)$_0$ $-$ M_K CMD. The (FUV $-$ NUV)$_0$ color is corrected for internal extinction using the relation between the total-infrared (TIR) to FUV ratio and the extinction in the FUV and NUV bands given by Buat et al. (2005). Only spiral and irregular/compact galaxies are used in this plot. Solid (dashed) line represents the best weighted (nonweighted) fit to the data. The narrow distribution in extinction-corrected UV slopes indicates that the tendency seen in the (FUV $-$ NUV) $-$ M_K CMD shown above for spiral galaxies is a direct consequence of the change in the amount of dust with the luminosity of the galaxy. (*e*) (FUV $-$ NUV) $-$ $M_{\rm FUV}$ CMD. (*f*) (FUV $-$ NUV) $-$ M_B CMD. These two latter diagrams show a similar behavior to that shown in (*c*). The high-luminosity end of the sample in the FUV is clearly dominated by spiral galaxies with a very narrow distribution in observed (FUV $-$ NUV) color.

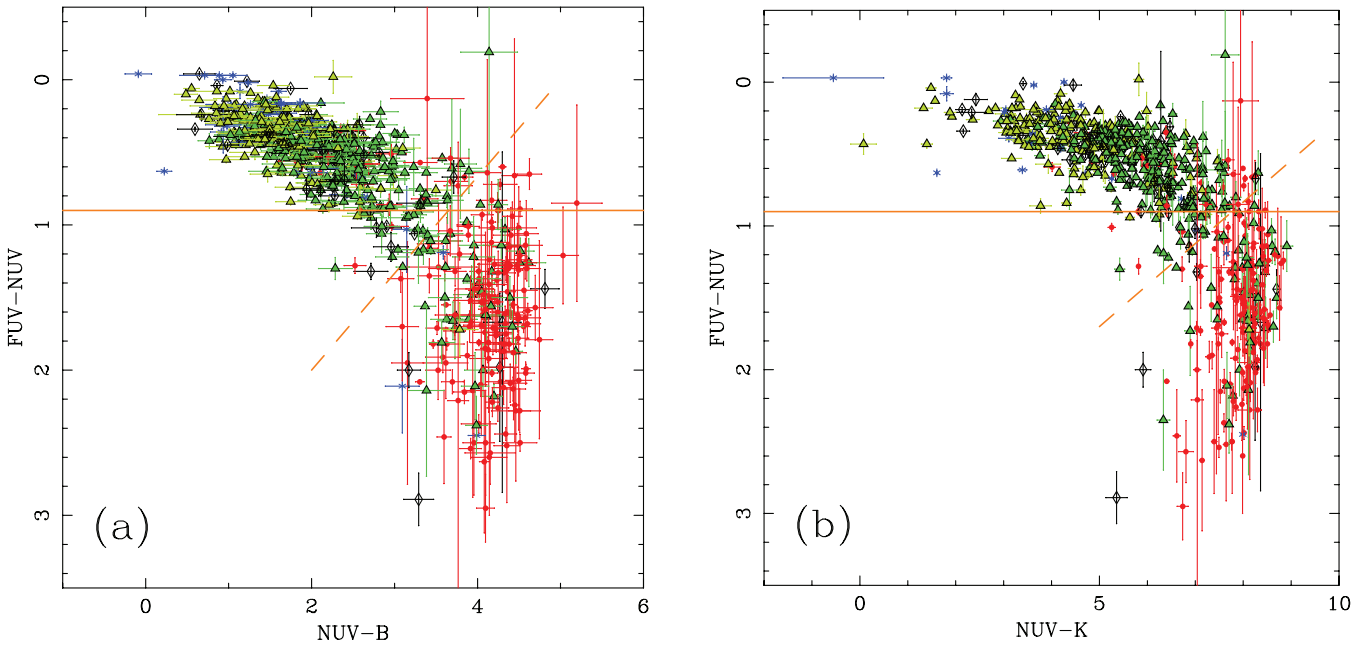

FIG. 7.—Color-color diagrams of the galaxies in the Atlas. (*a*) (FUV − NUV) − (NUV − *B*) color-color diagram. (*b*) (FUV − NUV) − (NUV − *K*) color-color diagram. Symbols have the same meaning as in Fig. 6. Lines in this plot represent various criteria proposed to separate elliptical/lenticular galaxies from spirals (see text for details). Note that, in order to keep with the stellar convention, the (FUV − NUV) axis has been flipped and red (FUV − NUV) colors are now plotted at the bottom of the figure.

derived in this way is independent of luminosity with an average value of $(\mathrm{FUV}-\mathrm{NUV})_0 = 0.025 \pm 0.049$ mag (i.e., $\beta_{\mathrm{GLX},0} = -1.94 \pm 0.11$; see Kong et al. 2004). We should note here that the measurements of the extinction in the FUV and NUV from which this intrinsic (FUV − NUV) color is derived are not fully independent since both are obtained by comparing the corresponding observed FUV and NUV flux with the same total-infrared emission (Buat et al. 2005). Consequently, there might be some additional weak dependency of the intrinsic (FUV − NUV) color with the luminosity that could be identified by analyzing both the detailed star formation history and dust properties (composition, geometry, temperature distribution) of individual galaxies.

Figure 6*e* shows that the most luminous galaxies in the FUV are spirals (both early- and late-type ones). In the optical (Fig. 6*f*) and NIR (Fig. 6*c*), on the other hand, the bright end of the luminosity function is populated by both elliptical and spiral galaxies. It is also worth noting that the galaxies in the bright end of the FUV luminosity function show a very narrow dispersion in the observed (FUV − NUV) color that results in a very similar shape for the bright end of the FUV and the NUV local luminosity functions (Wyder et al. 2005).

In Figure 7*a* we analyze the (FUV − NUV) − (NUV − *B*) color-color diagram of the galaxies in the Atlas. What is remarkable is the relatively narrow strip of this diagram where the galaxies are located. In the case of the spiral galaxies this is due in part to the well-known degeneracy in these colors between dust extinction and star formation history (see, e.g., Gil de Paz & Madore 2002). The ellipticals show a very narrow range in (NUV − *B*) color but a wide range of (FUV − NUV) colors, probably due to differences in the strength of the UV upturn from galaxy to galaxy. In the (FUV − NUV) − (NUV − *K*) color diagram (Fig. 7*b*) we find that ellipticals with redder (NUV − *K*) color tend to show bluer (FUV − NUV) colors. This is again a consequence of the weaker UV upturn present in optically blue, intermediate-mass ellipticals. The combination of the (FUV − NUV) color with either the (NUV − *B*) or the (NUV − *K*) color clearly improves the discrimination between elliptical/lenticular galaxies and spirals (see dashed lines in Figs. 7*a* and 7*b*). In the case of the (FUV − NUV) − (NUV − *B*) color-color diagram the origin {destination} of the cut-off line is [(FUV − NUV), (NUV − *B*)] = [2.0, 2.0]{5.0, 0.0}. For the (FUV − NUV) − (NUV − *K*) color-color diagram the corresponding origin {destination} of the cutoff line is [(FUV − NUV), (NUV − *K*)] = [5.0, 1.7]{9.5, 0.4}.

5.4. *Dust Extinction and the IRX-β Relation*

The relation found by Heckman et al. (1995) and Meurer et al. (1995, 1999) between the TIR-to-FUV ratio and the slope of the UV spectrum in starburst galaxies (IRX-β relationship; see also Seibert et al. 2005) can be used in principle to estimate the dust extinction in galaxies even if FIR data are not available. Some recent works have claimed that this relationship is valid only when applied to UV-selected starburst galaxies but not in the case of infrared-bright objects like the luminous/ultraluminous infrared galaxies (LIRGs/ULIRGs; Goldader et al. 2002) or even for normal spiral or irregular galaxies (see Bell et al. 2002 for results on the LMC). In Figure 8*a* we compare the TIR-to-FUV ratio with the observed (FUV − NUV) color, which is equivalent to the slope of the UV continuum (see Kong et al. 2004). Here we have only plotted galaxies with observed (FUV − NUV) color bluer than 0.9 mag. This criterion guarantees that the vast majority of the objects considered are either spiral or irregular galaxies. The dotted line represents the IRX-β relation given by Meurer et al. (1999). This figure demonstrates that the slope of the UV is indeed well correlated with the TIR-to-FUV and can be used to estimate (at least in a statistical way) the dust extinction in nearby galaxies. Similar results are found by Cortese et al. (2006) using a volume-limited optically selected sample of galaxies in nearby clusters.

The solid line in Figure 8*a* represents the best linear fit to the data. The dashed line is the same but excluding objects with

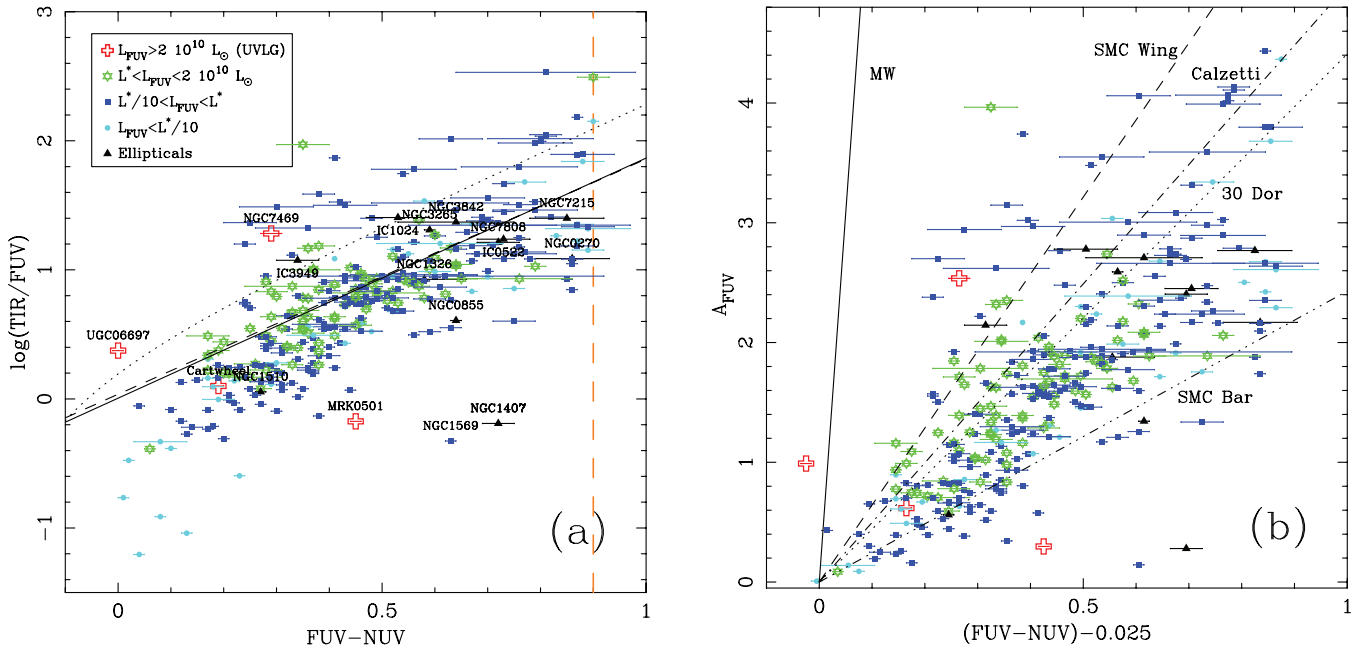

FIG. 8.—(*a*) IRX-β relation. The vertical long dashed line represents the cutoff in (FUV − NUV) color used to select the subsample of galaxies used to study the relation between the TIR-to-FUV ratio and the slope of the UV. This selection criterion guarantees that in the galaxies considered both the infrared and the UV emission are in the most part associated with the presence of recent star formation activity. The dotted line represents the relation derived by using a sample of starburst galaxies (Kong et al. 2004; Meurer et al. 1999). The best fit to the whole set of data is shown by a solid line. The best fit obtained excluding the lowest luminosity galaxies (*dots*) is shown by a dashed line. Symbols are coded by UV luminosity. Galaxies with higher UV luminosities (*green stars*) seem to be located somewhat closer to the relation derived for starburst galaxies that fainter objects (*blue squares*). Triangles correspond to the elliptical galaxies in the sample. Note that most of the ellipticals with (FUV − NUV) < 0.9 are known to have some degree of residual star formation. (*b*) A_{FUV} vs. (FUV − NUV) − 0.025. The latter term is equivalent to $A_{FUV} - A_{NUV}$ if an intrinsic (FUV − NUV) = 0.025 mag is assumed for all star-forming galaxies in the sample (see § 5.3). The lines drawn correspond to the total-to-selective extinction in the UV expected for different extinction laws (MW, *solid line*; LMC 30 Doradus, *dotted line*; SMC Wing, *dashed line*; SMC Bar, *triple-dot-dashed line*) and the attenuation law of Calzetti et al. (1994, *dot-dashed line*). The R_V values adopted for each of these laws are given in the text. Note that the inclusion of scattering would result in steeper relations between A_{FUV} and $A_{FUV} - A_{NUV}$ than those shown here. Therefore, an attenuation law based on the SMC Bar extinction law seems to be favored by these results. High–UV-luminosity galaxies are still adequately represented by the Calzetti attenuation law.

luminosities below $0.1L^*$ ($M^*_{FUV} = -18.12$; Wyder et al. 2005), for which the relation begins to depart from linearity. The results of these fits are

$$\log(\mathrm{TIR}/\mathrm{FUV}) = -0.18 + 2.05 \times (\mathrm{FUV} - \mathrm{NUV}); \quad \sigma = 0.36 \text{ dex}; \tag{11}$$

$$\log(\mathrm{TIR}/\mathrm{FUV}) = -0.15 + 2.00 \times (\mathrm{FUV} - \mathrm{NUV}); \quad \sigma = 0.36 \text{ dex} \left(\text{for } L > \frac{L^*}{10}\right). \tag{12}$$

Note that our sample suffers from a small deficiency of low-luminosity spirals. This fact might have an impact on the best-fit IRX-β relationship derived above. Cortese et al. (2006) have recently proposed a set of recipes that can be used to estimate the TIR-to-FUV ratio in star-forming galaxies using not only the (FUV − NUV) color but other parameters such as the oxygen abundance, the luminosity, the mean surface brightness, etc.

The majority of the objects in Figure 8*a* are found below the relationship defined for starburst galaxies. It is worth noting that objects with higher UV luminosity, some of them starburst galaxies, seem to fall closer on average [at least in the region with (FUV − NUV) < 0.6 mag] to the Meurer et al. relation than lower luminosity galaxies. According to Kong et al. (2004) the offset between normal galaxies and starbursts is primarily due to a lower ratio of present to past-averaged SFR in normal galaxies. However, the results obtained by Seibert et al. (2005) and Cortese et al. (2006) using *GALEX* data of nearby galaxies do not support this idea. These recent studies suggest that this offset might be due instead to a different geometry of the dust in normal galaxies compared with starbursts or, alternatively, to aperture effects present in the *IUE* data set used by Meurer et al. (1999).

The fact that we find such a good correlation between the TIR-to-FUV ratio and the (FUV − NUV) color and that the intrinsic (FUV − NUV) color seems to be rather constant for spiral and irregular galaxies suggests that the attenuation law in the UV for these galaxies is different from a pure Galactic extinction law. In the case of the Milky Way the extinction law shows a bump at 2175 Å that would result in a similar extinction in both bands, $A_{FUV} = 7.9E(B-V)$ and $A_{NUV} = 8.0E(B-V)$ (Bianchi et al. 2005). Thus, the observed trend in the (FUV − NUV) color with the TIR-to-FUV ratio is most probably due to a different extinction law since scattering, either for a shell or clumpy dust geometry, would result in an even lower FUV attenuation (compared with the NUV) than that expected from the Galactic extinction law alone (see, e.g., Roussel et al. 2005). The SMC Bar or 30 Doradus extinction laws and the attenuation law proposed by Calzetti et al. (1994) all show a weak 2175 Å feature and, especially in the case of the SMC Bar extinction law, a relatively steep FUV rise. In this sense, despite including scattering, the FUV rise of the Calzetti law is apparently too modest to reproduce the dependence between A_{FUV} and $A_{FUV} - A_{NUV}$ followed by the majority of the galaxies in our sample (see Fig. 8*b*).[12] Thus, although the Calzetti law, originally built for UV-bright

[12] We have adopted $R_V = 3.1$ for the Milky Way and LMC 30 Doradus extinction laws (Cardelli et al. 1989), $R_V = 4.05$ for the Calzetti law (Calzetti et al. 2000), $R_V = 2.87$ for the SMC Bar law (star AzV 398; Gordon & Clayton 1998), and $R_V = 2.66$ for the SMC Wing law (star AzV 456; Gordon & Clayton 1998).

starburst galaxies, still provides an adequate approximation to the relation between A_{FUV} and $A_{FUV} - A_{NUV}$ for galaxies with UV luminosities above L^*, an attenuation law based on the SMC-Bar extinction law is favored for the bulk of the galaxies in this Atlas.

We cannot exclude, however, that the FUV emission might be arising from young stars more deeply embedded in their parent molecular clouds than those responsible for the NUV emission. If that is the case, the differential extinction between the FUV and NUV emitting sources would lead to an artificial FUV rise in the global attenuation law even if the extinction law is rather flat in the UV.

In this same sense, it is worth noting that here we are referring to the attenuation law of the dust associated with the regions responsible for the UV emission, which could be quite different from the law we would obtain from regions dominating the emission at other wavelengths and also different from the extinction law that would be derived from line-of-sight absorption studies of individual stars.

5.5. *Structural Properties and UV Morphology*

Concentration indices have been commonly used in the past to infer the morphological types of barely resolved intermediate-redshift galaxies found in *Hubble Space Telescope* images (see, e.g., Abraham et al. 1996). One of the problems associated with these studies is the fact that in many cases the concentration indices derived for the high-redshift galaxies are measured in the rest-frame UV, while the local reference samples are usually observed in the optical (Bershady et al. 2000). In this sense, it is important to know the structural parameters in the UV of a sample of well-known nearby galaxies, like the one collected for this Atlas. Concentration indices C31 and C42 are provided in Table 4. The number of objects with these indices is small because we only computed the C31 (C42) concentration index for those galaxies whose radius containing 25% (20%) of the light was larger than $6''$. The same criterion applies to the effective radius, where the radius containing 50% of the light was imposed to be larger than $6''$ in order for it to be measured.

In Figure 9 we compare the concentration index C42 with the (FUV − K) color. As we commented in § 5.2 this color discriminates very well between elliptical and spiral galaxies and also between spiral galaxies of different types (see § 5.2). This figure shows that the C42 index improves the discrimination between ellipticals (*dots*) and lenticulars (*open circles*) and also between these and early-type spirals (*open triangles*). Y. H. Joe et al. (2008, in preparation) have recently carried out a more detailed study of the structural properties (including both concentration and asymmetry parameters) of nearby galaxies in the UV using the same sample presented in this Atlas.

Regarding the morphological classification of the UV surface-brightness profiles we first notice a large variety of morphologies even within each of the classes defined in § 4.4. This is partly a consequence of the high sensitivity of the UV to the recent star formation, which results in the presence of structures having relatively short evolutionary timescales that might dominate the UV profiles but that are not as obvious in the optical or NIR profiles. There is also the difficulty of dealing with degeneracies between some morphological classes. In this sense, some of the blue compact dwarf galaxies in the sample could be easily classified as having ER or EV profiles. In addition, some of the profiles inspected could be either classified as EEh or Ed. Despite these issues we successfully classify the profiles of 970 of the 1034 galaxy in the Atlas. Moreover, we find that most of the galaxies (615 out of 970) have UV profiles that can be grouped in three

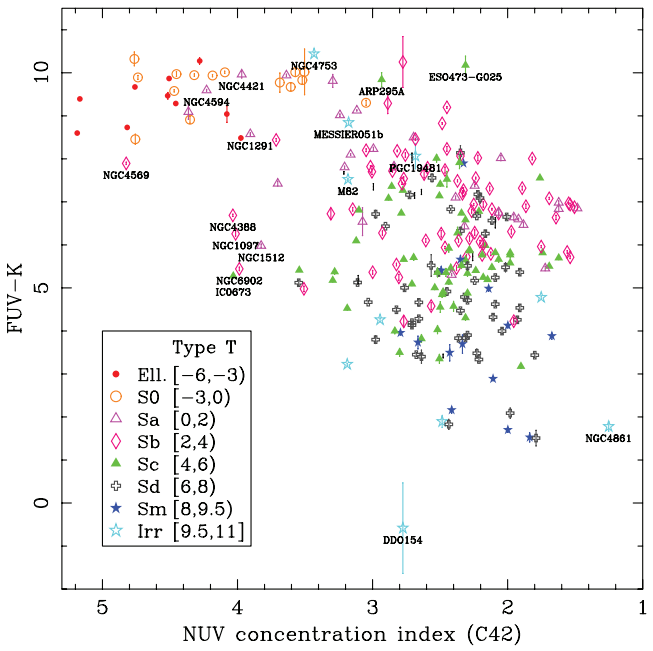

FIG. 9.—(FUV − K) color vs. the concentration index C42 in the NUV. Symbols are coded by morphological type. Although the galaxies are better segregated in (FUV − K) color than in the concentration index, the value of C42 can be used improve to the discrimination between ellipticals and lenticulars and between these and some early-type spirals.

main classes: (1) profiles that can be reproduced entirely by a de Vaucouleurs law (class VV), (2) pure exponential profiles (class EE), and (3) profiles with an exponential component in the outer region and significant flattening in the inner region (EF and Ef classes). Only 19 galaxies were classified as EV class, despite being the dominant morphology in the optical and near-infrared profiles of spiral galaxies.

This paucity of EV profiles seems to be due, at least in the case of late-type spirals, to the fact that even in the central regions the bulge is much fainter than the disk, which results in these galaxies being classified as having type EE or EF/Ef profiles (e.g., NGC 0628, M33, NGC 1042, NGC 2403). In early-type spirals, like the Sb galaxies NGC 0986, M31, M81, M95, the bulge is dominant only in the nucleus of the galaxy where is also commonly found associated with a flattening or decrease in the surface brightness of the disk toward the center. Because of the small spatial extension of these bulges in the UV surface brightness profiles Sb galaxies get usually classified as EFn, VFn, or EDn. Only lenticulars (e.g., NGC 1387, NGC 1546, NGC 4310, NGC 4477, NGC 6945, NGC 7252, M86), intermediate S0/a (NGC 2681, NGC 3816, NGC 3885, IC 0796), or very early-type spirals like the Sa galaxies NGC 1022, NGC 2798, NGC 4314, or NGC 4491 are sometimes best classified as having EV-type UV profiles. This is true for both UV bands although it is more frequent in the case of the NUV profile.

In Figure 10 we plot the distribution of galaxies classified within each of these groups: de Vaucouleurs profiles (v type), pure exponential profiles (e type), and flattened exponential profiles (f type); in the (FUV − K) versus morphological type diagram. Again, the morphological types used are those published in RC3. In the light of this figure it is fair to say that the majority of the elliptical galaxies in the Atlas follow a de Vaucouleurs profile in the UV, like is the case of the optical and NIR profiles of luminous elliptical galaxies. Note that because of our selection limits a small number of dwarf elliptical galaxies (which commonly show

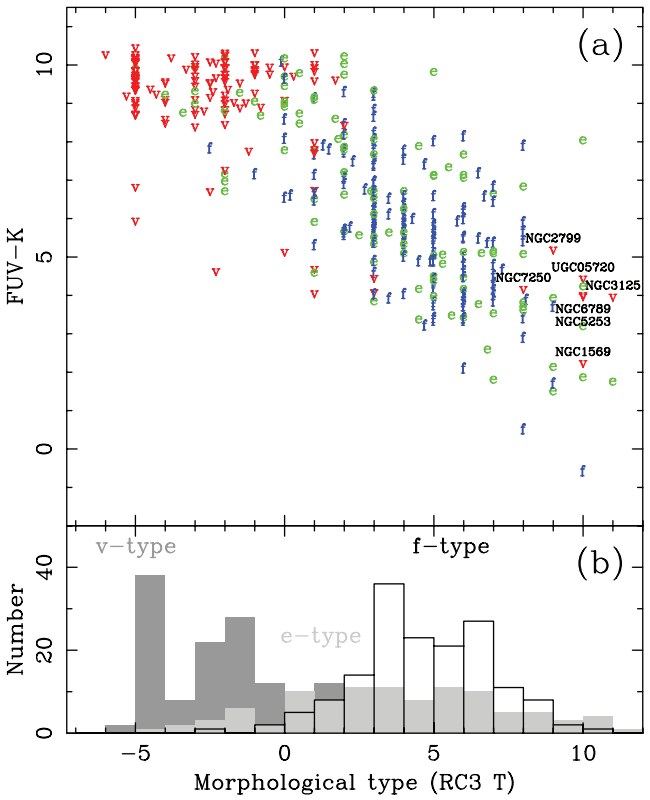

FIG. 10.—(*a*) (FUV − *K*) color vs. the morphological type. The symbols are coded by letters that represent the morphology of their UV profiles: "v" for galaxies following a de Vaucouleurs $R^{1/4}$ profile, "e" for galaxies with pure exponential profiles, and "f" for galaxies with exponential profiles in the outer regions and a flattened profile inside. (*b*) Morphological-type distribution for each class of the UV profile.

exponential light profiles in the optical) is expected to be found in this Atlas. A few v-type galaxies classified morphologically as late T-type objects are found to be well-known blue compact dwarf (BCD) galaxies: NGC 1569, NGC 3125, NGC 5253, NGC 6789, and UGC 05720 (Haro 2). See Doublier et al. (1997, 1999) for some other examples of BCD galaxies with $R^{1/4}$ profiles in the optical.

Regarding the distribution of the other two types of profiles we point out that, while galaxies with pure exponential profiles (a total of 173) are widely distributed in morphological type and color, galaxies with flattened exponential profiles (269) have, in the majority of the cases, morphological types T in the range $2 < T < 8$, i.e., they are truly spiral galaxies. In order to explain this behavior is necessary to understand first what is the mechanism(s) behind the flattening of the UV profiles.

In the spectrophotometric models of the evolution of disk galaxies of Boissier & Prantzos (2000; see also Boissier 2000), a similar flattening in blue bands is obtained. The main reason for it is that the rate the stars formed (i.e., SFR) in the inner disk has been higher than the infall of gas, leading to a progressive consumption of the gas in these regions. In the outer parts, however, star formation is less efficient and infall proceeds on longer timescales. As a result, the gas reservoir of the outer disk is not exhausted, and the shape of the exponential profile is preserved (in addition, an extinction gradient could enhance the difference between the inner regions, metal and dust rich, and outer regions suffering low metallicity and low extinction).

The dependence of the degree of flattening with the morphological type found, with most galaxies showing flattened-exponential profiles having types Sab–Sdm, is probably a consequence of the fact that (1) early-type galaxies have already consumed the majority of their gas at all radii, due to a high global star formation efficiency and low current infall, and (2) late-type spirals, because of their current large supply of gas and infall, still have enough gas to prevent its consumption at all radii. Note also that in some very early-type spirals (S0/a and Sa types) the presence of a relatively bright bulge might also difficult the detection of any flattening in the inner-disk profile.

The models referred above use as parameters the circular velocity (i.e., total mass), and the spin parameter (i.e., angular momentum). For a fixed spin parameter, the degree of flattening should depend on mass since e.g., the infall timescale depends on the mass. Indeed, at very low mass a modest flattening occurs, a more visible one at intermediate mass, and no flattening again in very massive galaxies (where the gas has been consumed over the whole galaxy) (Boissier 2000). However, using the *K*-band absolute magnitude as a tracer of the total mass of the system we found no difference between the distribution of galaxies with or without flattening in their profiles. This disagreement with the naive expectation from the models could be linked to the existence of the second parameter (at fixed velocity, the flattening of the star formation rate is more noticeable for smaller spin parameters), or more fundamental differences between EF/Ef and EE galaxies, not yet included in models. A more direct measure of the total mass and spin parameter, or detailed modeling of these galaxies (or a subsample of them) could help us to understand what makes the EF/Ef galaxies different from the EE ones.

6. CONCLUSIONS

We have presented an imaging Atlas of 1034 galaxies observed in two UV bands by the *GALEX* satellite. From these we have derived surface brightness and color profiles in the FUV and NUV *GALEX* bands. Asymptotic magnitudes and colors along with concentration indices have also been obtained. A morphological classification of the profiles is also carried out. Despite a small but non-negligible excess of high-luminosity and paucity of low-luminosity spiral galaxies (compared with the luminosity distribution of ellipticals both in our and the NFGS samples) it is shown that this sample adequately matches the distribution and full range of properties of galaxies in the local universe. We have augmented this data set with corollary data from the optical (RC3), NIR (2MASS), and far-infrared (*IRAS*). We emphasize here the special caution should be observed when comparing these results with those derived from a volume-limited sample. From a broad-based initial analysis of the UV properties of this sample we conclude the following:

1. The value of the integrated (FUV − *K*) color of galaxies provides an excellent criterion with which to discriminate elliptical/lenticular galaxies from spirals and irregulars. The best discrimination between these two classes of galaxies (quiescent vs. star-forming) is achieved if a cutoff color (FUV − *K*) = 8.8 mag is adopted. A reasonably good separation is also obtained by using a (FUV − NUV) cutoff color at 0.9 mag. These colors also allow for a continuous distinction (although with a significant dispersion) of spiral galaxies of different types.

2. Elliptical/lenticular galaxies with brighter FUV and *K*-band luminosities show bluer (FUV − NUV) colors than ellipticals with fainter luminosities but redder (NUV − *K*) colors. This is true for ellipticals galaxies specifically within the range of absolute magnitudes covered by this Atlas (i.e., $M_K < -21$ mag). This behavior is probably a consequence of luminous elliptical galaxies having

stronger UV upturns than their intermediate-mass counterparts (see Boselli et al. 2005).

3. We do not find a large dispersion in the intrinsic (corrected for internal extinction) (FUV − NUV) colors of the spiral/irregular galaxies in the Atlas ($\sigma_{(\mathrm{FUV-NUV})_0} = 0.05$ mag) nor a strong dependence of it with the galaxy luminosity. Consequently, the variations in the observed (FUV − NUV) colors with the luminosity or morphological type of the spiral and irregular galaxies in the sample are plausibly due to variations in the dust content (due for example to changes in metallicity) with these magnitudes. In the case of the (FUV − K) color the star formation history necessarily contributes to its dependence on luminosity and morphological type.

4. The change in the observed (FUV − NUV) color with the TIR-to-FUV ratio also suggests that the attenuation law in these galaxies differs from a pure Milky Way extinction law. In particular, attenuation laws with relatively steep FUV rise and no 2175 Å bump, like those based on a SMC Bar extinction law or the Calzetti law in the case of the most luminous objects, are favored.

5. A significant fraction (28%) of the UV profiles show some degree of flattening in the inner regions. The galaxies showing this kind of profile belong to a relatively small range of optical morphological types (compared with the pure-exponential profiles), $2 < T < 8$, i.e., they are all truly spiral galaxies. We interpret this as a consequence of the high past SFR but comparatively low current gas infall rate in the inner disks of spiral galaxies, leading to an efficient consumption of the gas in these regions and, consequently, to a flattening of the UV profiles compared with the outer disks, where the gas supply is still abundant. This is, indeed, expected to be particularly important in intermediate-type spirals.

The *GALEX* and corollary photometry data along with the profiles and UV images of galaxies in the sample can be accessed through a dedicated Web page.[13]

GALEX (*Galaxy Evolution Explorer*) is a NASA Small Explorer, launched in 2003 April. We gratefully acknowledge NASA's support for construction, operation, and science analysis for the *GALEX* mission, developed in cooperation with the Centre National d'Etudes Spatiales of France and the Korean Ministry of Science and Technology. A. G. d. P. is partially financed by the MAGPOP EU Marie Curie Research Training Network and the Spanish Programa Nacional de Astronomía y Astrofísica under grant AYA2003-01676. We thank Cren Frayer and Olga Pevunova for preparing the online version of the Atlas. We are also thankful to the referee for his/her valuable comments which helped to improve the paper.

Facilities: GALEX

[13] See http://nedwww.ipac.caltech.edu/level5/GALEX_Atlas/.

REFERENCES

Abraham, R. G., Tanvir, N. R., Santiago, B. X., Ellis, R. S., Glazebrook, K., & van den Bergh, S. 1996, MNRAS, 279, L47
Amram, P., Mendes de Oliveira, C., Boulesteix, J., & Balkowski, C. 1998, A&A, 330, 881
Bell, E. F., Gordon, K. D., Kennicutt, R. C., Jr., & Zaritsky, D. 2002, ApJ, 565, 994
Bershady, M. A., Jangren, A., & Conselice, C. J. 2000, AJ, 119, 2645
Bertin, E., & Arnouts, S. 1996, A&AS, 117, 393
Bianchi, L., et al. 2003a, in The Local Group as an Astrophysical Laboratory, ed. M. Livio & T. Brown (Baltimore: STScI), 10
———. 2003b, BAAS, 203, 91.12
———. 2005, ApJ, 619, L71
Bland-Hawthorn, J., Gallimore, J. F., Tacconi, L. J., Brinks, E., Baum, S. A., Antonucci, R. R. J., & Cecil, G. N. 1997, Ap&SS, 248, 9
Boissier, S. 2000, Ph.D. thesis, Univ. Paris
Boissier, S., & Prantzos, N. 2000, MNRAS, 312, 398
Boselli, A., Gavazzi, G., Donas, J., & Scodeggio, M. 2001, AJ, 121, 753
Boselli, A., Tuffs, R. J., Gavazzi, G., Hippelein, H., & Pierini, D. 1997, A&AS, 121, 507
Boselli, A., et al. 2005, ApJ, 629, L29
Bottinelli, L., Gouguenheim, L., Paturel, G., & de Vaucouleurs, G. 1984, A&AS, 56, 381
Brown, T. M. 2004, Ap&SS, 291, 215
Brown, T. M., Bowers, C. W., Kimble, R. A., Sweigart, A. V., & Ferguson, H. C. 2000, ApJ, 532, 308
Bruzual, G., & Charlot, S. 2003, MNRAS, 344, 1000
Buat, V., Boselli, A., Gavazzi, G., & Bonfanti, C. 2002, A&A, 383, 801
Buat, V., & Xu, K. 1996, A&A, 306, 61
Buat, V., et al. 2005, ApJ, 619, L51
Burstein, D., Bertola, F., Buson, L. M., Faber, S. M., & Lauer, T. R. 1988, ApJ, 328, 440
Cairós, L. M., Caon, N., Vílchez, J. M., González-Pérez, J. N., & Muñoz-Tuñón, C. 2001, ApJS, 136, 393
Calzetti, D., Armus, L., Bohlin, R. C., Kinney, A. L., Koornneef, J., & Storchi-Bergmann, T. 2000, ApJ, 533, 682
Calzetti, D., Kinney, A. L., & Storchi-Bergmann, T. 1994, ApJ, 429, 582
Cardelli, J. A., Clayton, G. C., & Mathis, J. S. 1989, ApJ, 345, 245
Cole, S., et al. 2001, MNRAS, 326, 255
Condon, J. J., Cotton, W. D., & Broderick, J. J. 2002, AJ, 124, 675
Cortese, L., et al. 2006, ApJ, 637, 242
Cowie, L. L., Songaila, A., Hu, E. M., & Cohen, J. G. 1996, AJ, 112, 839
Dale, D. A., Helou, G., Contursi, A., Silbermann, N. A., & Kolhatkar, S. 2001, ApJ, 549, 215
Davidge, T. J. 2003, AJ, 125, 3046
de Vaucouleurs, G. 1977, Evolution of galaxies and stellar populations, ed. R. B. Larson, & B. M., Tynsley (New Haven: Yale Univ. Obs.), 43
de Vaucouleurs, G., de Vaucouleurs, A., Corwin, H. G., Buta, R. J., Paturel, G., & Fouqué, P. 1991, Third Reference Catalogue of Bright Galaxies (Berlin: Springer) (RC3)
Deharveng, J.-M., Boselli, A., & Donas, J. 2002, A&A, 393, 843
Donas, J., Deharveng, J. M., Laget, M., Milliard, B., & Huguenin, D. 1987, A&A, 180, 12
Doublier, V., Caulet, A., & Comte, G. 1999, A&AS, 138, 213
Doublier, V., Comte, G., Petrosian, A., Surace, C., & Turatto, M. 1997, A&AS, 124, 405
Drozdovsky, I. O., & Karachentsev, I. D. 2000, A&AS, 142, 425
Feldmeier, J. J., Ciardullo, R., & Jacoby, G. H. 1997, ApJ, 479, 231
Freedman, W. L., & Madore, B. F. 1990, ApJ, 365, 186
Freedman, W. L., Wilson, C. D., & Madore, B. F. 1991, ApJ, 372, 455
Freedman, W. L., et al. 1994, ApJ, 427, 628
———. 2001, ApJ, 553, 47
Funes, J., Kennicutt, R. C., Jr., Lee, J. C., Sakai, S., Tremonti, C. A., & van Zee, L. 2007, in Island Universes: The Structure and Evolution of Disk Galaxies (Berlin: Springer), 441
Gallart, C., Aparicio, A., Freedman, W. L., Madore, B. F., Martínez-Delgado, D., & Stetson, P. B. 2004, AJ, 127, 1486
Gavazzi, G., Bonfanti, C., Sanvito, G., Boselli, A., & Scodeggio, M. 2002, ApJ, 576, 135
Gavazzi, G., Boselli, A., Donati, A., Franzetti, P., & Scodeggio, M. 2003, A&A, 400, 451
Gavazzi, G., Boselli, A., Scodeggio, M., Pierini, D., & Belsole, E. 1999, MNRAS, 304, 595
Gavazzi, G., Marcelin, M., Boselli, A., Amram, P., Vílchez, J. M., Iglesias-Páramo, J., & Tarenghi, M. 2001, A&A, 377, 745
Gavazzi, G., Pierini, D., & Boselli, A. 1996, A&A, 312, 397
Gavazzi, G., & Scodeggio, M. 1996, A&A, 312, L29
Gil de Paz, A., Aragón-Salamanca, A., Gallego, J., Alonso-Herrero, A., Zamorano, J., & Kauffmann, G. 2000a, MNRAS, 316, 357
Gil de Paz, A., & Madore, B. F. 2002, AJ, 123, 1864
———. 2005, ApJS, 156, 345
Gil de Paz, A., Madore, B. F., & Pevunova, O. 2003, ApJS, 147, 29
Gil de Paz, A., Zamorano, J., & Gallego, J. 2000b, A&A, 361, 465
Gil de Paz, A., et al. 2004, BAAS, 205, 42.01
———. 2005a, ApJ, 619, L115
———. 2005b, ApJ, 627, L29
Gladders, M. D., López-Cruz, O., Yee, H. K. C., & Kodama, T. 1998, ApJ, 501, 571

Gladders, M. D., & Yee, H. K. C. 2005, ApJS, 157, 1
Goldader, J. D., et al. 2002, ApJ, 568, 651
Gordon, K. D., & Clayton, G. C. 1998, ApJ, 500, 816
Gordon, K. D., Clayton, G. C., Misselt, K. A., Landolt, A. U., & Wolff, M. J. 2003, ApJ, 594, 279
Gordon, K. D., Clayton, G. C., Witt, A. N., & Misselt, K. A. 2000, ApJ, 533, 236
Heckman, T. M., et al. 1995, ApJ, 452, 549
———. 2005, ApJ, 619, L35
Herrnstein, J. R., et al. 1999, Nature, 400, 539
Huchra, J., Davis, M., Latham, D., & Tonry, J. 1983, ApJS, 52, 89
Jansen, R. A., Fabricant, D., Franx, M., & Caldwell, N. 2000, ApJS, 126, 331
Jarrett, T. H., Chester, T., Cutri, R., Schneider, S. E., & Huchra, J. P. 2003, AJ, 125, 525
Jensen, J. B., et al. 2003, ApJ, 583, 712
Karachentsev, I. D., & Drozdovsky, I. O. 1998, A&AS, 131, 1
Karachentsev, I. D., Karachentseva, V. E., Huchtmeier, W. K., & Makarov, D. I. 2004, AJ, 127, 2031
Karachentsev, I. D., Musella, I., & Grimaldi, A. 1996, A&A, 310, 722
Karachentsev, I. D., et al. 2002, A&A, 383, 125
———. 2003a, A&A, 398, 479
———. 2003b, A&A, 404, 93
Kauffmann, G., et al. 2003, MNRAS, 341, 33
Kelson, D. D., et al. 1996, ApJ, 463, 26
Kennicutt, R. C., Jr. 1998, ARA&A, 36, 189
Kennicutt, R. C., Jr., et al. 2003, PASP, 115, 928
Kent, S. M. 1985, ApJS, 59, 115
Kong, X., Charlot, S., Brinchmann, J., & Fall, S. M. 2004, MNRAS, 349, 769
Kuchinski, L. E., Madore, B. F., Freedman, W. L., & Trewhella, M. 2001, AJ, 122, 729
Kuchinski, L. E., et al. 2000, ApJS, 131, 441
Lauger, S., Burgarella, D., & Buat, V. 2005, A&A, 434, 77
Lonsdale, C., Helou, G., Good, J. C., & Rice, W. 1985, Catalogued Galaxies and Quasars Observed in the *IRAS* Survey (Pasadena: Jet Propulsion Laboratory)
Lupton, R., et al. 2004, PASP, 116, 133
Macri, L. M., et al. 2001, ApJ, 559, 243
Madore, B. F., et al. 1998, Nature, 395, 47
Makarova, L. N., & Karachentsev, I. D. 2003, Astrophysics, 46, 144
Makarova, L., Karachentsev, I. D., Takalo, L. O., Heinaemaeki, P., & Valtonen, M. 1998, A&AS, 128, 459
Marcum, P. M., et al. 2001, ApJS, 132, 129
Marlowe, A. T., Meurer, G. R., & Heckman, T. M. 1999, ApJ, 522, 183
Martin, D. C., et al. 2005, ApJ, 619, L1
Meurer, G. R., Heckman, T. M., & Calzetti, D. 1999, ApJ, 521, 64
Meurer, G. R., Heckman, T. M., Leitherer, C., Kinney, A., Robert, C., & Garnett, D. R. 1995, AJ, 110, 2665
Monet, D. G., et al. 2003, AJ, 125, 984
Morrissey, P., et al. 2005, ApJ, 619, L7
Moshir, M., et al. 1990, *IRAS* Faint Source Catalog, version 2 (Pasadena: IPAC)
O'Connell, R. W. 1999, ARA&A, 37, 603
Ohl, R., et al. 1998, ApJ, 505, L11
Östlin, G. 2000, ApJ, 535, L99
Paturel, G., Teerikorpi, P., Theureau, G., Fouqué, P., Musella, I., & Terry, J. N. 2002, A&A, 389, 19
Pérez-González, P. G., Gil de Paz, A., Zamorano, J., Gallego, J., Alonso-Herrero, A., & Aragón-Salamanca, A. 2003, MNRAS, 338, 525
Perrett, K. M., Hanes, D. A., Butterworth, S. T., Kavelaars, J., Geisler, D., & Harris, W. E. 1997, AJ, 113, 895
Rejkuba, M. 2004, A&A, 413, 903
Rejkuba, M., Minniti, D., Gregg, M. D., Zijlstra, A. A., Alonso, M. V., & Goudfrooij, P. 2000, AJ, 120, 801
Rice, W., et al. 1988, ApJS, 68, 91
Rich, R. M., et al. 2005, ApJ, 619, L107
Rifatto, A., Longo, G., & Capaccioli, M. 1995, A&AS, 114, 527
Roberts, M. S., & Haynes, M. P. 1994, ARA&A, 32, 115
Roussel, H., Gil de Paz, A., Seibert, M., Helou, G., Madore, B. F., & Martin, C. 2005, ApJ, 632, 227
Sakai, S., & Madore, B. F. 1999, ApJ, 526, 599
Salzer, J. J., Lee, J. C., Melbourne, J., Hinz, J. L., Alonso-Herrero, A., & Jangren, A. 2005, ApJ, 624, 661
Sandage, A., & Tammann, G. A. 1990, ApJ, 365, 1
Schlegel, D. J., Finkbeiner, D. P., & Davis, M. 1998, ApJ, 500, 525
Schulte-Ladbeck, R. E., Hopp, U., Crone, M. M., & Greggio, L. 1999, ApJ, 525, 709
Seibert, M., et al. 2005, ApJ, 619, L55
Sersic, J. L., & Donzelli, C. 1993, A&AS, 98, 21
Sharina, M. E., Karachentsev, I. D., & Tikhonov, N. A. 1999, Astron. Lett., 25, 322
Silbermann, N. A., et al. 1996, ApJ, 470, 1
Sullivan, M., Mobasher, B., Chan, B., Cram, L., Ellis, R. S., Treyer, M. A., & Hopkins, A. 2001, ApJ, 558, 72
Sullivan, M., Treyer, M. A., Ellis, R. S., Bridges, T. J., Milliard, B., & Donas, J. 2000, MNRAS, 312, 442
Sullivan, M., Treyer, M. A., Ellis, R. S., & Mobasher, B. 2004, MNRAS, 350, 21
Theureau, G., Rauzy, S., Bottinelli, L., & Gouguenheim, L. 1998, A&A, 340, 21
Thilker, D. A., et al. 2005, ApJ, 619, L79
Thim, F., Tammann, G. A., Saha, A., Dolphin, A., Sandage, A., Tolstoy, E., & Labhardt, L. 2003, ApJ, 590, 256
Tikhonov, N. A., & Galazutdinova, O. A. 2002, A&A, 394, 33
Tolstoy, E., Saha, A., Hoessel, J. G., & McQuade, K. 1995, AJ, 110, 1640
Tonry, J. L., et al. 2001, ApJ, 546, 681
Tosi, M., Sabbi, E., Bellazzini, M., Aloisi, A., Greggio, L., Leitherer, C., & Montegriffo, P. 2001, AJ, 122, 1271
Treyer, M. A., Ellis, R. S., Milliard, B., Donas, J., & Bridges, T. J. 1998, MNRAS, 300, 303
Tully, R. B. 1988, Nearby Galaxies Catalog (Cambridge: Cambridge Univ. Press)
van de Steene, G. C., Jacoby, G. H., Praet, C., Ciardullo, R., & Dejonghe, H. 2004, in Planetary Nebulae beyond the Milky Way, ed. J. R. Walsh & L. Stanghellini (Berlin: Springer) (astro-ph/0407348)
van den Bergh, S. 2000, Galaxies of the Local Group (Cambridge: Cambridge Univ. Press)
Verdes-Montenegro, L., Bosma, A., & Athanassoula, E. 2000, A&A, 356, 827
Wiklind, T., Combes, F., & Henkel, C. 1995, A&A, 297, 643
Windhorst, R. A., et al. 2002, ApJS, 143, 113
Wyder, T. K., et al. 2005, ApJ, 619, L15
Yahil, A., Tammann, G. A., & Sandage, A. 1977, ApJ, 217, 903
Yi, S. K., Lee, Y.-W., Woo, J.-H., Park, J.-H., Demarque, P., & Oemler, A., Jr. 1999, ApJ, 513, 128
Yi, S. K., et al. 2005, ApJ, 619, L111